DESIGN, CONSTRUCTION, AND EVALUATION OF A FIXED MIRROR SOLAR CONCENTRATOR

A THESIS

Presented to

The Faculty of the Division of Graduate

Studies and Research

By

John Fenton Rollins

In Partial Fulfillment

of the Requirements for the Degree

Master of Science in Mechanical Engineering

Georgia Institute of Technology

August 1974

DESIGN, CONSTRUCTION, AND EVALUATION OF A FIXED MIRROR SOLAR CONCENTRATOR

Approved:

James R. Williams, Chairman

Prateen V. Desai

Jesse D. Walton

Date approved by Chairman: 8/20/74

ACKNOWLEDGEMENTS

I would like first, to express my sincere appreciation to my Advisor, Dr. James R. Williams for suggesting the topic and providing guidance and encouragement during the duration of this project.

Appreciation is extended to Mr. J. D. Walton and Dr. P. V. Desai for serving on the reading committee and reviewing the manuscript.

I am particularly grateful to Mr. Glen Robinson of Scientific Atlanta for providing the funds which made this project possible.

I would also like to thank Dr. John L. Russell for providing the initial research literature and Mike McKee for his time and effort during the project.

I would like to thank my parents. It was their concern, patience and support throughout my college education which provided the opportunity for this experience.

Finally, I would like to thank my wife, Katie, for putting up with me during this project. It was her patience, understanding, and at times, personal assistance which made the completion of this project possible.

Special permission was received from the Division of Graduate Studies to vary from the thesis manual requirements for numbering of figures.

TABLE OF CONTENTS

TABLE OF CONTENTS (Concluded)

LIST OF TABLES

LIST OF ILLUSTRATIONS

* Photographic Figures

LIST OF ILLUSTRATIONS (Continued)

* Photographic Figures

LIST OF *ILLUSTRATIONS* (Continued)

---

* Photographic Figures

LIST OF ILLUSTRATIONS (Concluded)

NOMENCLATURE

$\bar{s}$	unit vector of incident ray of sunlight
$\bar{s}'$	unit vector of reflected ray of sunlight
$\bar{n}$	unit vector normal to reflecting surface at point of reflection
Γ	angle of reflection
Γ'	angle of incidence
θ	angle measured from z axis to intersection of center of mirror slat and reference circle
Q	angle between any two light ray projections in the yz plane
Δ	angle between center line and z axis
θ_{TS}	angle between tangent slat position and C_L
FMC	fixed mirror concentrator
α β γ	direction cosines of $\bar{s}$
ϕ	angle projection of incident sunlight in yz plane makes with xy plane as measured from positive y axis counterclockwise (solar angle)
τ	angle between focal plane and plane perpendicular to incident light rays from one mirror slat
I	normalized value of direct solar heat flux
Ω	16 minute arc
ω	focal plane angle
D	length of line from center of slat to center of focal plane, in yz plane
C_L	center line of concentrator also axis of symmetry
R	radius of reference circle

NOMENCLATURE (Continued)

θ_{in}	angle defining aperture of fixed mirror concentrator
θ_{η}	position angle on reference circle
TS	tangent slat
L_1	horizontal projection of first slats half width
L_2	horizontal projection of second slat's half width
L_3	horizontal distance between the centers of two adjacent slats
ψ	angle between horizontal and line thru centers of two adjacent slats
λ	1/2 the angle subtended by a chord between two adjacent slats
W	width of mirror slat
W_c	width of concentrator
ES	edge slat, last slat forming one of two edges or lips of concentrator
θ_F	the position on the reference circle of the center of the focal plane
h	height of vertical edge between two mirror slats
ρ	reflectivity
S	total direct solar energy incident on FMC
S_E	total solar energy reaching focal plane after edge losses only
S_E^*	correct value of solar energy reaching focal plane after edge losses only at $\phi = 78°$ and $\phi = 90°$
L_{CP}	cross pipe shadow loss
S_T	area under the theoretical heat flux density curve falling within target area
CE	concentration efficiency
I_R	intensity level of direct radiation after a single reflection of a mirror slat

NOMENCLATURE (Concluded)

D_P	pivot arm distance
η	scanner angle
θ_P	pivot arm angle
ϕ_x	solar angle in xz plane
θ_{TS}	position angle of tangent slat
θ_{ES}	position angle of edge slat
I_F	energy arriving at focal plane
I_A	energy passing plane A
θ_F	position angle of focal plane

SUMMARY

The purpose of this project was to design, construct and evaluate a 60 square foot fixed mirror solar concentrator. The design utilized economical, readily available materials and required no special assembly techniques. The final design which was constructed consisted of an aluminum and plywood frame supporting 23 reflecting slats. Each reflecting slat was formed by bonding two rear surfaced window glass mirror sections to an aluminum channel. Two methods of concentrator alignment, one using a laser alignment apparatus and the other using incident sunlight were successfully employed.

The theoretical heat flux profiles at the focal plane of the concentrator were determined and used to calculate the theoretical concentration efficiency and theoretical edge loss of the concentrator over a range of solar angles. The theoretical heat flux profiles and theoretical concentration efficiency were later compared to experimentally determined results.

A photomultiplier tube scanning mechanism was designed, built, and then used to measure the actual heat flux profiles at the focal plane of the concentrator. This was done over the same range of solar angles used in the theoretical analysis. These experimentally determined heat flux profiles were then used to calculate the actual concentration efficiency of the concentrator.

A comparison of the experimental and theoretical heat flux

profiles and concentration efficiency showed very close agreement. This is particularly important due to the fact that low cost materials and standard assembly techniques were used in the construction of the concentrator.

CHAPTER I

INTRODUCTION

Background and History

In the United States, a square mile of land receives about 15×10^{12} BTU of solar energy every year. In 1970, the total energy consumed by the United States was about 6.5×10^{16} BTU. Assuming a 10% conversion efficiency, this would mean that 43,000 square miles or about 1.5% of the land area in the 48 states could have supplied the total United States' energy requirement in 1970, utilizing solar energy alone [1]. Today solar energy remains practically unused except in the natural sense, but with the increasing scarcity and high cost of fossil fuels it is once again being examined as a possible partial solution to the energy problem.

The history of man's attempts to utilize solar energy as a power source dates back about 100 years. In 1878 at a Paris exhibition, sunlight was utilized in a focusing concentrator to produce steam that operated a small steam engine. In later years solar engines and heaters became larger and more complicated, but they all consistently suffered the same draw back. They could not compete economically with the relatively cheap and abundant fossil fuels.

Solar energy collectors may be classified in three categories. These are (1) low temperature flat plate collectors with no concentration, (2) linear concentrating collectors obtaining medium temperatures, and (3) high temperature concentrating collectors. Table 1 summarizes

these three categories [2].

Table 1. Classification of Solar Collectors

Category	Example	Temperature °F	Efficiency per cent
no concentration	flat plate	150- 300	30-50
med. concentration	parabolic cylinder	500-1200	50-70
high concentration	parabodial	1000-4000	60-75

Concentrating solar collectors offer several advantages over non-concentrating types when used for heating, cooling, and the generation of electric power [1]. These are:

1. more compact heat storage
2. year round collection of high temperature heat
3. higher thermal efficiencies in heat engines, cooling devices, and generating devices
4. smaller collector areas for cooling and power generating devices.

Most concentrating collectors however, have one major problem. They must be constantly oriented toward the sun. Parabolic cylinders and parabodial concentrators suffer degradation of focus when the sunlight is not exactly incident along the axes of the parabola. As a result of this, practical and economic size limitations result when attempting to design such a concentrator which must not only follow the sun, but withstand the maximum possible wind loadings as well. Daniels [3] reported that a practical limit in some areas is about eight feet in

diameter for the circular type.

Systems using constantly oriented concentrators have, as yet, not been able to economically compete with fossil fuel systems. A large part of the cost of such steerable concentrators is associated with mechanical mechanism which supports and moves the reflecting surface. To reduce this cost and bring concentrating systems into the range of economic feasibility two general approaches have been tried: (1) use simple automatic mechanisms to steer many separate, smaller reflectors instead of a single reflecting surface. These smaller reflectors would require less supporting structure than the larger single surface. (2) Develop concentrators with fixed reflecting surfaces and movable heat absorbing devices. These heat absorbing devices would be much smaller than the reflecting surface thereby also requiring a smaller supporting structure.

Review of Literature

Along with the idea of focusing many separate smaller reflectors, Gunter [4] in 1906 proposed a concentrator consisting of a number of long, narrow reflecting surfaces laid side by side each set at a predetermined angle. With a single, simple mechanism all the reflectors could be rotated at the same speed keeping the sunlight constantly focused on a fixed heat absorbing device. This concentrator had the added advantage that all the reflecting surfaces could be quickly rotated to a position facing the ground for protection against sudden hail storms. Desai and Lindsey [5] have recently built and tested such a concentrator which shows good promise. The results of these tests

will be available soon.

Fairbanks and Morse [6] described a simple orientation device called a thermal heliotrope which might be used to steer many small reflectors. This consists of a bimetallic helical coil along with one or more sun shades that produces torque and the correct angular displacement of a solar concentrating system when sunlight hits the coil. The device is electrically passive, has few parts, and it could be mass produced at a low unit cost.

Another system associated with the first approach is called the solar furnace. The tower concept [7] is a good example. Here, mass produced heliostats are used to orient many separate flat mirrors which focus sunlight into a boiler. The boiler is mounted on top of a tower in the center of a field covered with such heliostat-oriented mirrors. The boiler produces high temperature steam for use in driving a turbine. One such solar furnace has been built in Italy [8]. Martin Marietta and Georgia Institute of Technology are also working on a similar power plant. This system uses arrays of heliostat-oriented mirrors to focus sunlight into a cavity type boiler near the ground. The French furnace at Odellio is going to be used to demonstrate the system which will generate about 300 kilowatts of electric power [9].

The second approach consisted of developing concentrators with fixed reflecting surfaces and movable heat absorbing devices. Tabor [10] discussed the possibility of using a cylindrical, parabolic mirror with an east-west mounting. If the mirror was only given a weekly tilt a concentration of approximately three could be realized without diurnal movement. This concentration could be increased to about four

with the aid of a small auxiliary fixed mirror.

Steward [11] proposed a stationary spherical reflector mounted with the axis pointed south and tilted at an angle of 60 degrees from the vertical to favor the winter sun. A movable heat collecting device intercepts the reflected rays which are focused along a straight line. The concentration factor was to be determined after tests, however, an operating temperature of greater than 500°F was assumed. One difficulty associated with Steward's proposed system seemed to be the somewhat complicated mechanism needed to position the heat collecting device.

Winston [12] described an interesting design of a stationary, concentrating collector which does not form a focused image. This concentrator consists of a trough-like reflecting light channel of a specific shape which concentrates incident radiant energy at the bottom of the trough. These troughs could be grouped together, side by side, into units and covered with glass plates. In this way, they also have the unique ability to accept both direct and diffuse solar radiation. The complete stationary system would be capable of accepting solar energy over an average eight hour day and concentrating it by a factor of 10 without diurnal tracking of the sun. Seasonal adjustments, however, would be needed to keep such a concentration factor. Without these seasonal adjustments the concentration factor is reduced to about three which indicates a somewhat narrow acceptance angle. Since multiple reflections are involved in the concentration of sunlight, an extremely clean surface with a very high reflectivity is needed for efficient operation. This could present problems in economically producing such a system which would work efficiently.

One of the more promising fixed mirror concentrating designs has recently been proposed by Russell [13]. This design consists of long, narrow reflecting mirrors positioned at certain set angles on the inside of a reference cylindrical surface. This cylindrical surface and the mirrors remain stationary. Incident sunlight from any direction that reflects off the fixed mirrors is focused into a sharp line parallel to the fixed mirrors and lying somewhere on the top portion of the reference cylindrical surface. A heat absorbing pipe is then mounted on arms which are pivoted at the center of the reference cylinder. A simple sun sensing or timing device is used to keep the heat absorbing pipe in the concentrator's focus, which slowly moves across the top of the reference cylinder as the sun changes position.

The fixed mirror concentrator (FMC) has several advantages over other stationary systems:

1. A sharp focus is always formed for any incident sunlight.
2. The heat absorption element is easily positioned due to its single degree of freedom movement.
3. The reflecting surfaces are flat as opposed to parabolic or circular reflectors, which are more expensive and difficult to produce.
4. The design is simple, easily lending itself to mass production techniques.
5. The design can be built in modular sections which could be used individually or grouped together into solar farms for central station power production [14].

Definition and Purpose of Research

This project involved the design, construction, and evaluation of a fixed mirror concentrator of at least 50 square feet. The purpose

of the research was to compare the theoretical performance characteristics of the design with what was experimentally measured. Comparisons were made of heat flux profiles and the concentration efficiency over a range of sun angles.

The performance characteristics measured were of a working concentrator similar to commercial models which might become available. No attempt was made to design and construct a concentrator which would exhibit the maximum performance characteristics possible, without regard to cost. With this in mind, the design involved low cost, readily available materials and simple hand assembly techniques.

Method of Attack

The project was divided into three areas:

1. Design and construction of the fixed mirror concentrator.
2. Design of the equipment and experimental testing of the concentrator.
3. Theoretical analysis of the concentrator.

Since funds for construction were limited to $1,000, the first step involved the preliminary cost estimate of various fixed mirror concentrator designs. A low cost design involving materials which could be obtained quickly and economically was arrived at and the concentrator was constructed.

The second step involved the design and construction of a photomultiplier scanning mechanism used to measure the heat flux profile at the focal area. The equipment was mounted on the concentrator and experimental test carried out.

Finally, a theoretical analysis was performed and the results compared with the experimental tests.

CHAPTER II

GENERAL CONCEPTS OF THE FIXED MIRROR CONCENTRATOR

Two Dimensional Principle

The following general concepts of the FMC are summarized from Russell's report on the principles of the FMC [13]. Consider two long mirror slats S_1 and S_2 laid a distance apart with their long axes parallel and their planes not parallel. Two parallel planes of light, A and B, are incident on slats S_1 and S_2 and are reflected off into light planes A_1 and B_1 which intersect along line F as shown in Figure 1. Now consider a plane perpendicular to planes of both slats S_1 and S_2 and light planes A, B, A_1, and B_1 is shown in Figure 2. Note, lines a, b, a_1, and b_1 are not light rays but simply the projections in the plane perpendicular to slats S_1 and S_2 of any light rays in planes A, B, A_1, and B_1. The laws of reflection are valid for these projections as shown in Figure 2.

It can be geometrically proven that as angle aS_1S_2 in Figure 2 varies the locus of point F is a circle which inscribes the triangle FS_1S_2. This circle shall be known as the reference circle. It follows that any other slat which lies on the reference circle (as do S_1 and S_2) and is angled so that it reflects an incident light plane which is parallel to planes A and B, through line F; will also direct this reflected light plane through F no matter what direction the incident light plane comes from, as long as it is parallel to planes A and B. It is therefore possible to construct a cylindrical concentrator

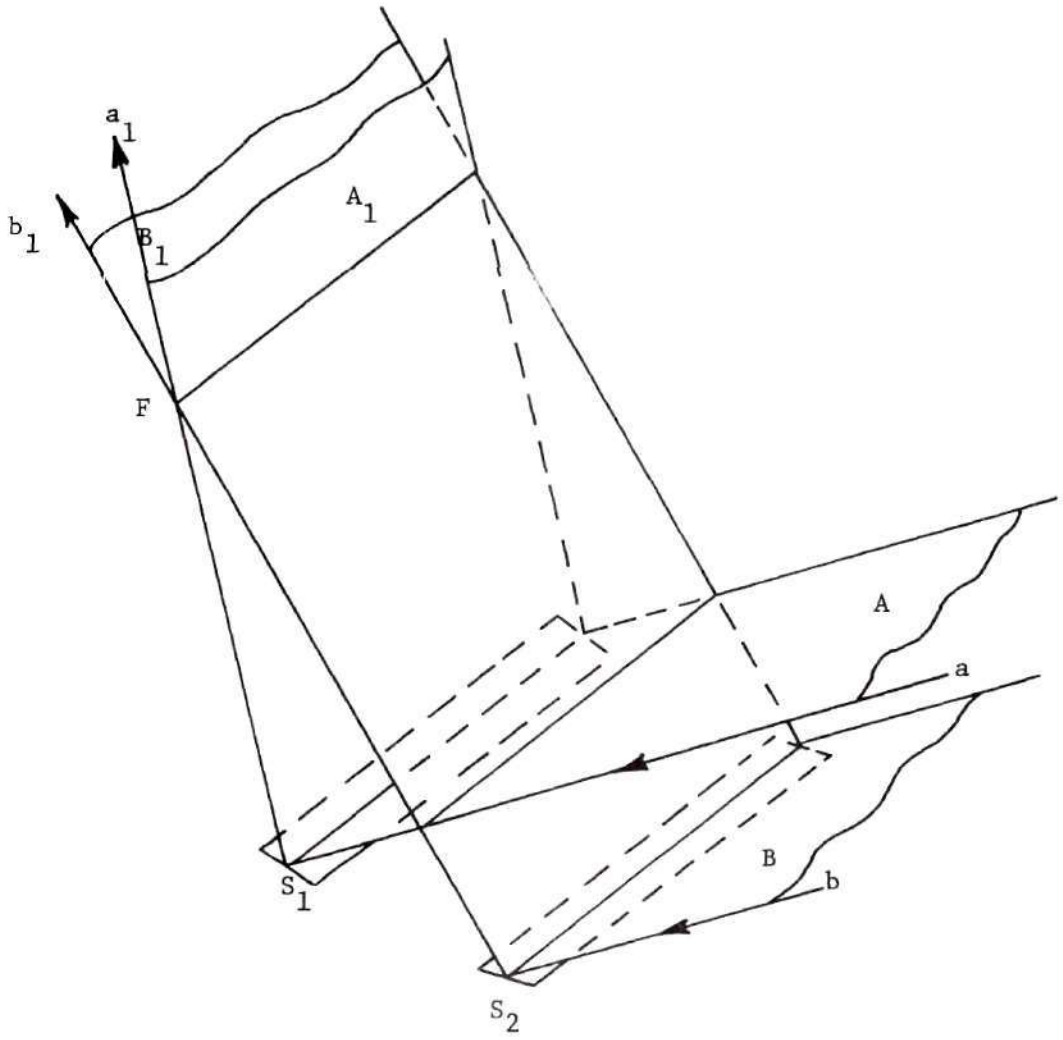

Figure 1. Planes of Light Incident on Two Mirror Slats

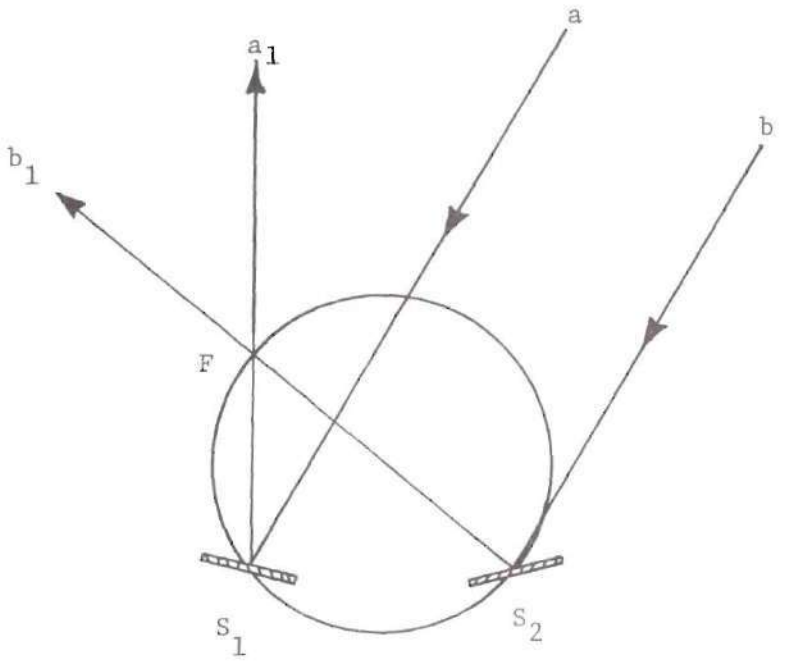

Figure 2. Intersection of a Plane Perpendicular to Slats S_1 and S_2

which would be composed of a reference cylinder on the lower portion of which are positioned a number of fixed mirror slats (like S_1 and S_2). When these thin slats are properly oriented, they will focus incident parallel light from any direction into a sharp line which lies on the upper portion of the reference cylinder. The focal distance of this array of fixed mirrors in 2R, where R is the radius of the reference circle. Note that a conventional cylindrical mirror of radius R has focal distance of R/2. The important feature of this particular concentrator is the fact that the array of mirrors mounted on the reference circle are fixed in position, and they form a concentrator which exhibits no degeneration of focus when the incident light changes direction. This is to be compared with the severe off axis aberration of parabolic concentrators. It is a relatively easy matter to mount a heat collecting tube on arms of radius R which pivot about the center of the reference cylinder as shown in Figure 3. By simply rotating the heat collecting tube it can be kept exactly in the focus of the fixed mirror concentrator for all incident light angles.

The above discussion is essentially a two dimensional description of the fixed mirror concept. The next section discusses the situation in which a ray of incident sunlight, while lying in plane A or B of Figure 1, does not lie in a plane perpendicular to the mirror slats. In other words, its projection in the plane perpendicular to the mirror slats (Figure 2) is not parallel to the actual ray.

Three Dimensional Principle

In Figure 4 let a ray of sunlight be incident on the unit vector $\bar{s}$. Let $\bar{s}'$ be the reflected ray of sunlight also of unit length. Let $\bar{n}$

be a unit vector normal to the reflecting surface at the point of reflection. The law of reflection says that

$$\bar{s} \times \bar{n} = \bar{s}' \times \bar{n} \tag{1}$$

or in other words the angle of incidence equals the angle of reflection. In Figure 4, Γ' is the angle of incidence and Γ is the angle of reflection as measured from the normal vector $\bar{n}$.

It can be shown that

$$\bar{s}' = \bar{s} - 2\bar{n}\,(\bar{s}\cdot\bar{n}) \tag{2}$$

which is the general solution $\bar{s}'$ in terms of $\bar{s}$ and $\bar{n}$.

Figure 5 shows a fixed mirror concentrator with its axis of rotation as the x axis. The length of the reflecting slats are long when compared to the reference circle radius. The width of the reflecting slats is very small. If a slice is taken out of this concentrator perpendicular to the x axis a reflecting element, shown in Figure 6, is formed. If the fixed mirror concentrator is thought of as being composed of a stack of the reflecting elements shown in Figure 6, then the final reflected image of uniform incident sunlight is formed by the summation of reflections from each of the reflecting elements in the concentrator.

If a reflecting element as shown in Figure 6 is situated in the yz plane at $x = 0$, then the position of each reflecting slat can be specified by the angle θ. If these slats focus parallel rays of light from any direction into a line on the reference cylinder, then their angle of inclination to the xy plane is $\theta/4$ as shown in Figure 7.

The vector $\bar{n}$ is the unit vector normal to the thin reflecting

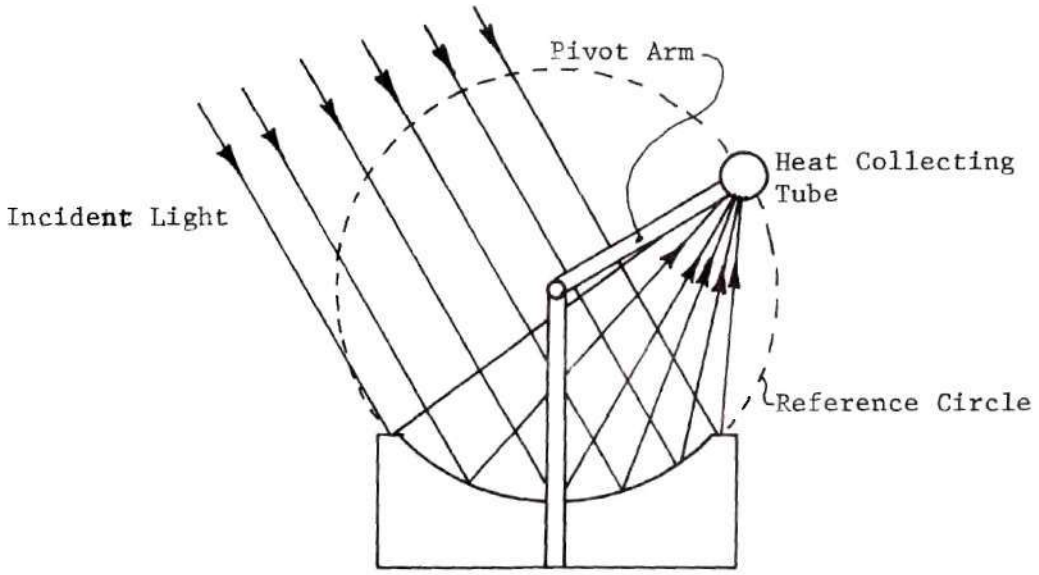

Figure 3. The Fixed Mirror Concentrator

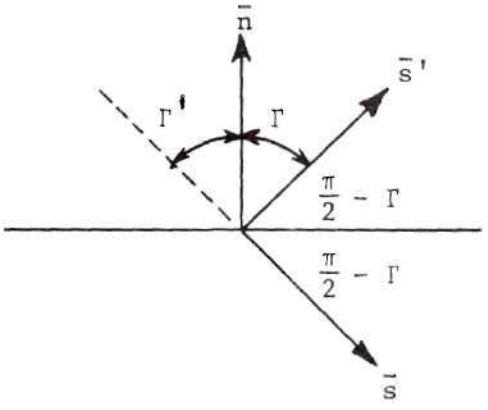

Figure 4. Reflection Notation

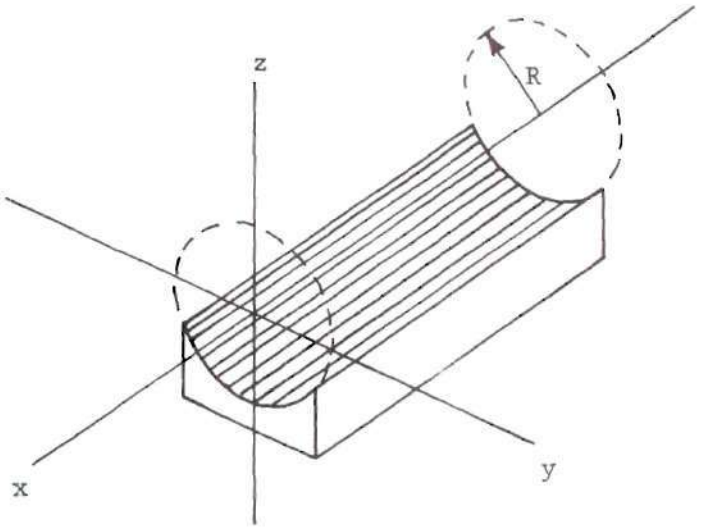

Figure 5. Concentrator with Axis of Rotation as the x Axis

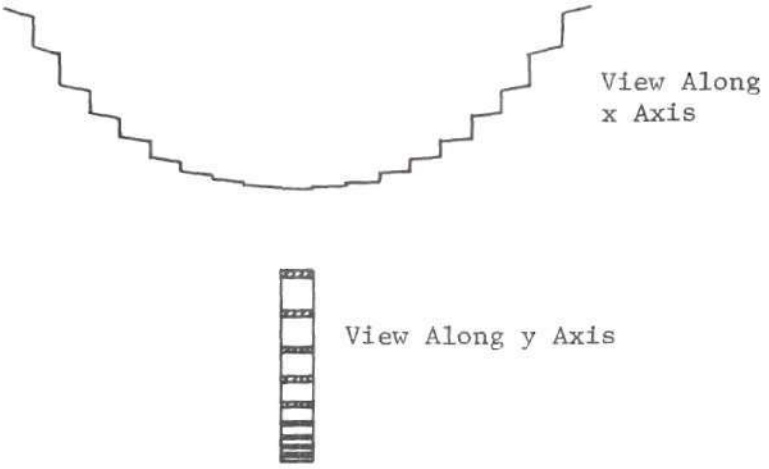

Figure 6. Reflecting Element

slat at (θ) on the reference cylinder, where

$$\bar{n} = \begin{pmatrix} \sin^{\circ} \theta/4 \\ \cos \theta/4 \end{pmatrix}$$

Let $\bar{s}$ be defined as before, and let

$$\bar{s} = \begin{pmatrix} \alpha \\ \beta \\ \gamma \end{pmatrix}$$

where α, β, and γ are the direction cosines of $\bar{s}$ with the x, y, and z axes.

The vector $\bar{s}$ can always be expressed as the sum of two perpendicular components, one of which is parallel to the x axes ($\bar{s}_{||}$) and one of which is in the yz plane, perpendicular to the x axes ($\bar{s}_{\perp}$). From this let

$$\bar{s} = \bar{s}_{||} + \bar{s}_{\perp} \tag{3}$$

as shown in Figure 8. Similiarly let the unit vector $\bar{s}'$ be defined as

$$\bar{s} = \bar{s}'_{||} + \bar{s}'_{\perp} \tag{4}$$

By substituting Equation (3) in Equation (2) and then substituting in Equation (4) the following results are obtained.

$$\bar{s}'_{||} = \bar{s}_{||} = \begin{pmatrix} \alpha \\ o \\ o \end{pmatrix} \tag{5}$$

$$\bar{s}'_{\perp} = \bar{s}_{\perp} - 2\bar{n} \, (\bar{s}_{\perp} \cdot \bar{n}) \tag{6}$$

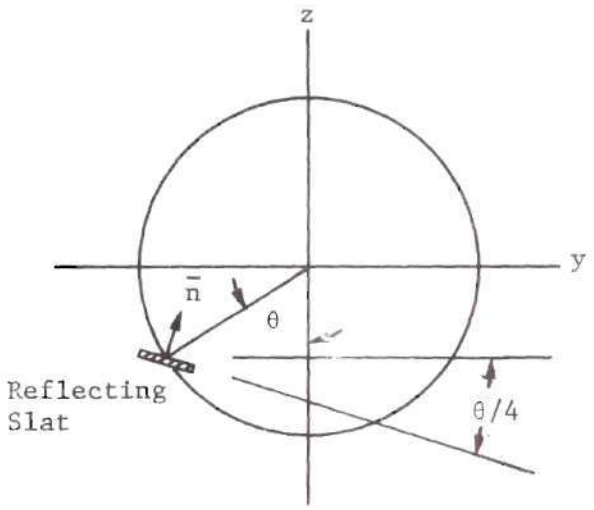

Figure 7. Slat in yz Plane at x=o

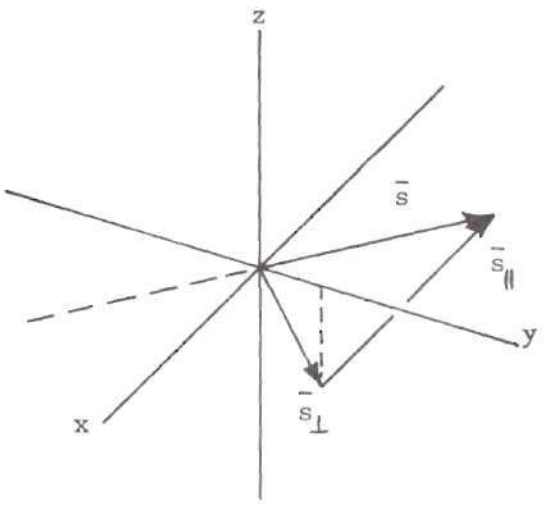

Figure 8. Vector $\bar{s}$

Equations (5) and (6) state that any light ray component parallel to the x axis is unchanged by reflection.

The relationship of $\bar{s}_{\perp}'$ to $\bar{s}_{\perp}$ on a given slat at position (θ) on the reference circle will now be examined. It can be shown that

$$\bar{s}_{\perp}' = \begin{pmatrix} \beta \cos^{\circ} \theta/2 - \gamma \sin \theta/2 \\ -\beta \sin \theta/2 - \gamma \cos \theta/2 \end{pmatrix}$$

Looking at Equations (4) and (5) it can be seen that

$$|\bar{s}_{\perp}'| = \sqrt{1 - \alpha^2} \tag{7}$$

The angle Q between the perpendicular projections in the yz plane of any two reflected rays (that is, the angle between $\bar{s}_{\perp}'(\theta_1)$ and $\bar{s}_{\perp}'(\theta_2)$ is defined by

$$\text{Cosine of } Q = \frac{\bar{s}_{\perp}'(\theta_1) \cdot \bar{s}_{\perp}'(\theta_2)}{1 - \alpha^2} \tag{8}$$

It can be shown that

$$\bar{s}_{\perp}'(\theta_1) \cdot \bar{s}_{\perp}'(\theta_2) = 1 - \alpha^2 \cos\left(\frac{\theta_1 - \theta_2}{2}\right) \tag{9}$$

Substituting Equation (9) into Equation (8)

$$Q = \left(\frac{\theta_1 - \theta_2}{2}\right) \tag{10}$$

Since the angle Q between any two reflected light ray projections in the yz plane is constant at half the difference of the position angles θ_1 and θ_2, the point of intersection in the yz plane of the two

light rays must trace out a circle in the yz plane that passes through the two reflecting slats at θ_1 and θ_2. Futhermore, if the two slats at θ_1 and θ_2 are angled at $\theta_{1/4}$ and $\theta_{2/4}$ with respect to the xy plane, then for incident rays of light whose projections in the yz plane are parallel to the z axis, the point of intersection of the two projections in the yz plane, of the reflected rays off slats at θ_1 and θ_2, will be where the z axis crossed the reference circle.

If $\alpha = 0$ for several parallel rays of incident sunlight which all lie in yz plane, for very thin reflecting slats, the focal spot of the reflected rays will be a point on the reference circle in the yz plane. Given a single reflecting element as shown in Figure 6, situated at $x = 0$ on the fixed mirror concentrator, the following is true. If parallel rays of light that have $\alpha \neq 0$ (they do not lie in the yz plane) strike the thin slats on the reflecting element at $x = 0$, they will be reflected up and pass through line F on the reference cylinder. The reflected rays $\bar{s}'_{||}(\theta) + \bar{s}'_{\perp}$ will however, not pass through line F at the same points on the reference cylinder surface.

From Equations (3), (4), and (5) it can be seen that from any number of different reflecting slats, the reflected ray components $\bar{s}'_{||}$, coming off the slats will have the same length and direction. From Equation (7) it can be seen that the reflected ray components $\bar{s}'_{\perp}$ will have the same length but <u>different</u> directions. The result is that reflected light rays cut the focal line F on the reference cylinder at different places because the path length to line F in the yz plane is different from each reflecting slat in one reflecting element. This is shown in Figure 9.

The rays with the longest path length in the yz plane to line F, will intersect line F at the furthest horizontal distance from the point of reflection. As a result, the rays from each reflecting element are spread into a fan that cuts the focal line F in several places. (Figure 9) The resultant focused image on line F is then a superposition of all the reflected rays from the stack of reflecting elements that make up the concentrator.

As can be seen in Figure 9(b), for a very long, perfect concentrator, the amount of light being reflected to any point on line F should be constant except at the two ends of line F, where the end effects will be important. The end effects are caused by the superposition of ray fans which starts off gradually, builds to a constant overlapping of reflected rays, and then gradually tapers off. On an actual fixed mirror concentrator where the reflected rays are focused at a heat collecting tube kept on the focal line F (Figure 9), all or only part of the incident light rays might actually hit the heat collecting tube. This of course, would depend on the length of the concentrator and heat collecting tube, and the projected angle (ϕ_x) which the incident light rays make in the xz plane. As seen in Figure 9(b), section A on line F would receive no reflected light. Light rays from section B would also not hit line F which stops at point C. The above end effects would affect the positioning of an actual fixed mirror concentrator to obtain optimum performance. Generally, short fixed mirror concentrators should be oriented with their x axis running north and south to reduce the end effects as much as possible. Long fixed mirror concentrators in which the end effects play a relatively

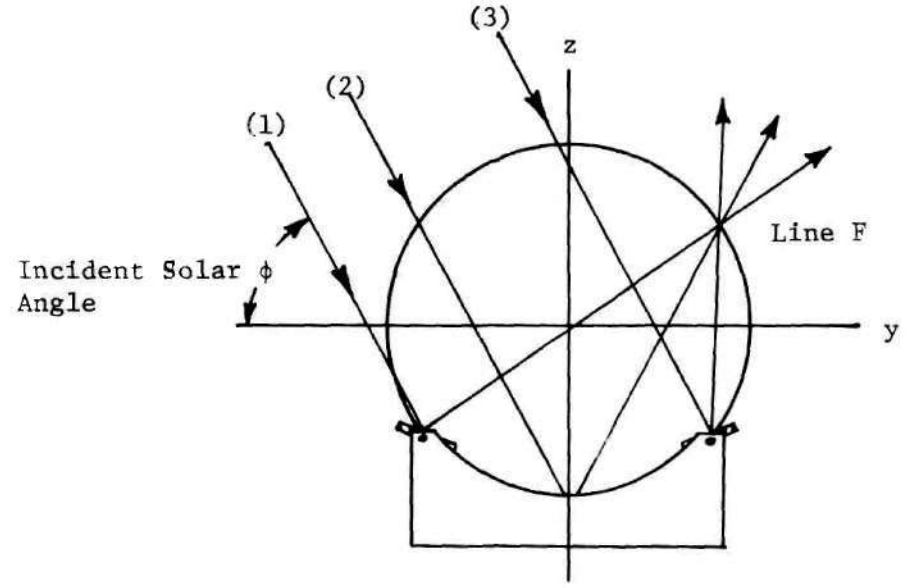

(a) yz Projection

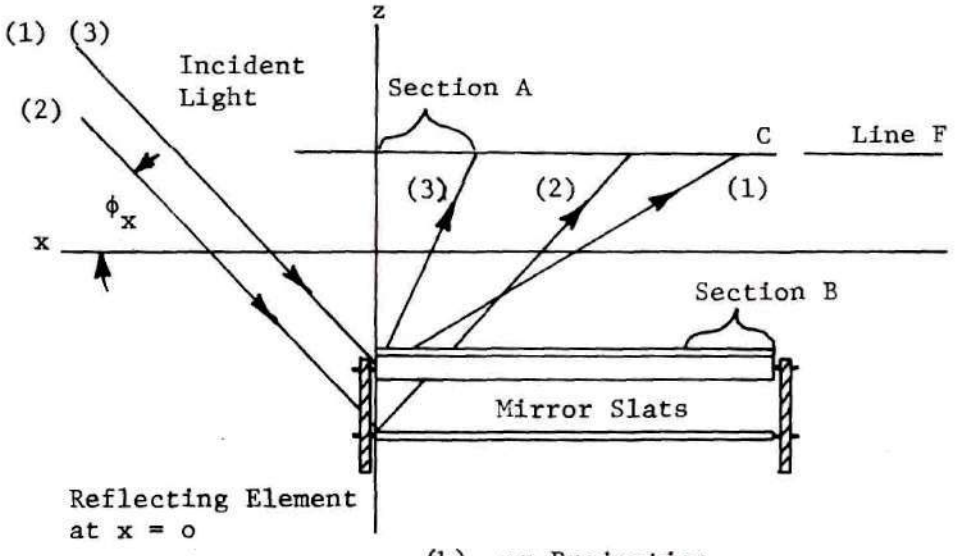

(b) xz Projection

Figure 9. Reflecting Path Lengths

smaller roll when compared to edge losses should be oriented east and west to reduce these edge losses which will be discussed next [17]. A long concentrator is one whose length along its x axis is many times the diameter of its reference cylinder. A short concentrator is one whose length and reference cylinder diameter are approximately the same.

Edge Losses

The analyses that follows will not take into account the end effects as described above. It will only concern that section of a long, perfect fixed mirror concentrator where the reflected fans are in the constantly overlapping stage. As a result the analysis which follows will be done two dimensionally in the yz plane.

Figure 10 shows the labeling of the geometry associated with any fixed mirror concentrator [17]. As it can be seen, a fixed mirror concentrator need not be symmetrical in any way and, in fact, probably would not be to provide optimum performance for a given location. The center line C_L, bisects the aperture angle θ_{in} into two equal parts. The center line C_L, may be set at an angle Δ to the vertical z axis. The tangent slat TS, or the single slat on the FMC which is tangent to the reference circle is set at an angle θ_{TS} from the center line C_L.

The particular FMC designed, constructed and evaluated in this thesis will be symmetrical with $\Delta = 0$ degrees; $\theta_{TS} = 0$ degrees; and $\theta_{in} \approx 90$ degrees.

The surface of a fixed mirror concentrator is not smooth. It consists of reflecting slats placed on step like terraces which are connected by vertical edges. Figure 11(a) shows the projection of

incident light in the yz plane on two mirror slats. Lines (ac) and (de) are two adjacent mirror slats. Line (cd) is the vertical edge between them. The light which is incident on the concentrator but not reflected up to the heat collecting tube is represented by incoming light sections B and C in Figure 11(a). These sections of light are known as the edge loss.

Sections of light A, B, and C falling on slat section (ab), slat section (bc), and edge (cd) respectively, are incident on the slat and edge as shown in Figure 11(a), on all mirror slats to one side of the tangent slat and including the tangent slat. The light in section B is reflected into the edge (cd) and lost. The light in section C hits edge (cd) directly and is also lost. Note, Figure 11(b) shows how the mirror slats on the other side of the tangent slat suffer no edge losses since all the incident light is reflected by some mirror slat even though portions of many mirror slats will be in the shadow of adjacent edges. As the sun changes position in the sky it will cross a plane set perpendicular to the tangent slat and along its axis. When this happens, the side of the FMC suffering the edge losses reverses to the opposite side. Summing these losses on an area basis over all the slats affected at a particular solar angle and dividing this by the total light incident on the concentrator, will give the total edge loss as a percentage of incident light. Russell [13] has done computer calculations, assuming parallel incoming light rays, to find the edge losses for various FMC configurations and solar angles. These edge losses range from approximately zero to 40% of the total incident solar energy for solar angles of 0 degrees to 140 degrees as measured from the

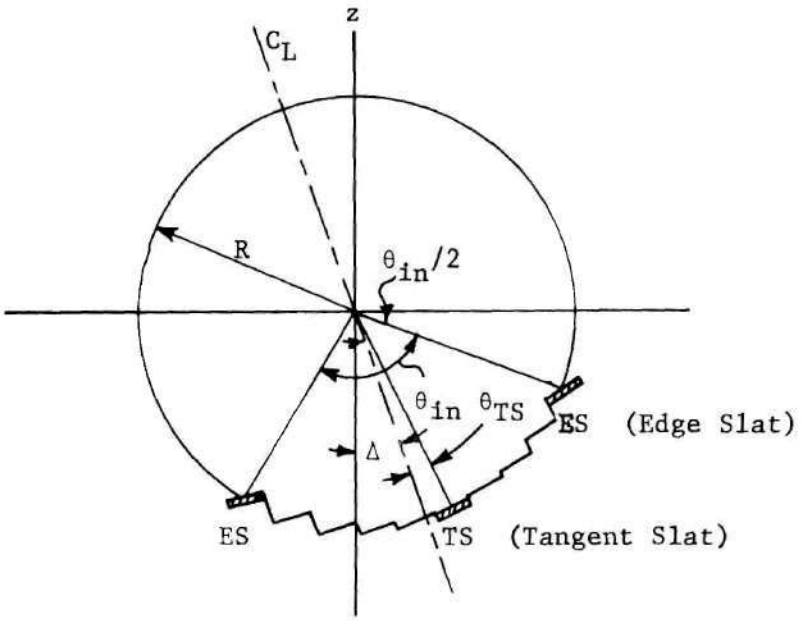

Figure 10. Labeling of Geometry of a FMC

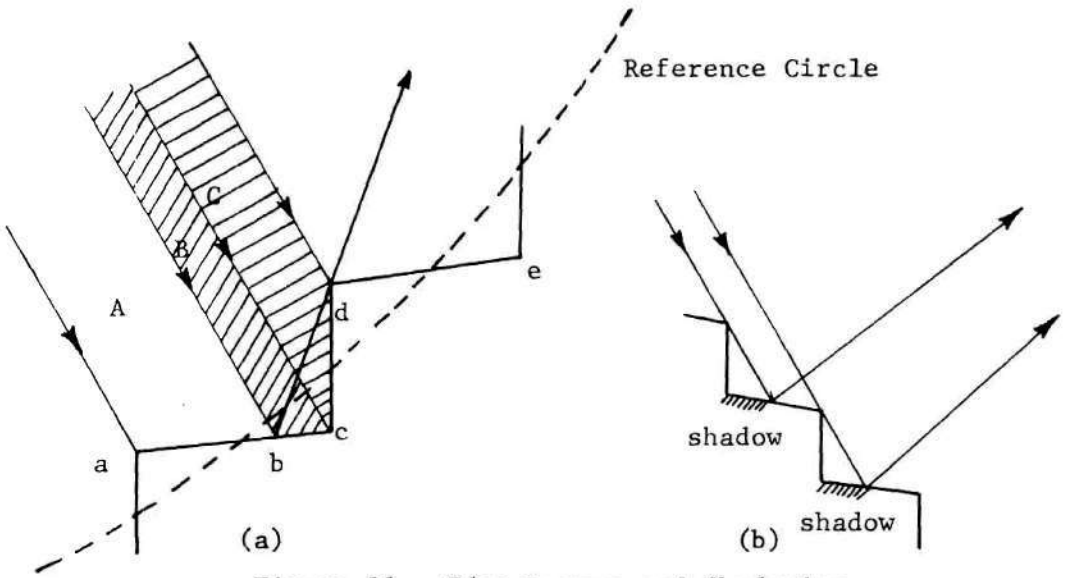

Figure 11. Edge Losses and Shadowing

eastern horizon. This is for a fixed mirror concentrator with its x axis pointed north or south.

CHAPTER III

DESIGN AND CONSTRUCTION OF THE FIXED MIRROR CONCENTRATOR

Choice of the Reflecting Surface

A collector greater than 50 square feet was chosen to provide a workable concentrator that would lend itself to experimental use. The subtended angle was chosen to be 90 degrees.

The reflecting surfaces were chosen from four different surfaces which were examined:

1. 1/4 inch thick polished plate glass rear surfaced mirrors weight - .0208 lb/in^2
2. 1/8 inch thick window glass rear surfaced mirrors weight - .0113 lb/in^2
3. Front surfaced mirrors
4. Aluminized mylar

The ideal reflecting surface should have high reflectivity, good weathering properties, and reasonable cost. It should be free of surface distortions so that a good, sharp reflected image of the sun is formed. Finally, it should be easy to work with, requiring no special construction techniques. Front surfaced mirrors were eliminated due to their high cost and poor weathering ability. Aluminized mylar was not chosen because it would have to be bonded to some type of frame to construct each reflecting slat. It was thought that great difficulty would arise in obtaining a relatively undistorted image from such a system. Such a mylar covered frame would, however, be lighter in

weight, contributing to an overall reduction in the weight of the supporting concentrator frame. Thus the choice remained between the window glass and plate glass mirrors.

Both rear surfaced plate glass and window glass mirrors possess good weathering properties. Plate glass mirrors weigh approximately twice as much as window glass mirrors and the cost of plate glass mirrors cut into strips for a fixed mirror concentrator is approximately one third greater than window glass mirrors. The reflectivity for both is good, being between 80% and 90% [15]. The reflectivity of the rear surfaced plate glass mirror is, overall, probably 1% or 2% less than the rear surfaced window glass mirror due to the absorption of light by iron compounds in the glass [3] which is twice as thick as the window glass. These iron compounds give the glass a greenish tint when viewed on edge.

Visual observation of the image reflected off a single plate glass mirror slat showed a clear, sharp image with very few distortions, (hot or dark areas within the image). Visual observations of the image reflected off a window glass mirror slat showed a slightly distorted image with numerous light and dark areas. The image was, however, well defined. This fact, along with the greater cost and weight of the plate glass mirrors led to the choice of rear surfaced window glass mirrors as the reflecting surface. A slat width of four inches was chosen.

Design of the Framework

Two basic framework designs were evaluated with respect to

their cost, the availability of needed materials, and the time needed for construction. The first was an all wood frame consisting of a rectangular bottom support to be constructed of 2 inch x 6 inch lumber. Sheets of plywood were to be mounted on both ends and in the middle of the bottom support, and at right angles to it. A terraced quarter circle was to be cut in each plywood sheet. The reflecting mirrors were to be bonded to aluminum channels and set inside the cut plywood, on the terraced steps to form the concentrating surface. Screws going through the aluminum channel and into the terraced steps of the plywood sheet, along with small springs, were to be used to adjust each reflecting slat angle. A welded frame of steel tubing would rotate the heat collecting pipe or instrument package over the concentrator. The total cost for this framework was calculated to be $687.00 (1974) with all the materials easily available. The two major drawbacks of this design were the construction time and general difficulty in working with wood to obtain good framework alignment.

The second framework examined, and subsequently used, consisted of aluminum pipe joined together using slip-on fittings with set screws. Two pieces of 3/4 inch plywood were mounted on each end of the aluminum frame. The mirror sections were bonded to aluminum channels. These were then mounted between the two plywood pieces with bolts that went through the plywood and into a fitting, which slipped into each end of the aluminum channels. The holes were drilled along the required circular path in each plywood end piece so that when the aluminum channels were mounted they could be tilted to form the correct concentrating surface. The heat absorbing pipe and instrument

support were an integral part of the aluminum frame, being made of the same aluminum pipe and fittings. The aluminum pipe size of 1.5 inch I.P.S. diameter was chosen to be compatable with the available slip-on fittings which would easily handle the structural load. The aluminum 6061-T6 alloy pipe was chosen because it has medium strength and good corrosion resistance. It was also relatively economical when compared to other alloys and treatments. Total projected cost of the concentrator materials with an aluminum frame was $900 (1974).

Although the aluminum framework cost more, it did have several advantages over the wooden framework. First, it had superior weathering properties and construction was easier and faster. Second, the design is light weight when compared with wood, and this facilitates moving the concentrator from one location to another. It also makes the design of the tilting mechanism and the actual tilting of the concentrator to obtain desired experimental positions much easier. For these reasons the aluminum framework was chosen over the wooden one.

Design and Construction of the Mirror Slats

In mounting the mirrors on the aluminum channels several problems had to be overcome. Ideally, each reflecting slat would be perfectly flat, free of distortion, and mounted at a correct, constant angle. The actual mounting method used (see Figure 12) attempted to accomplish this with materials that were available at a reasonable cost. The aluminum channel was used to provide a flat supporting structure on which the reflecting mirrors would rest. Because of the

method of suspending the aluminum channel between the two plywood end pieces, a slight downward deflection in the middle of the beam was unavoidable. In addition, the beam had to resist any twisting force applied through uneven curing of the glue that bonded the mirror sections to the channel or that occured when the wing nuts were tightened to lock the mirror slat (aluminum channel with two mirror sections) into the correct position.

A good light weight section which would reduce to a minimum the midspan deflection, resist applied torque, and facilitate mounting with the end bolt method would be a rectangular, hollow, extruded aluminum beam. Unfortunately, at the time of construction it was not available from aluminum suppliers contacted. A second choice was a deep aluminum channel. Suppliers were contacted and the choice was narrowed down to the two best channels available at a reasonable cost, which would perform the desired function. These were 1/8 inch x 1 inch deep x 3 inches wide and 1/8 inch x 2 inches deep x 3 inches wide channels of architectural grade aluminum. The two channels were examined for maximum midspan deflection with the given window glass mirror loading [16]. Maximum deflections were calculated to be 0.1104 inches and 0.0155 inches for the one inch and two inch deep channel respectively. The two inch channel was, however, approximately one third more expensive, and for this reason, the 1/8 inch x 1 inch deep x 3 inches wide channel was chosen for the design. With a perfect reflecting surface this midspan sag would cause the focus of the concentrator to be slightly intensified in the central portion of the heat collecting pipe, and reduced at the edges. This did not appear to present a

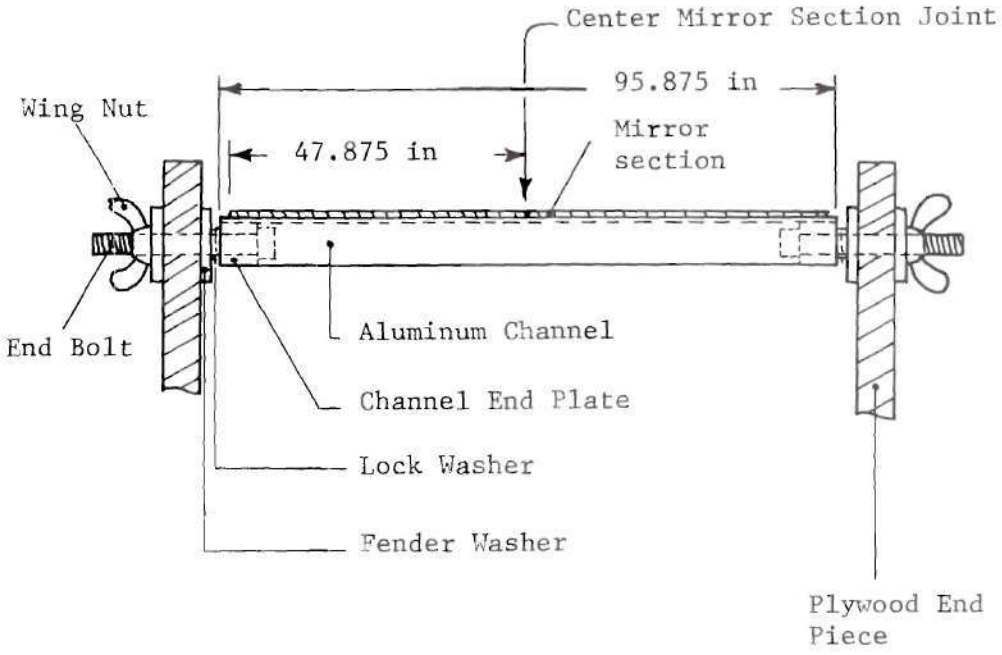

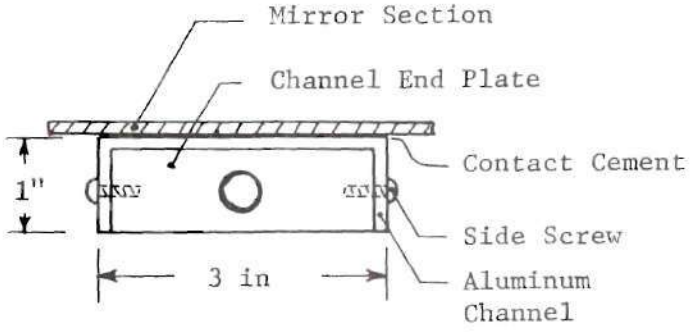

Figure 12. Mirror Slat Construction and Mounting Between Two Plywood End Pieces

significant problem.

The aluminum channels were delivered in 16 foot lengths. After cutting in two sections and allowing for mirror cutting errors, a slat length of 7 feet 11 and 7/8 inches and a mirror section with dimensions of 4 inches wide x 47 inches long was arrived at. Two mirror sections were bonded to each aluminum channel since one section of the required length was impossible to obtain. The channels and channel end plates were cut, bored, threaded, and readied for assembly.

In assembling the individual mirror slats one problem arose. Since each mirror slat was composed of an aluminum channel and two separate mirror sections, it was necessary that each of the two mirror sections be bonded to the channel at the same angle. The junction in the center of the aluminum channel where the two mirror sections touched should be perfectly aligned, otherwise there would be a discontinuity in the slat's reflected image. To eliminate this problem the following method was used to bond the mirror sections to the aluminum channels.

The mirror sections and aluminum channel were given a thin coat of contact cement. The mirror sections were carefully placed upside down on a large lathe bed and aligned end to end. In this way the two mirror sections assumed the same, flat, even position from one end, through the junction between the two, to the other end. The mirror sections were carefully clamped in this position. Next, the aluminum channel, in an upside down position, was carefully laid on the two mirror sections and instantly bonded by the contact cement. The procedure was repeated for the 23 mirror slats which were then set

aside for the contact cement to completely dry. As a final check, a test was conducted to determine the actual angular misalignment at the junction of the two mirror sections.

Mirror Slat Alignment Test

Each individual, completed mirror slat was laid out horizontally. An argon laser beam was directed at the center of the junction between the two mirror sections. The circular light beam was reflected off the junction onto a wall a known distance away. The reflected image for a perfectly aligned mirror slat is shown in Figure 13(a). The image reflected off a mirror slat which is slightly misaligned is shown in Figure 13(b).

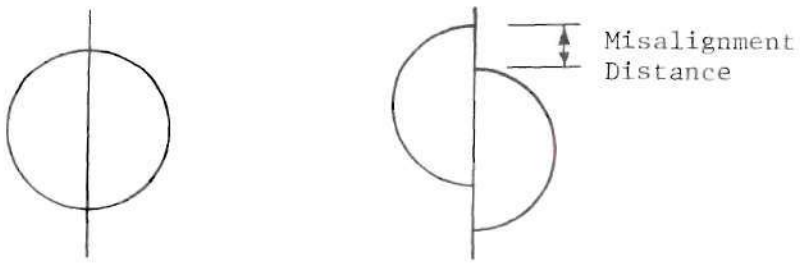

(a) Perfect Alignment (b) Misalignment

Figure 13. Slat Alignment Test Images

By measuring the position up the wall of the reflected image and the misalignment distance, the angular difference between the two mirror sections was calculated. For the 23 mirror slats that were mounted on the concentrator the average misalignment between each of two mirror sections on each slat was 0.0191 degrees. The maximum misalignment was 0.0613 degrees, and the minimum, zero degrees.

Design of Plywood End Pieces

Exterior grade 3/4 inch A-A plywood was chosen for the two end pieces instead of another material of stronger, more ideal properties, purely for economical reasons. The method used to lay out the position of the holes in the plywood where the end bolts would be located, is as follows. Figure 14 shows the labeling of the geometry used.

Initially, the slat width W, and θ_{in} = 90 degrees are given. The value, θ_{in} extends between the outer edges of the outside mirror slats as shown in Figure 14(a). It was desired to obtain a concentrator of at least 50 square feet with the approximate dimensions of eight feet x eight feet. The problem then, was to determine the radius of the reference circle (R) which would let the width of the concentrator (W_c) be approximately seven to eight feet and allow an exact number of mirror slats of width (W = four inches) to be located within θ_{in} = 90 degrees. (Figure 14(a)) The process was one of trial and error.

In Figure 14(b), edge (AB) is perpendicular to the tangent slat which in the case of this particular concentrator is located on the

center line C_L. A first value for the radius of the reference circle (R) was chosen. Next, starting at the tangent slat (θ_1 = 0 degrees) a first value of θ_2, the position along the reference circle of the next adjacent mirror slat was chosen. Looking at Figure 14(b),

$$L_1 + L_2 = \frac{W}{2}\left(\cos\ \theta 1/4 + \cos\ \theta 2/4\right) \tag{1}$$

Now, looking at Figure 14(c) it can be seen that

$$L_3 = 2R \sin\left(\frac{\theta_2 - \theta_1}{2}\right) \cos\left(\frac{\theta_1 + \theta_2}{2}\right) \tag{2}$$

It is obvious that $L_3 = L_1 + L_2$. So when

$$\frac{W}{2}\left(\cos\ \theta 1/4 + \cos\ \theta 2/4\right) = 2R \sin\left(\frac{\theta_2 - \theta_1}{2}\right) \cos\left(\frac{\theta_1 - \theta_2}{2}\right) \tag{3}$$

is satisfied by the proper choice of θ_2, that value of θ_2 is the correct one for the given radius R. Knowing the correct value for θ_2, the correct values for θ_3 and so on, were determined.

One special mirror slat case should now be noted. Since the mirror slats have a thickness of 1/8 inch, and the angular difference between the tangent slat and the next adjacent slat $\left(\theta 2/4 - \theta 1/4\right)$ is less than one degree, theoretically, the two edges of the tangent slat should touch the edges of the slats on either side of it. Now, the accuracy of cutting window glass mirror sections is usually on the order of ±0.125 inches. To allow for this, the width used in the tangent slat calculations was set at 4.25 inches. This would leave a gap of 0.125 inches on either side of the tangent slat to allow for

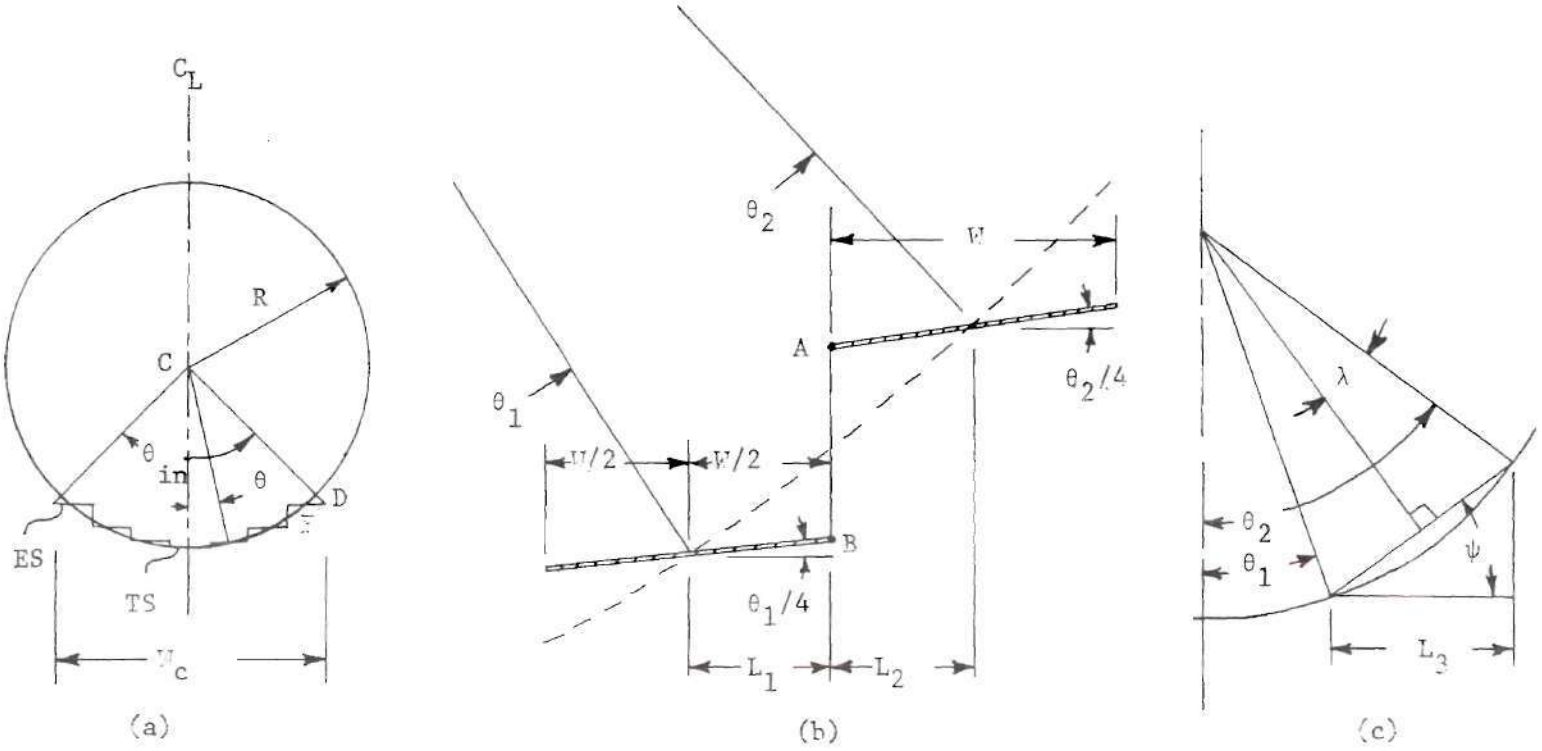

Figure 14. Labeling of Geometry Used in Design of Plywood End Pieces

the mirror cutting irregularities. All other slat widths were taken to be four inches, since any oversize irregularity of a given mirror slat would simply extend under or over the two adjacent slats.

Once the final value of θ for the outside mirror slat was determined, the value of θ_{in} for the concentrator with the given radius R, slat width W, and width W_c could easily be determined by examining triangle CDF in Figure 14(a). If the calculated value of θ_{in} equaled 90 degrees the correct radius had been assumed. If not, another radius (R) was chosen and the process repeated until the correct value of R was determined.

The above calculations were carried out to an accuracy of two decimal places in determining the θ values. The final reference circle radius determined was R = 63.92 inches. The length of an arc of this radius and 0.01 degrees wide is approximately 0.011 inches long. For use in laying out the end bolt holes in a piece of plywood, an accuracy of ±0.01 inches is more than can be obtained in the actual cutting and boring.

As a final check the horizontal distance between the center of the tangent slat and the center of the outside edge slat was calculated using Equation (1) and summing the results from all the slats; and again, using Equation (2) with the values θ_{TS} and θ_{ES}. The difference in the two calculated lengths was less than 0.0042 inches. The results of these calculations are summarized below.

Final Concentrator Specifications

Radius of reference circle	R = 63.9167 inches
Width of mirror slats	W = 4 inches
Number of mirror slats	23 (11 on each side of tangent slat)
Aperture angle	θ_{in} = 90 degrees
Width of concentrator	W_c = 91.6965 inches

To locate the end bolt holes in the two plywood end pieces, a reference arc of radius R = 63.92 inches was first drawn. Knowing the calculated values of L_1 and L_2 for all the mirror slats, the positions along a horizontal line below the reference circle of each mirror slat was determined. A vertical line was then drawn to the reference circle to pinpoint the position of the center of each mirror slat on the reference circle. Since rear surfaced window glass mirrors were used, this position is defined as the center of the rear surface of the window glass mirrors where most of the reflection occurs. From this, knowing the value of $\theta/4$ and the design of the channel end plate, (Figure 12(b)) the location of the end bolt hole was marked on the plywood. One plywood end piece was marked, cut, and bored; and then used as a pattern for the other plywood end piece to assure good mirror slat alignment between the two.

Final Assembly

In the final assembly, the wheel bases and wheels were attached to the base of the concentrator. Next, the mirror slats were mounted on the concentrator. To do this the channel end plates were bolted on the plywood end pieces. Next, the completed mirror sections were laid on the channel end plates and side screws (See Figure 12 (b)) on

one end of the concentrator were screwed down tightly. The side screws on the other end of each mirror slat were screwed down, but left loose. Next, the pivot arms and cross pipe as shown in Figure 15 were fitted on the framework.

The final section to be added to the concentrator was the heat collecting tube. A cross section of this is shown in Figure 16. This heat collecting tube was designed for demonstration purpose only. Its main use was as a target to align the concentrator. This tube was constructed of four inch diameter aluminum stovepipe which was painted flat black. Wooden insulators were used to fasten the tube to the cross pipe and pivot arms. Finally, fiberglass insulation was wrapped around the upper portion and outlet sections of the tube. Figure 17 shows the mounted tube, without insulation, on the completed concentrator.

It should be noted that the main use of the heat collecting was an alignment tool. No attempt was made to design an efficient collecting device. The large, uninsulated area of flat black surface on this particular tube undoubtedly contributed to massive convective and radiative losses in actual operation. As a point of interest though, with an atmospheric wind velocity of about three MPH, an outside air temperature of 70° F, and an air flow rate inside the heat collecting tube of approximately 21 ft^3/min, an exit air temperature of 214° F was obtained on a clear day. These measurements were made with a turbine type wind anamometer and a mercury thermometer held inside the exit end of the heat collecting tube.

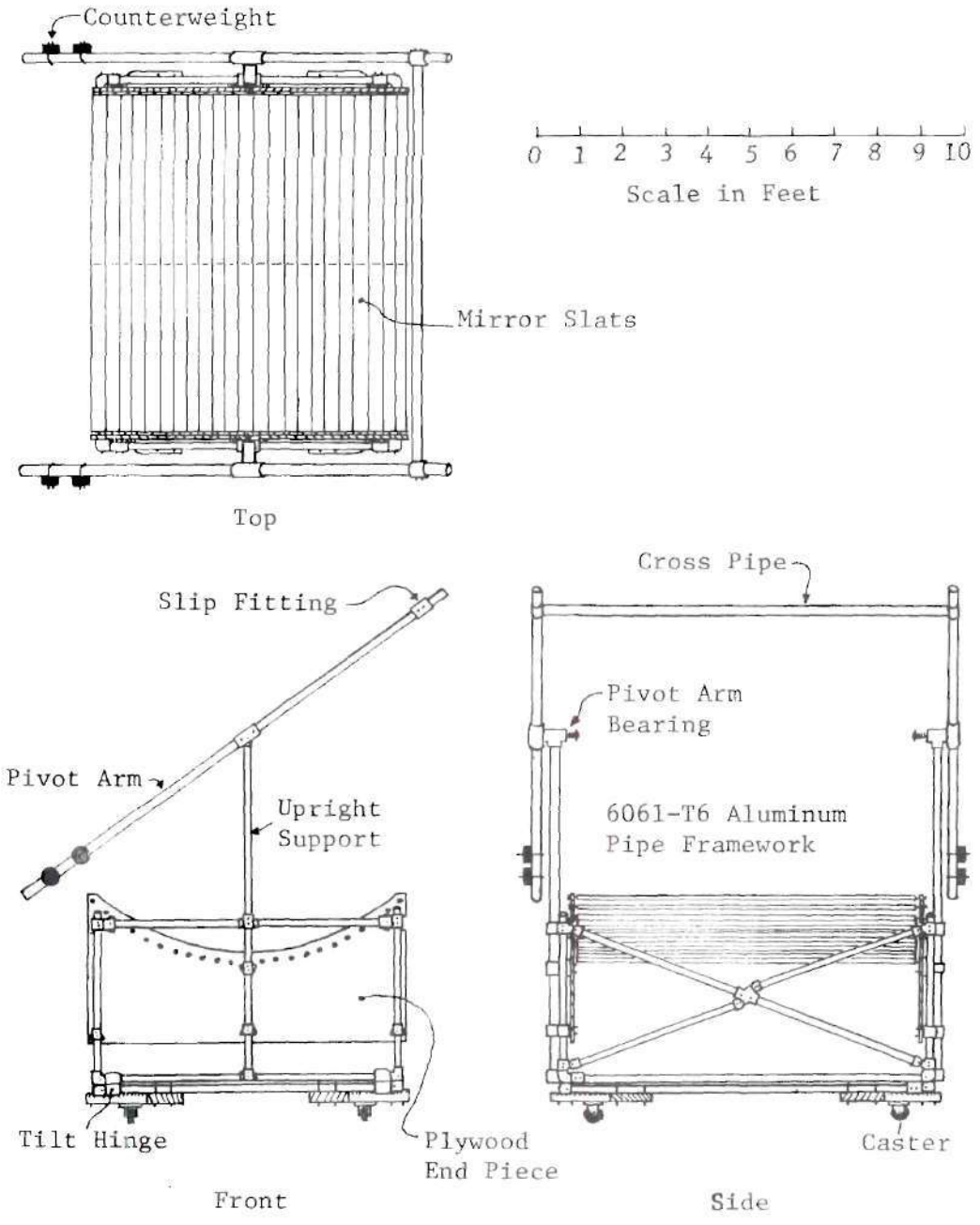

Figure 15. General Views of Concentrator

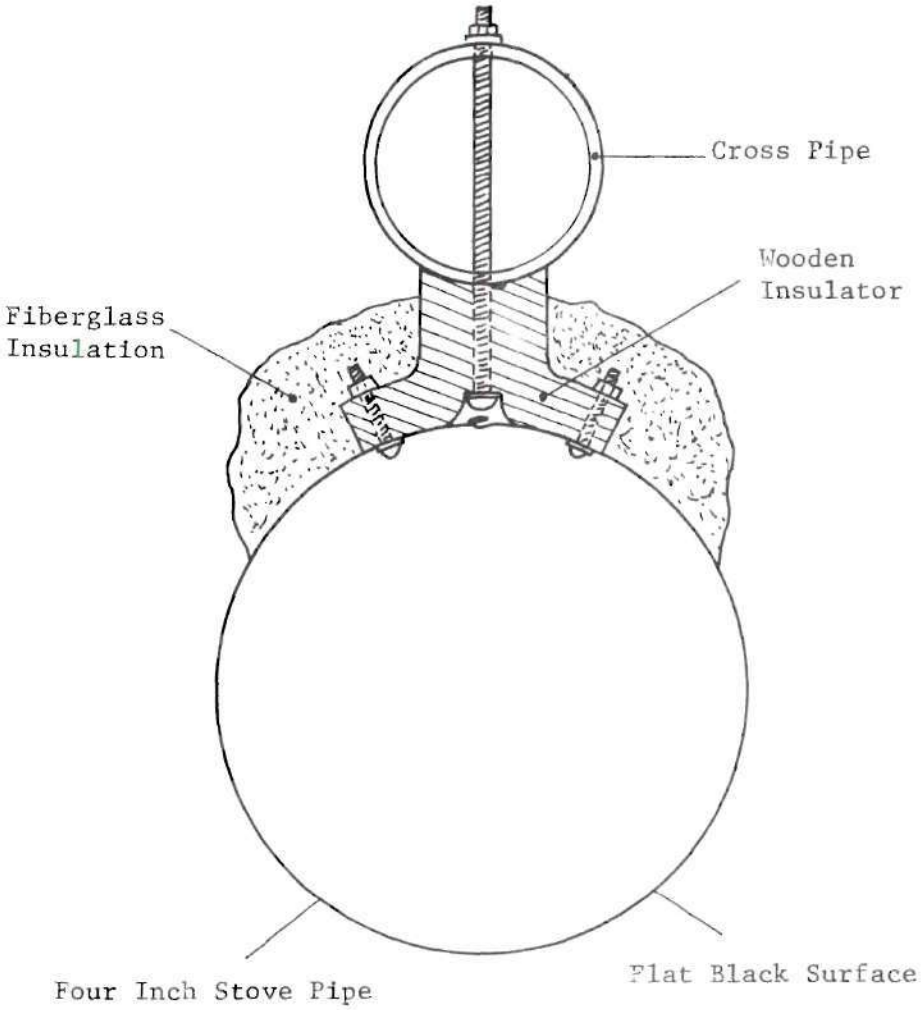

Figure 16. Cross Section of Heat Collecting Tube

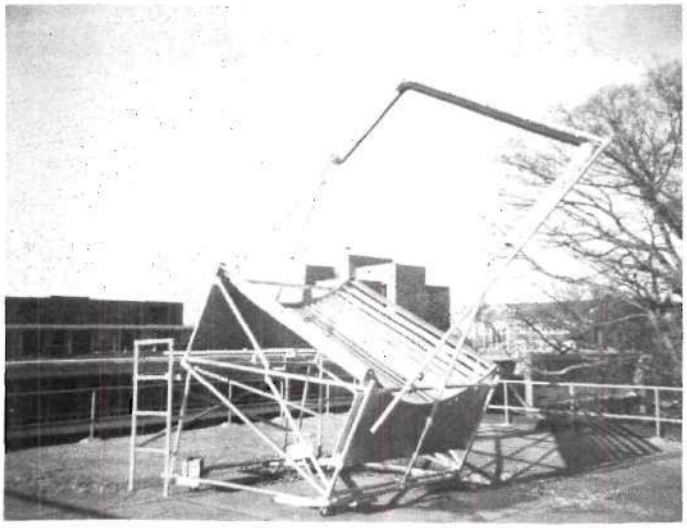

Front

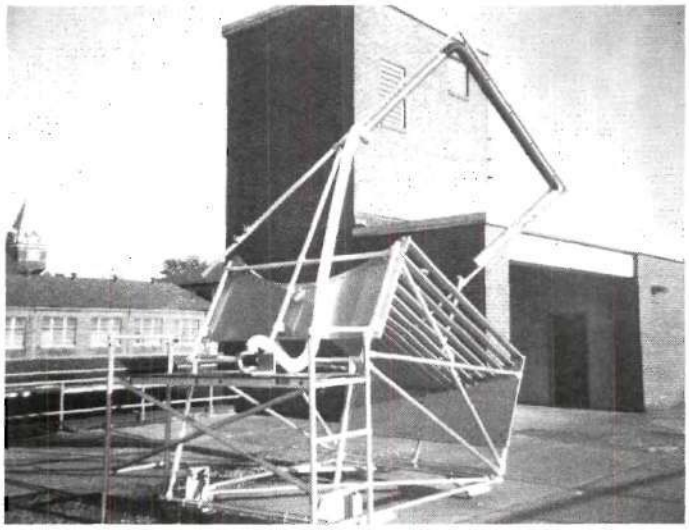

Rear

Figure 17. Mounted Heat Collecting Tube on Completed Concentrator

Laser Alignment Technique

As discussed previously, parallel light which is incident in a direction perpendicular to the tangent slat or parallel with the center line C_L, when viewed in the yz plane, will be reflected to the heat collecting tube when the pivot arm is in its vertical position as shown in Figure 18. The procedure followed during alignment was very simple. A vertical light beam from a laser was aimed down at each mirror slat. The slat was tilted until the light beam was centered on the heat collecting tube, and then the slat's end bolts were tightened by turning the wing nuts thus locking the mirror slat in position.

An argon laser and reflecting mirror apparatus was built as shown in Figure 19. The argon laser directs a parallel beam of light at a front surfaced mirror as shown. The mirror was mounted on an adjustable mount which rotates about the mirror pivot axis. A plumb line was mounted a short distance away from the mirror. The mirror pivot axis and the laser beam intersect on the front reflecting surface of the mirror. By rotating the mirror to a 45 degree angle, the incoming laser beam is directed vertically downward. The plumb line is mounted two inches away (measured in the x direction) from the center of the vertically reflected laser beam. When the plumb and the center of the reflected laser image line up two inches away from each other (again measured in the x direction) on the floor directly below the alignment mirror, it can be said that the reflected laser beam is traveling downward parallel with the z axis and hits the floor which is parallel to the xy plane, at a 90 degree angle (measured from reflected laser beam to xy plane).

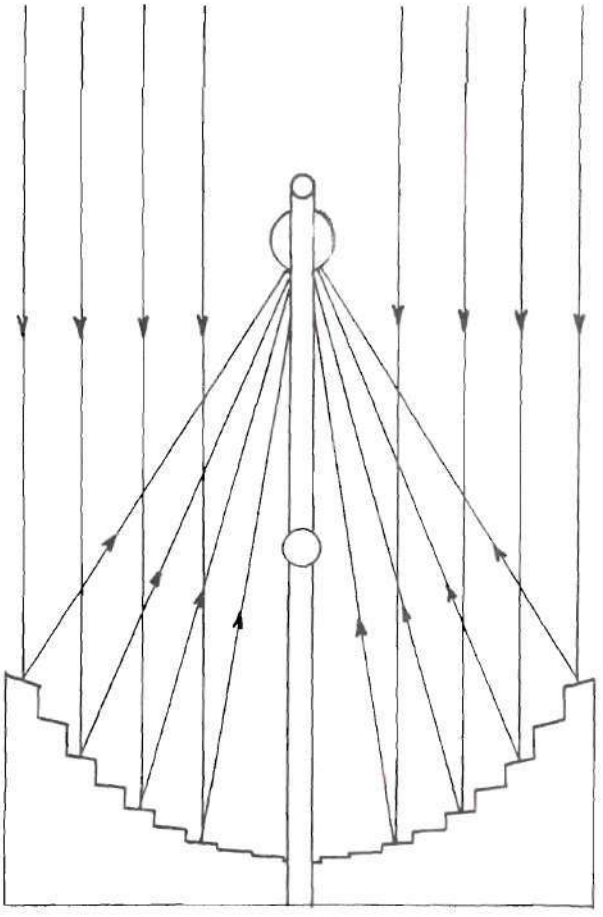

Figure 18. Light Reflected to Heat Collecting Tube

Now, a straight line (path A) is drawn below the laser, parallel to the x axis and passing through the reflected laser beam image and plumb line. By adjusting the adjustable mirror mount and position of the mirror pivot axis, it is possible to make the reflected laser image follow exactly path A. The laser image following a path similar to paths B or C would indicate an incorrect adjustment in either the mirror pivot axis or adjustable mirror mount. When the mirror is slowly rotated about its axis and the laser image stays on path A which is centered under the plumb line, it can be said that the reflected laser beam sweeps through an arc that stays in the xz plane, which is perpendicular to the yz plane. A person looking toward the yz plane at this reflected beam as it sweeps in the xz plane would only see a line perpendicular to the horizontal xy plane.

The entire apparatus (laser, mirror, and plumb line) was placed on a movable overhead crane platform which was positioned over the concentrator as shown in Figure 20. The overhead crane could be moved in the y direction. The concentrator was positioned so that the plumb line from the alignment apparatus hung directly over the center mirror section joint of each slat as it was slowly moved in the y direction (see Figure 12) across the width of the concentrator. The concentrator was then leveled paralled to the horizontal xy plane and the pivot arms placed in an upright position parallel to the z axis. In this way, by slowly moving the overhead crane, the plumb line and reflected laser beam could be positioned over the center of the width of each mirror slat. By rotating the given mirror slat about its end bolts it was positioned to reflect the vertical laser beam up to the heat collecting

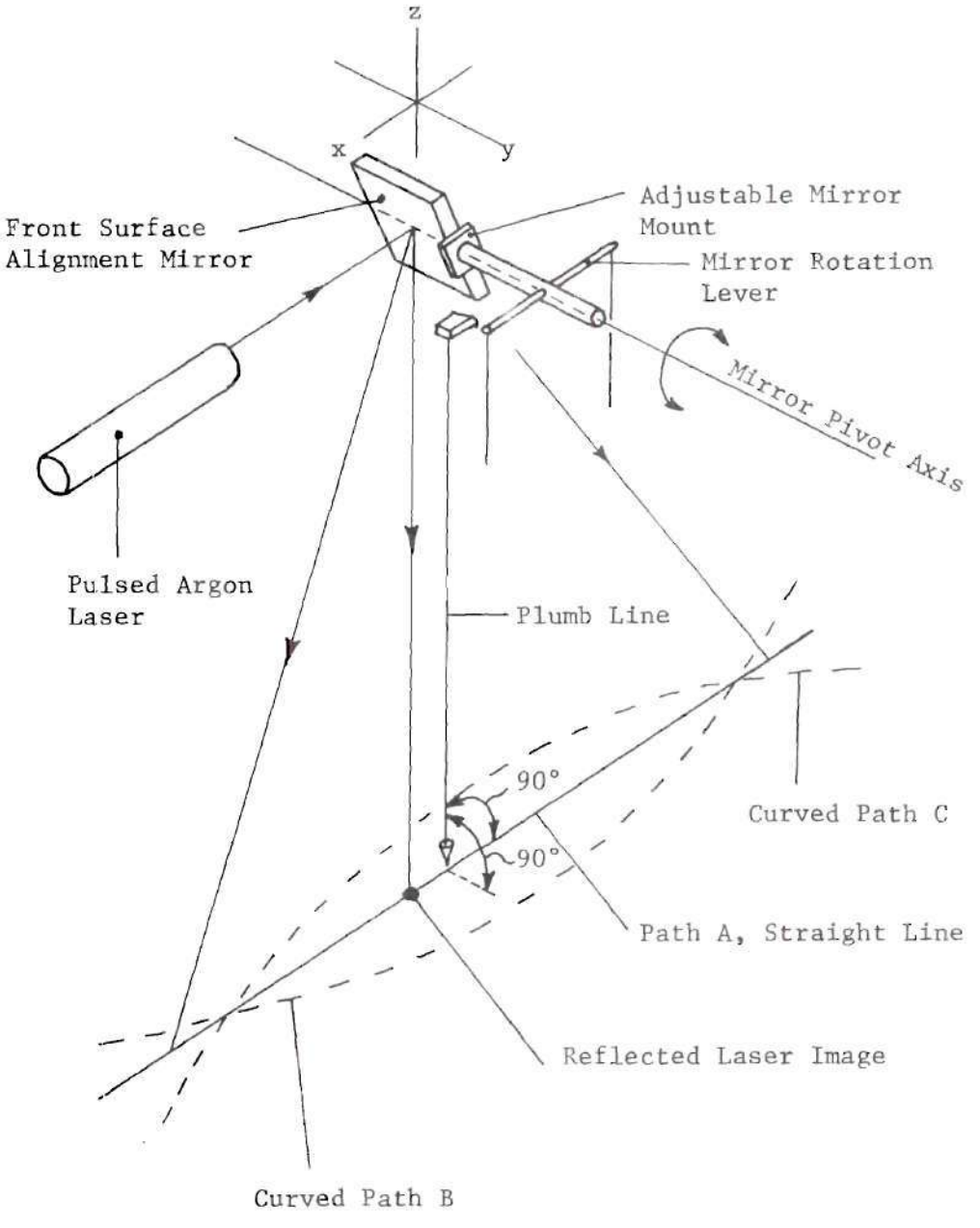

Figure 19. Laser Alignment Apparatus

tube. By rotating the alignment apparatus reflecting mirror, the laser beam scanned longitudinally along the given mirror slat and insured that the entire slat was correctly positioned. Once this was done, the two wing nuts of the given mirror slat were tightened, locking the slat in position. The two remaining side screws on the slat were then lightly tightened and the mirror slat scanned once again with the laser apparatus as a final check. If it was still aligned properly, the overhead crane was then moved to a position where the plumb line was centered over the next mirror slat and the alignment process repeated.

As another check, when the plumb line was centered over a slat, the laser beam should scan along a straight line from one end bolt through the plumb to the other end bolt (straight line path A). If it did not, then either the adjustable mirror mount or mirror pivot axis was out of adjustment. This problem never arose, but it did provide a constant check on the accuracy of the alignment apparatus.

A special case was the alignment of the tangent slat. Due to its position on the reference circle, incoming vertical light does not reach the tangent slat which is in the shadow of the heat collecting tube. In order to align the tangent slat the following method was used. The heat collecting tube was rotated so that the pivot arms were parallel with the y axis, and the laser apparatus was then moved into position directly over the tangent slat. The vertical laser beam was then reflected off of the end portions of the tangent slat onto the top portion of the upright supports, on top of which the pivot arm bearings are mounted (see Figure 20). When the laser beam image was centered on the upright support, the tangent slat was aligned properly,

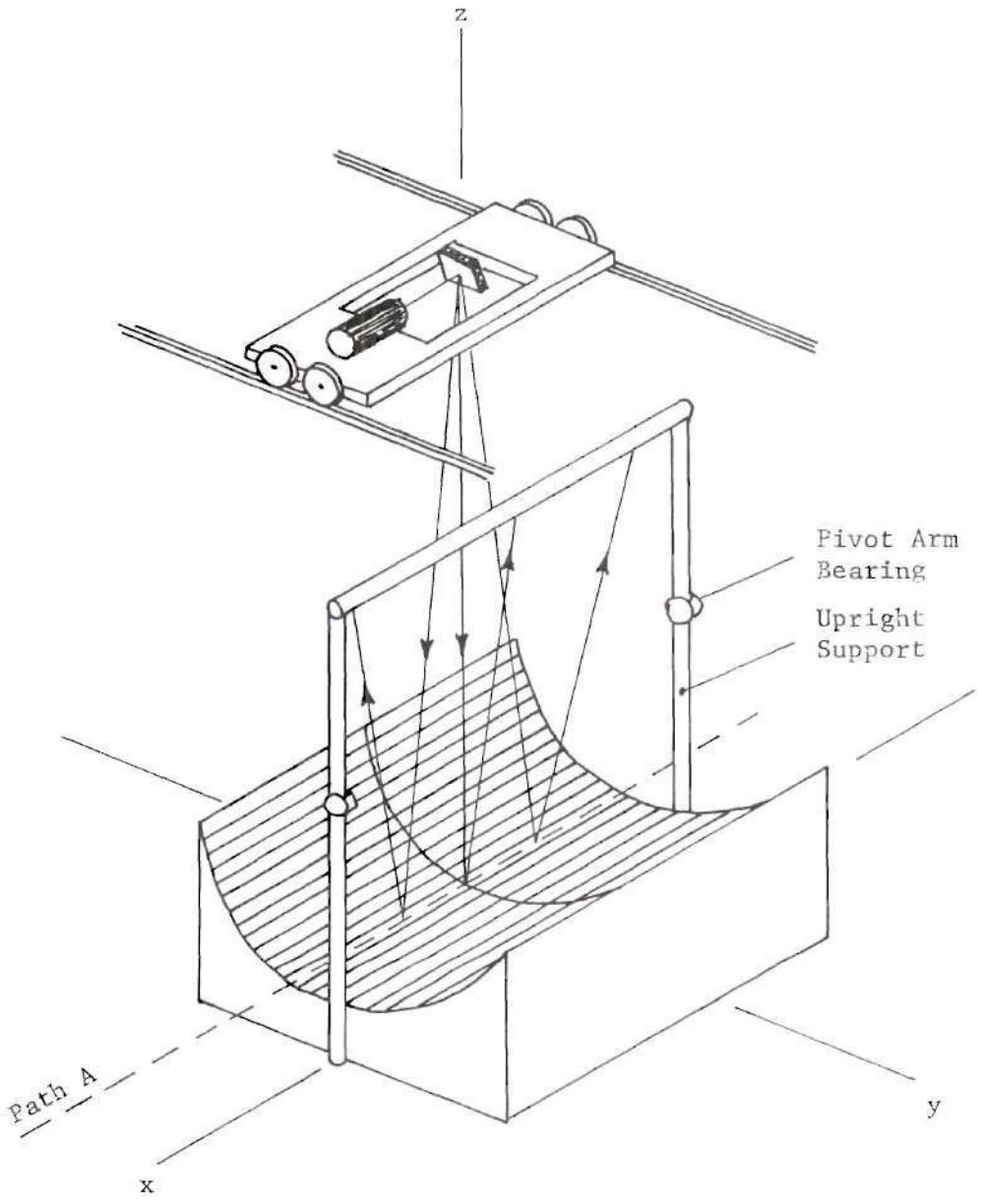

Figure 20. Alignment Apparatus Positioned Over Concentrator

perpendicular to the incoming laser light as viewed in the yz plane.

When the laser beam reflected off of a given mirror slat, the reflected image was then centered on the heat collecting tube. In effect, the center of each mirror slat was focused on a line exactly in the center of the heat collecting tube. This was surprisingly easy to do. As shown in Figure 21, when the mirror slat was correctly positioned, an image as shown in Figure 21(b) was produced. Any misalignment produced an image similar to Figure 21(a).

As a final note it was mentioned that the side screws of each mirror slat on one end of the concentrator were not tightened completely. This was to let each mirror slat slide on the channel end plate if the aluminum channels changed length due to thermal expansion or if the aluminum framework or plywood end pieces shifted or warped. Without this, the mirror slats might buckle slightly and shift out of focus. Figure 22 shows the completed concentrator.

New Alignment Technique

The original plan called for a concentrator which could be moved from position to position, on wheels, to set up any desired sun angle which was being tested. The surface that the concentrator was rolled over was very uneven, pitted, and full of small rocks. As a result, when the instruments were finally adjusted and it came time to begin the actual tests, it was determined by examining the focused image on the heat collecting tube that many of the mirror slats were no longer in good focus. Apparently the end-bolt, wing-nut locking mechanism did not produce sufficient force to keep the slats in position under

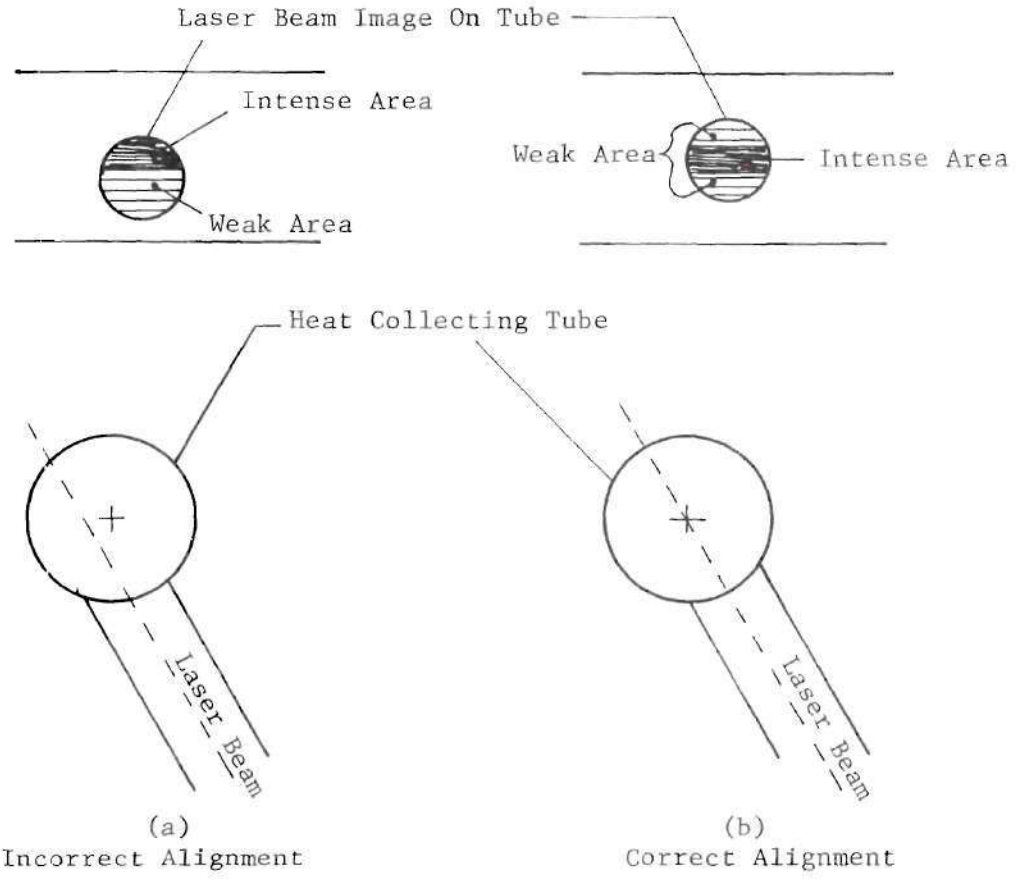

Figure 21. Position of Reflected Laser Image on Heat Collecting Tube

Front

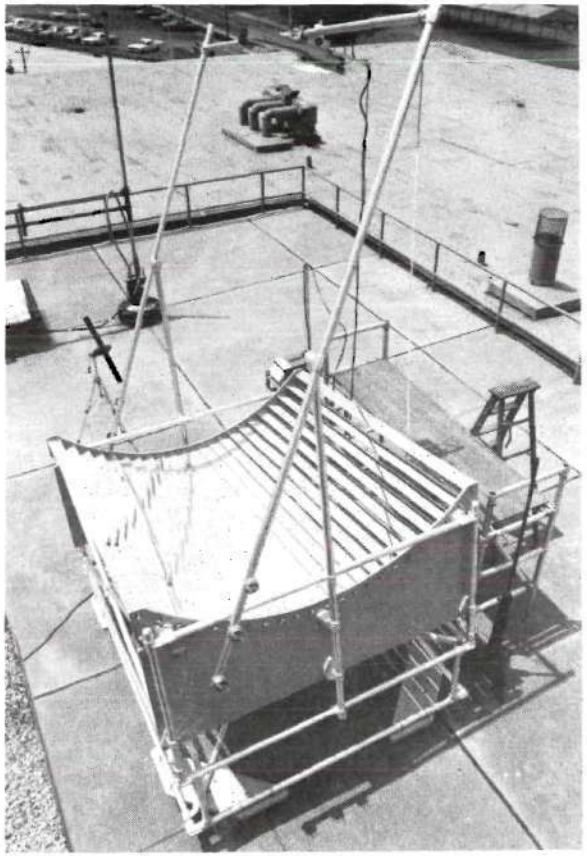

Rear

Figure 22. Completed Concentrator

the vibration caused by moving the concentrator over the uneven surface. In order to realign the mirror slats a new, faster technique was developed. It should be noted here, that given a flat target plate set at one angle to focus on, the width of each image reflected off of a given mirror slat will be different due to the various, different slat angles. Ideally, the center line along each mirror slat should be focused on a single line, whose point projection lies on the reference circle. If one tries to align the concentrator by simply superimposing the various slat images for one solar angle, there is a good probability that even though a sharp focused image is obtained, the center lines of each mirror slat will not be focused on the same line. As a result, the concentrator will be out of focus for other sun angles. The problem then, is to focus the center line of each slat on the same line whose point projection is on the reference circle.

To do this a focusing target consisting of sections of white cardboard with several parallel centering lines drawn on it was mounted on the cross pipe. Its projection in the yz plane is shown in Figure 23. Next, strips of paper one inch wide were taped down the center of the length of each mirror slat. Strips of paper four inches wide were then taped on top of each mirror slat and one inch paper strip, covering both completely. The pivot arms were placed in the vertical position. When the sun reached its solar noon position, the focusing target cast a shadow exactly on the tangent slat. At this time the four inch paper strips were removed from the two edge slats (ES in Figure 23), leaving the two slats, each with one inch paper strips down the center exposed to the sun. Their reflected images

were then centered on the focusing target. This was done by superimposing the two dark lines of each image formed by the one inch paper strips which did not reflect any light. The dark line within the two edge slat's reflected image was then centered on the focusing target.

Next one by one, each slat was focused by removing its four inch paper strip and centering the dark line within its reflected image on the dark line within the image of the two edge slats. The four inch paper strip was then replaced and the next slat refocused. The entire operation took about two hours. During this time the sun changed its solar angle. By simply keeping the focusing target centered on the darkline within the reflected image of the two edge slats, the realignment process continued. The tangent slat, formally in the target's shadow was aligned when the solar angle changed and the focusing target was moved off its original position.

No tests could be run to determine which method of concentrator alignment was the best, however visual observations of the focused image shortly after the initial laser alignment and observations of the image after realignment using the new technique, detected no difference.

After the realignment was completed, epoxy glue was put on the wing-nut end bolt assembly to further lock the mirror slats in position.

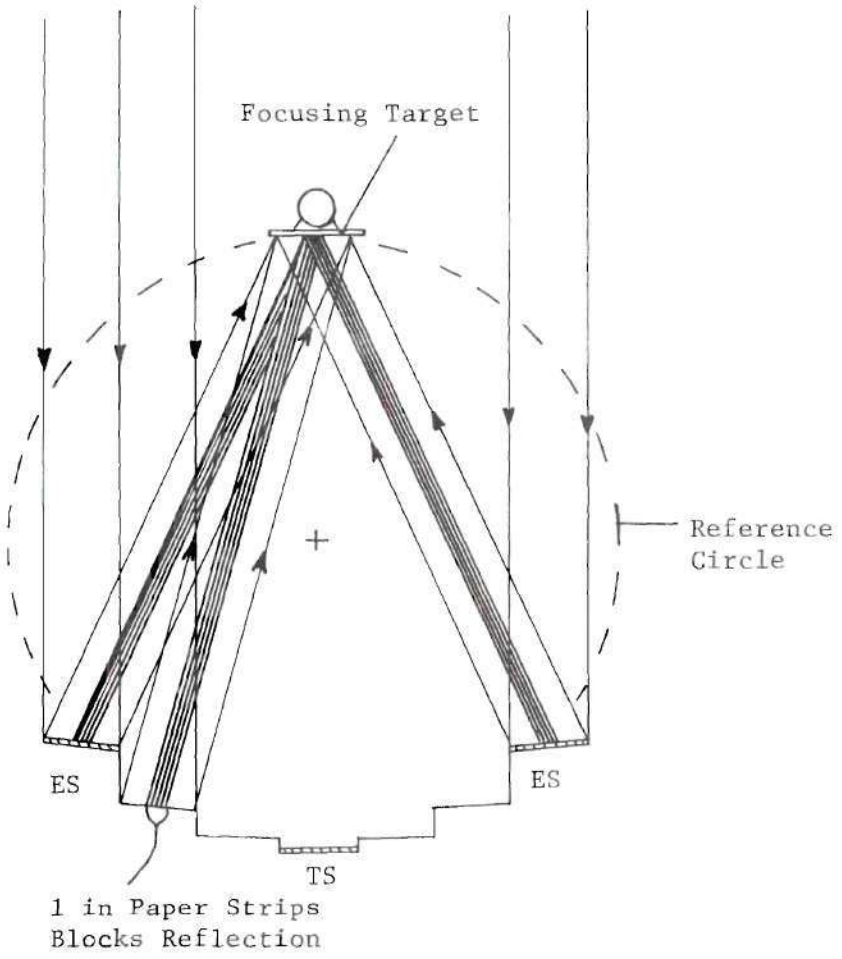

Figure 23. New Alignment Method

CHAPTER IV

THEORETICAL ANALYSIS

Heat Flux Profile at the Focal Plane

Background

The following analyses is carried out two dimensionally in the yz plane as discussed in the previous section. The following assumptions are made:

1. The reflecting mirror slats behave as front surface mirrors
2. Reflectivity, p is constant, independent of angle of incidence and wavelength
3. Perfect alignment as calculated in the design of the system
4. Specular reflection
5. Apparent angular diameter of sun is 32 minutes
6. Uniform radiation from sun's disk

Theoretically, if the sun were a point source, a fixed mirror concentrator with infinitely thin mirror slats would focus incident parallel light into an infinitely thin line on the reference cylinder. An actual fixed mirror concentrator, of course, has mirror slats which are not infinitely thin. The sun also has an apparent angular diameter of 32 minutes. Because of these two facts, the actual fixed mirror concentrator does not focus incident sunlight into a thin line on the reference cylinder. Instead, the line spreads out into a wider area. A fixed mirror concentrator with practical mirror slats will focus the

exact center of each mirror slat onto the theoretical focus line F, as shown in Figure 24. It can also be seen in Figure 24 that the solar energy reflected off the mirror slats is concentrated into an area surrounding line F which is much larger than line F. If a plane, perpendicular to the yz plane is passed through line F, then the heat flux can be defined as the amount of reflected solar energy per unit area per unit time passing any given point along the given planes projection in the yz plane, as seen in Figure 24. In this analysis the focal plane shall always be perpendicular to the reflected rays from the tangent slat.

The total heat flux (usually measured in BTU/hr ft^2) through the focal plane is simply the summation of the heat flux from all the individual mirror slats focused on the focal plane. For the moment assume that the incident light rays are all parallel. Because of the fact that the mirror slats are all at different angles to the focal plane, the width of their projected heat flux images on the focal plane will not be the same. Also, because of this fact, the maximum intensity of the solar energy reflected from any one mirror slat and measured at the focal plane will vary from slat to slat. Figure 25 shows reflected light incident on the focal plane at a given angle τ. The intensity of the energy arriving at the focal plane I_F is given by

$$I_F = I_A \cos \tau \tag{1}$$

where I_A is the intensity of the energy passing plane A.

If a given mirror slat is examined it can be seen that because of edge losses and mirror shadowing, the reflected image from the

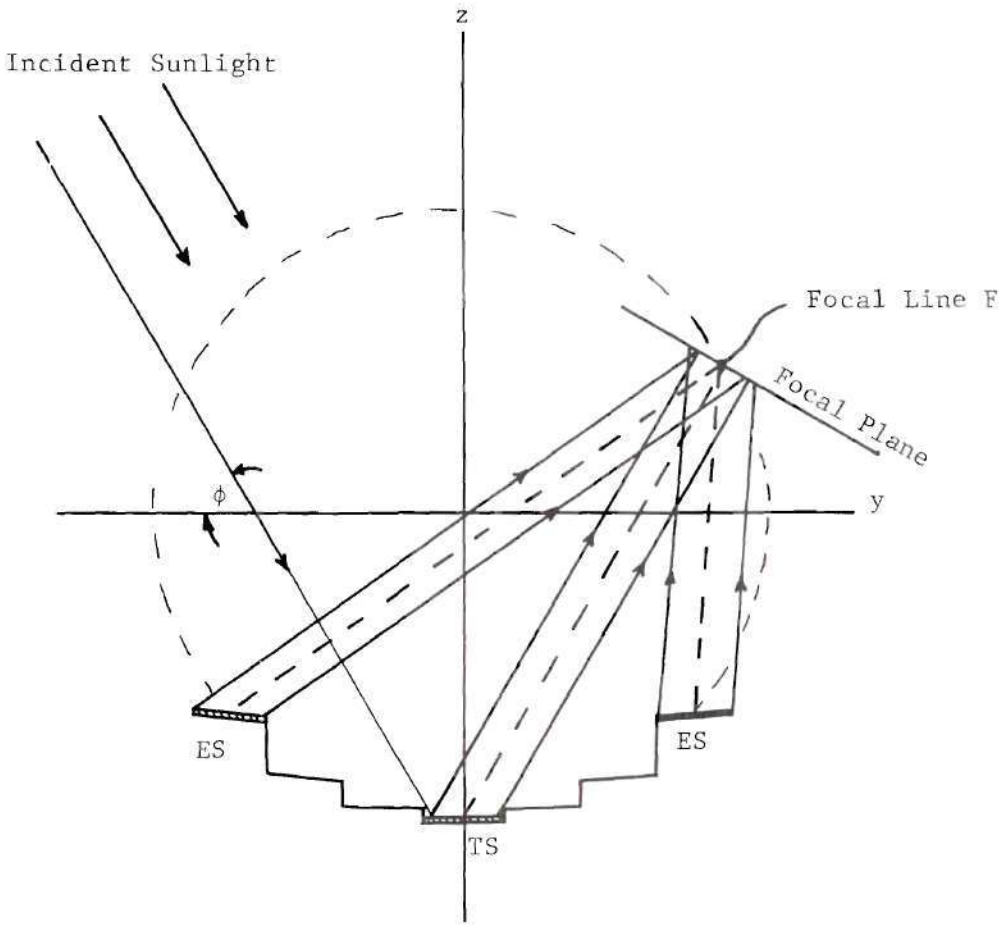

Figure 24. Wide Slats Focusing Reflected Light

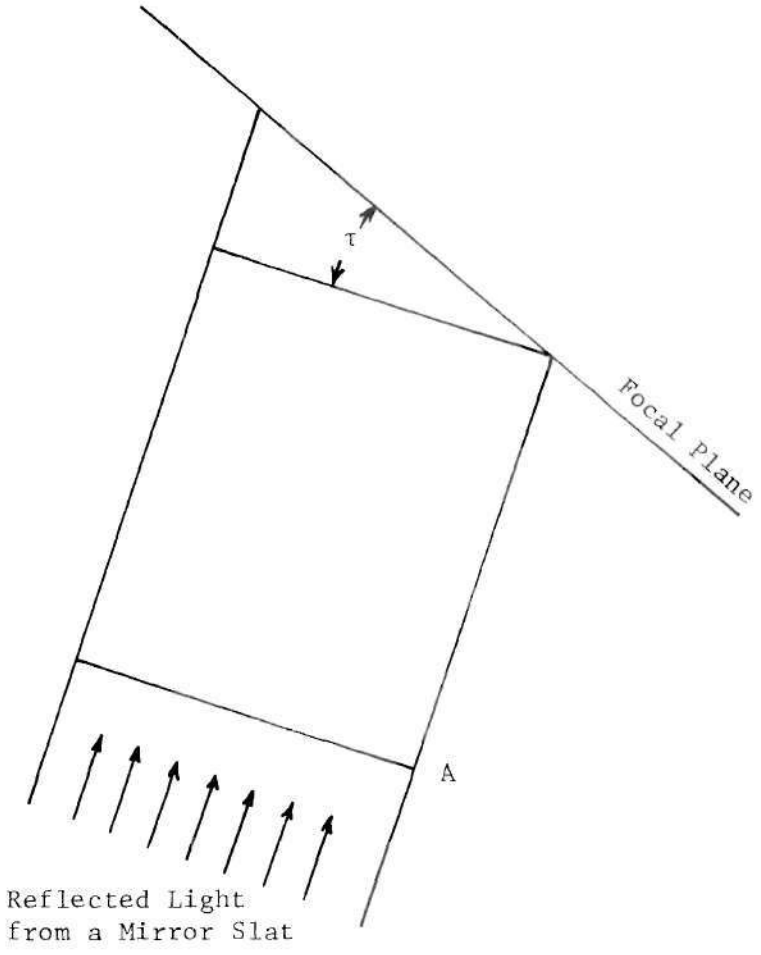

Figure 25. Reflected Light Incident on the Focal Plane

mirror slat on the focal plane is reduced in width to a varying degree depending on the particular slat. Figure 26(a) shows the effects of the edge loss on a given mirror slat. Only the light in section A, incident between points a and b on the slat is reflected to the focal plane. The light incident on the slat between points b and c is reflected into edge (cd) and lost. It can be seen that the amount of light (solar energy) actually reflected to the focal plane from a given slat, will depend on the angular tilt of the slat which is $\theta/4$, the height of the edge (cd) and the incident solar angle ϕ. Similarly, in Figure 26(b), it can be seen how a slat on the opposite side of the concentrator will suffer mirror shadowing. Edge (cd) shadows the section of the slat shown, allowing only a portion of the slat to actually reflect any light back to the focal plane. As before, the slat orientation, solar angle and height of edge (cd) determine how wide a section of light will reflect off of a given slat. Examining Figure 24, it can be seen that the only slats that do not suffer mirror shadowing or edge loss are the two edge slats, ES.

From the above discussion it can be seen that assuming parallel incident light rays, a curve representing the total heat flux profile across the width of the focal plane could be determined by simply adding the superimposed heat flux profiles at the focal plane due to each mirror slat. Furthermore, assuming perfectly flat mirror slats, the heat flux at the focal plane due to each mirror slat would be a rectangle, whose width and height representing width and energy intensity respectively, would be determined by the mirror reflectivity, edge losses or mirror shadowing, the angle between the mirror slat and

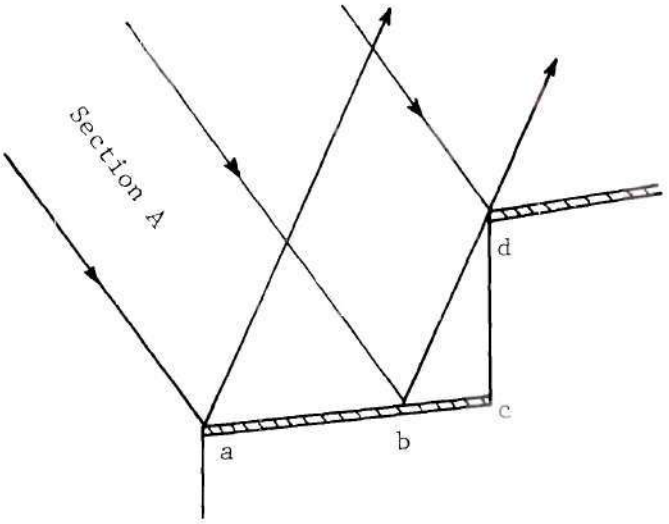

(a) Edge Loss

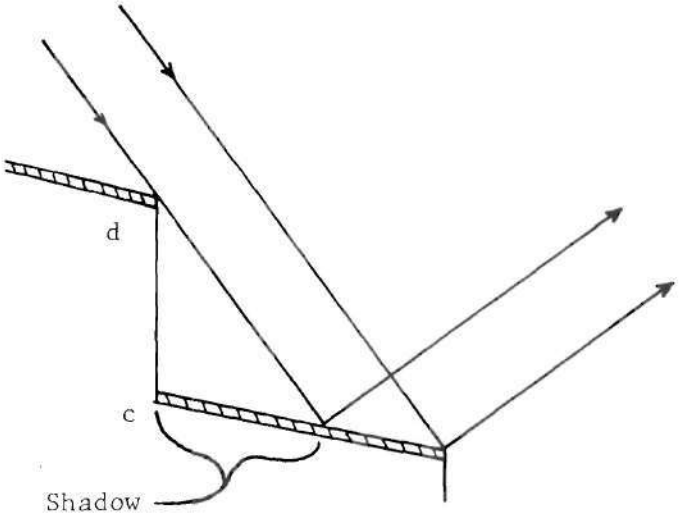

(b) Mirror Shadowing

Figure 26. Width Reduction of Reflected Image

focal plane and the incident solar angle ϕ. Profiles such as this are shown in Figure 27. Figure 27(a) represents the heat flux profile at the focal plane from the reflected light off a single mirror slat. Figure 27(b) represents the total heat flux profile at the focal plane from the reflected light off all the mirror slats focused on the center of the focal plane assuming parallel incident light and perfectly flat mirror slats.

Now obviously, the light incident on any solar concentrator is not strictly parallel since the sun is not a point source. For the purposes of this type of analysis, the sun is usually considered a disk of angular diameter 32 minutes which gives off uniform radiation. The effect of the sun's disk on the heat flux profile produced by a single mirror slat is now discussed.

For this analysis a solar energy observer will be located at the point P that moves along the focal plane. Figure 28 shows how an observer at point P would "see" the entire solar disk reflected off a mirror slat. In this case the solar disk is represented by two light rays (1) and (3), 32 minutes apart and another ray (2) from the center of the sun. The angle of 32 minutes shall be represented by 32 minutes = 2Ω. As shown, the three light rays converge and are reflected up to point P with the angles as indicated. The angle ϕ from the horizontal to ray (2) is the incident solar angle which indicates the direction of incident solar energy. The focal plane is set at angle ω to the horizontal. The mirror slat is in this case, set with $\theta/4$ = 0 degrees. An observer at point P then "sees" all of the sun's disk. If the reflectivity of the mirror slat is 100% then the

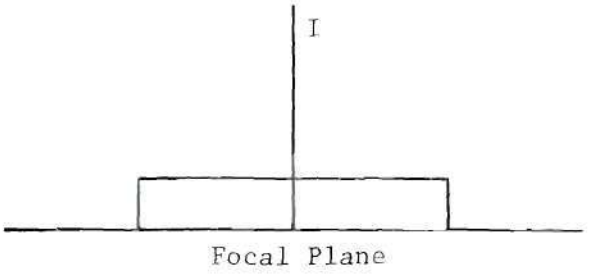

(a) Single Mirror Slat

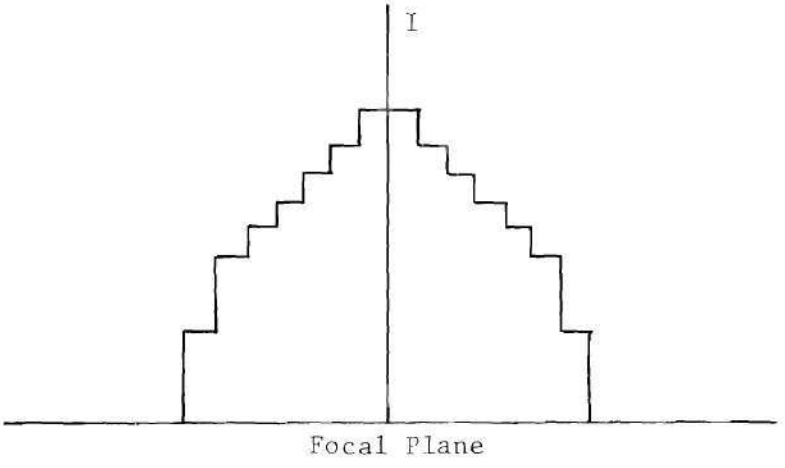

(b) All Mirror Slats

Figure 27. Theoretical Heat Flux Profiles From a Parallel Light Source With Perfectly Flat Mirror Slats

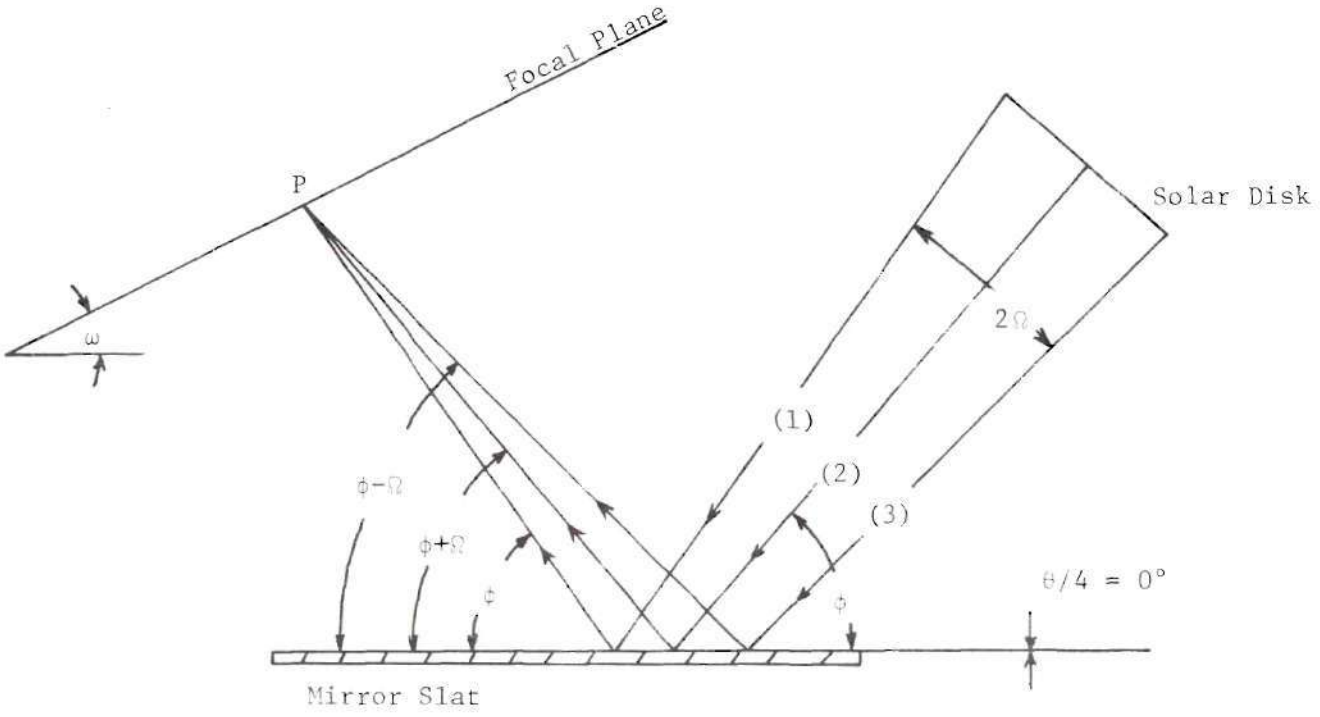

Figure 28. Reflection of Solar Disk as Seen by an Observer at Point P

observer at the point P sees all the incoming direct solar energy I, and the intensity reaching P from the sun's image is equal to the direct solar intensity I falling on the mirror slat. Now the rest of the focal plane will be examined to see how the reflected solar intensity varies.

In Figure 29(a) at position (a) along the focal line, an observer at point P begins to see the solar disk. In Figure 29(b) at position (b), an observer at point P sees half the solar disk or a solar energy intensity of I/2. In Figure 29(c) at position (c), an observer at point P sees all of the solar disk and a solar energy value of I. Figure 29(d) shows the composite result with rays (1), (2), and (3) leaving the edge of the reflecting surface marking the locations of the 0, I/2, and I, direct solar energy levels seen by an observer at point P on the focal plane.

As shown in Figure 29 the intensity of solar energy I, measured at point P is proportional to the amount of the solar disk seen by an observer at point P. By examining the area within a circle and to the left of a line, as that line moves across the circle; it is seen that more and more of the area of the circle will be exposed. By calculating the exposed area and the position of the line on the diameter of the circle, the curve connecting points a, b, and c of the heat flux profile on the focal plane, in Figure 29(d) can be calculated. This curve shown in Figure 30 can then be used, knowing the position on the focal plane of any points a, b, and c, to complete the single slat heat flux profile. An example of such a heat flux profile, assuming 100% mirror reflectivity, is shown in Figure 31.

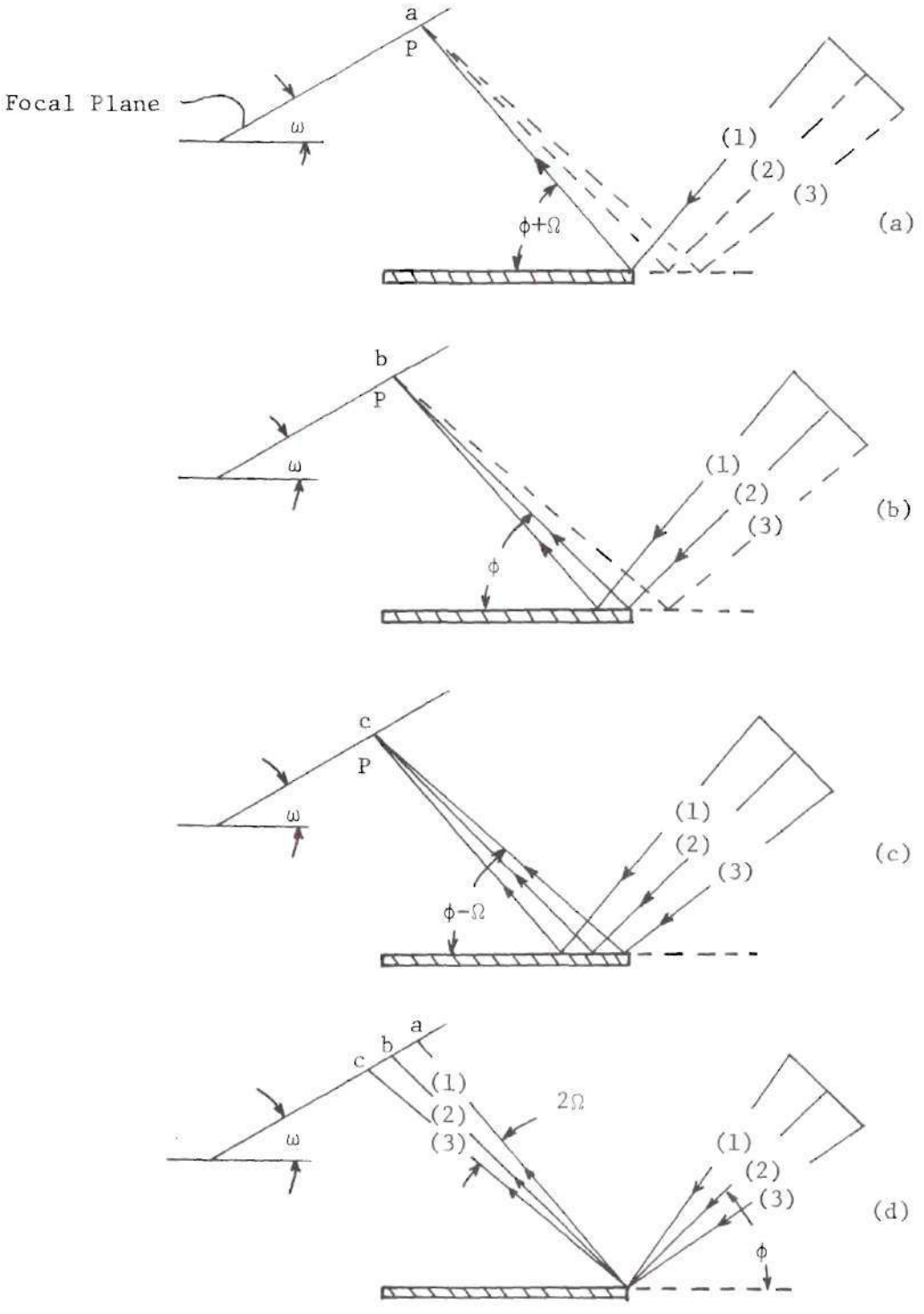

Figure 29. Formation of Heat Flux Profile

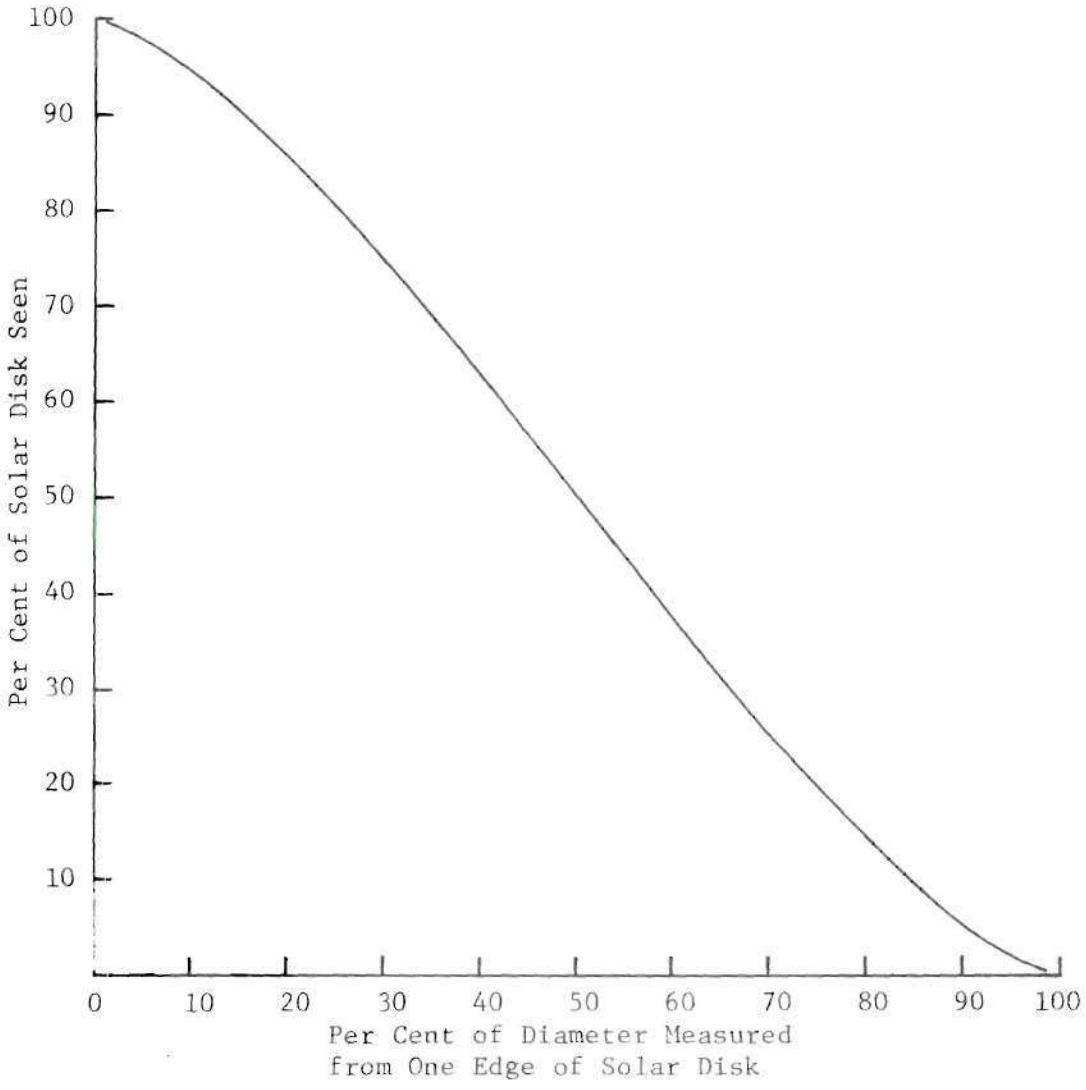

Figure 30. Heat Flux Fall Off Curve

General Method of Attack

The general method used in analyzing the theoretical heat flux profile at the focal plane will now be discussed. As mentioned above, the total heat flux at the focal plane is made up of the addition of all the reflected energy off each individual mirror slat which is focused at the center of the focal plane. Therefore, given an incident solar angle ϕ, the heat flux profiles at the focal plane for each individual mirror slat in the concentrator are calculated using a method to be discussed in detail. These profiles are then added together to produce the total heat flux profile at the focal plane for the given value of ϕ.

The reference system used in locating a particular slat is shown in Figure 32. Basically the tangent slat was given a number 0. The concentrator was then divided into a right and left side with the other slats numbered as shown. The number, 7_R, locates the seventh slat on the right side.

In analyzing the concentrator it was desired to pick a range of solar angles ϕ, from sunrise to sunset, for use in calculating the heat flux profiles. In this way concentrator efficiencies, heat flux profiles, and concentration factors were calculated covering an entire day. The particular solar angles ϕ at which the calculations were done, were chosen to produce a complete range of focal plane positions θ_F as shown in Figure 32. It should be noted, that given any particular solar angle ϕ, the position θ_F of the focal plane is automatically determined. Therefore, the focal plane positions θ_F were first chosen to completely cover the reference circle. Then, the

corresponding solar angles ϕ were easily calculated by examining the isosceles triangle OCF in Figure 32. Table 2 lists the solar angles ϕ and corresponding focal plane positions θ_F which will be analyzed.

Table 2. Solar Angles ϕ to be Analyzed

Solar Angle ϕ Degrees	Focal Plane Position θ_F Degrees	Time of ϕ, Atlanta, Georgia July, EST
27.5	55	8:11 AM 5:13 PM
33.75	67.5	8:35 AM 4:49 PM
45	90	9:23 AM 4:00 PM
56.25	112.5	10:16 AM 3:08 PM
67.5	135	11:06 AM 2:25 PM
78.75	157.5	11:56 AM 1:36 PM
90	180	12:44 PM

Since the particular fixed mirror concentrator designed for this thesis is symmetrical about its center line C_L, which is also the z axis; only focal plane positions θ_F on the right side of the center line C_L were analyzed. The results for the focal plane positions θ_F and corresponding solar angles ϕ for the left side of the concentrator are mirror images of the heat flux profiles calculated for the right side.

Single Mirror Slat Heat Flux Profiles

The method used to arrive at the heat flux profiles for a single mirror slat will now be discussed. The method used was graphical in nature so extreme care was used in drawing and measuring the various angles and lengths involved. To reiterate, this analysis was done in the yz plane. The first step was to lay out the given slat and edge

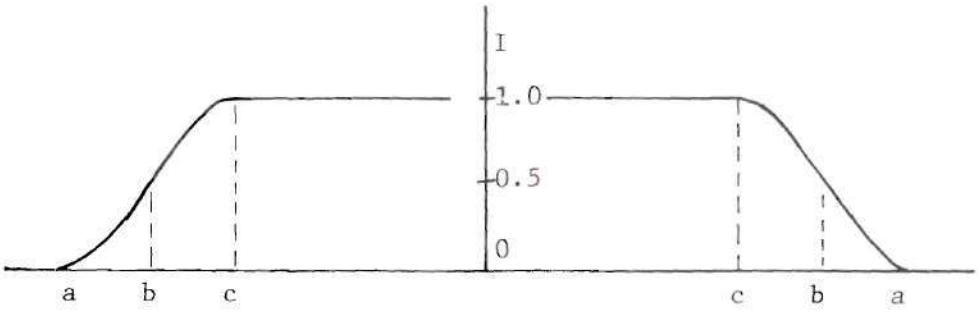

Figure 31. Heat Flux Profile at the Focal Plane From a Single Mirror Slat Assuming 100 Per Cent Reflectivity

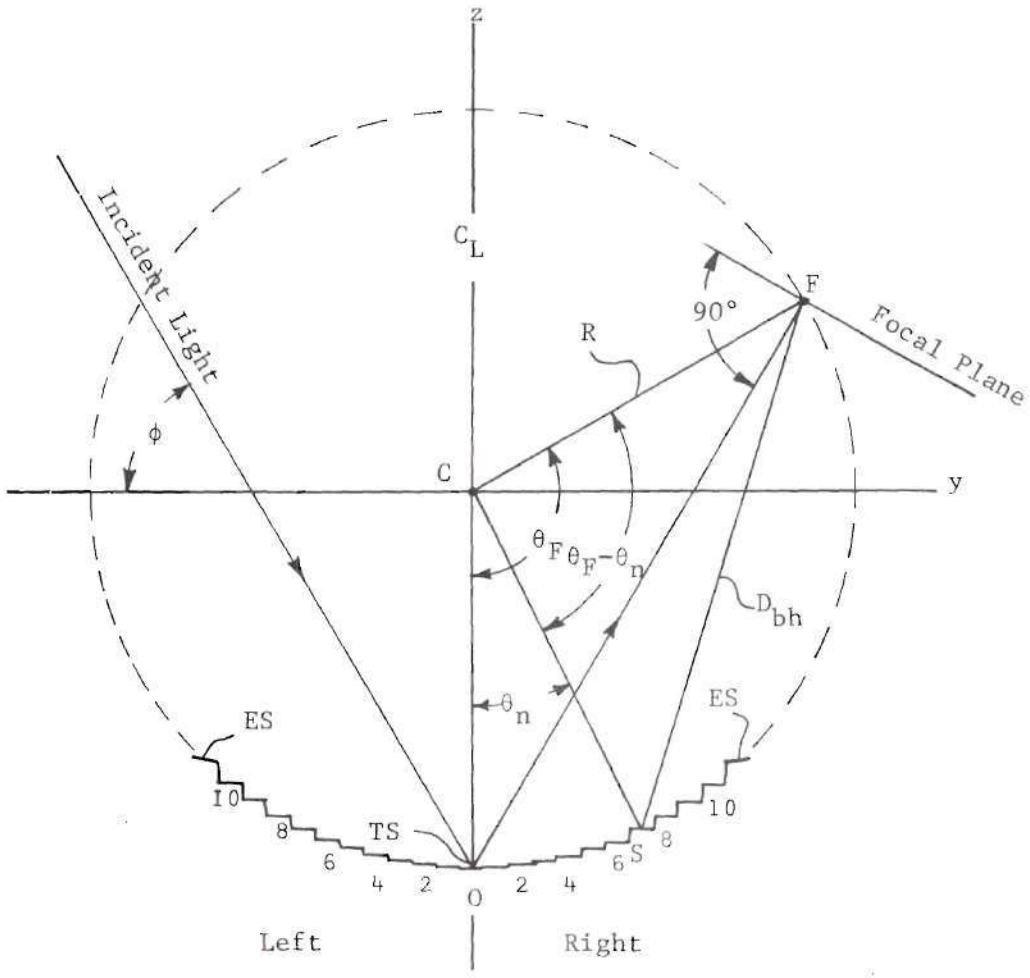

Figure 32. Slat Reference System

in a full scale drawing. An example of this is shown as lines (ad) and (de) in Figure 33. The point b is the midpoint of slat (ad). The point f is the center of the next adjacent slat. The reference circle passes through points b and f. In laying out the slat and edge, the height h of edge (de) had to be calculated. Equation (2), along with the geometry shown in Figure 34 was used in the calculation of the value of h in inches.

$$h = \left(\tan \frac{\theta_1+\theta_2}{2}\right)\left(L_1+L_2\right) - 2\left(\sin {}^{\theta}1/4 + \sin {}^{\theta}2/4\right) \qquad (2)$$

where $L = 2 \cos \theta/4$

Next, the focal plane, line (kn), at the proper angle, (90 - ϕ degrees) was drawn in as shown. The three reflected rays (ag), (bh), and (cj) were then added. These parallel rays are the reflected rays from the center of the sun's disk (ray (2) in Figure 29). Ray (ag) is reflected from the edge of the mirror slat, point a. Ray (bh) indicates the direction and location of a line that connects the center of the reflecting slat, point b, with the center of the focal plane, point h. The position of ray (cj) is dictated by the position of the slat (ad) and edge (de). The positioning of similar reflected rays will be discussed in detail later. Point h is the center of the focal plane and was used as a reference point to locate other points on the focal plane.

It can be seen that rays (ak) and (en) correspond to ray (1) in Figure 29, which marks the location on the focal plane where the heat

flux profile begins. Similarly, rays (a1) and (em) locate the points on the focal plane where the maximum heat flux is first reached. Rays (ag) and (cj) locate the point on the focal plane where the heat flux is half the maximum value, as in Figure 29. Knowing the angle Ω, as shown between the above rays, it is possible to calculate the distances (kg), (gl), (mj), and (jn) by examining triangles akg, agl, emj, and ejn respectively. To do this, the distances D_{ag}, D_{bh}, and D_{ej} must be calculated.

The first step in these calculations was the calculation of the distance D_{bh} from point b to point h. By examining the isosceles triangle SCF in Figure 32, the distance D_{bh}, from the center of the slat to the center of the focal plane was easily calculated. From here the distances d_1, d_2, d_3, and d_4 were measured with a scale on the full scale diagram, Figure 33. With these numbers, the desired distances D_{ag} and D_{ej} were easily calculated by adding or subtracting the appropriate numbers d_1, d_2, d_3, and d_4 from D_{bh}.

From Figure 33 it can be seen that the two pair of triangles akg and emj, as well as the triangles agl and ejn are similar. Knowing the distances D_{ag} and D_{ej} as calculated above and the angles as shown in Figure 33 within the four triangles, the distances (kg), (gl), (mj), and (jn) were calculated. The distances along the focal plane (hg) and (hj) were then measured directly from Figure 33. With the positions of points k, g, l, m, j, and n located with respect to the reference point h on the focal plane, it was now possible to plot the final heat flux profile.

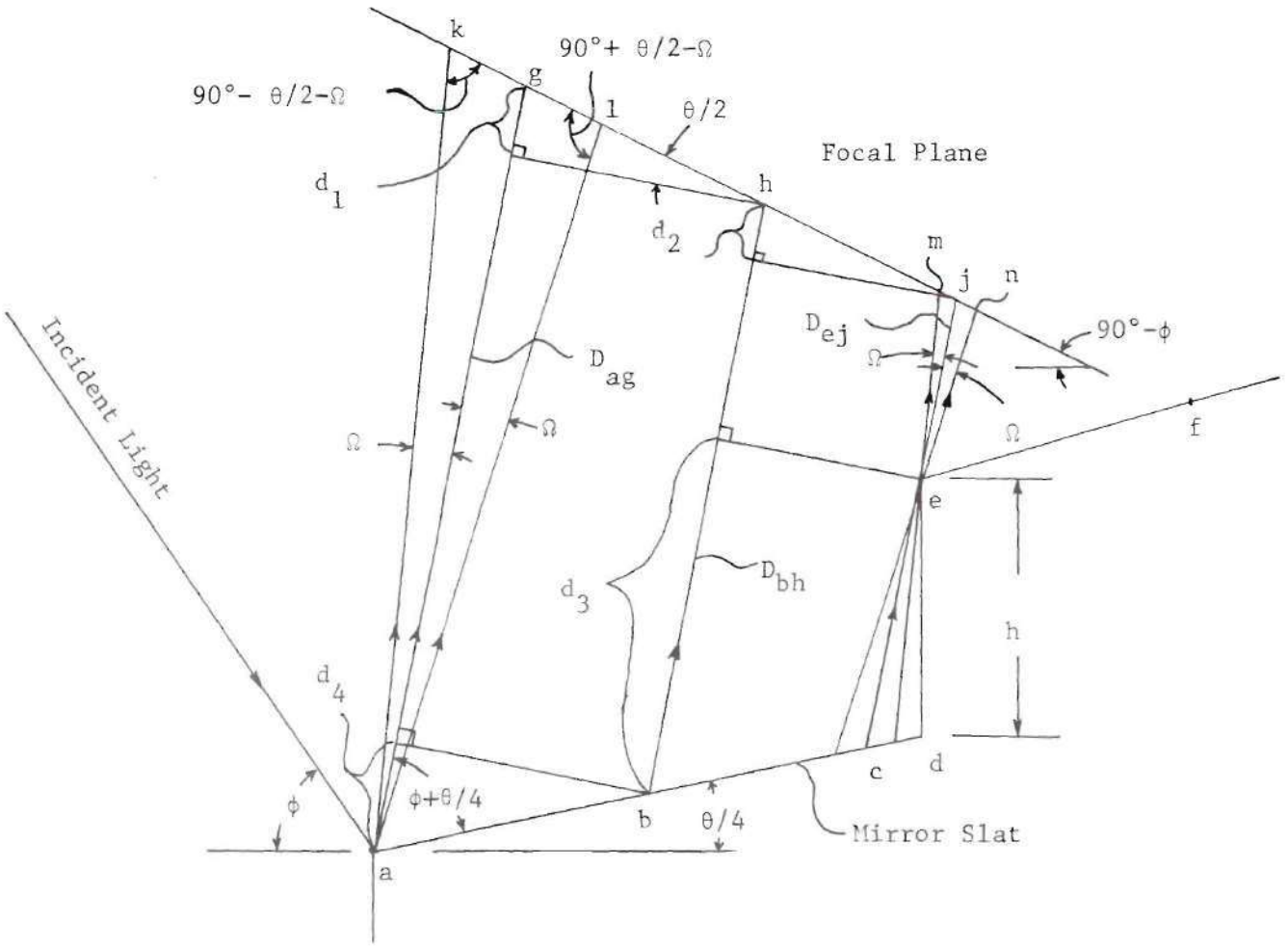

Figure 33. Heat Flux Construction Diagram

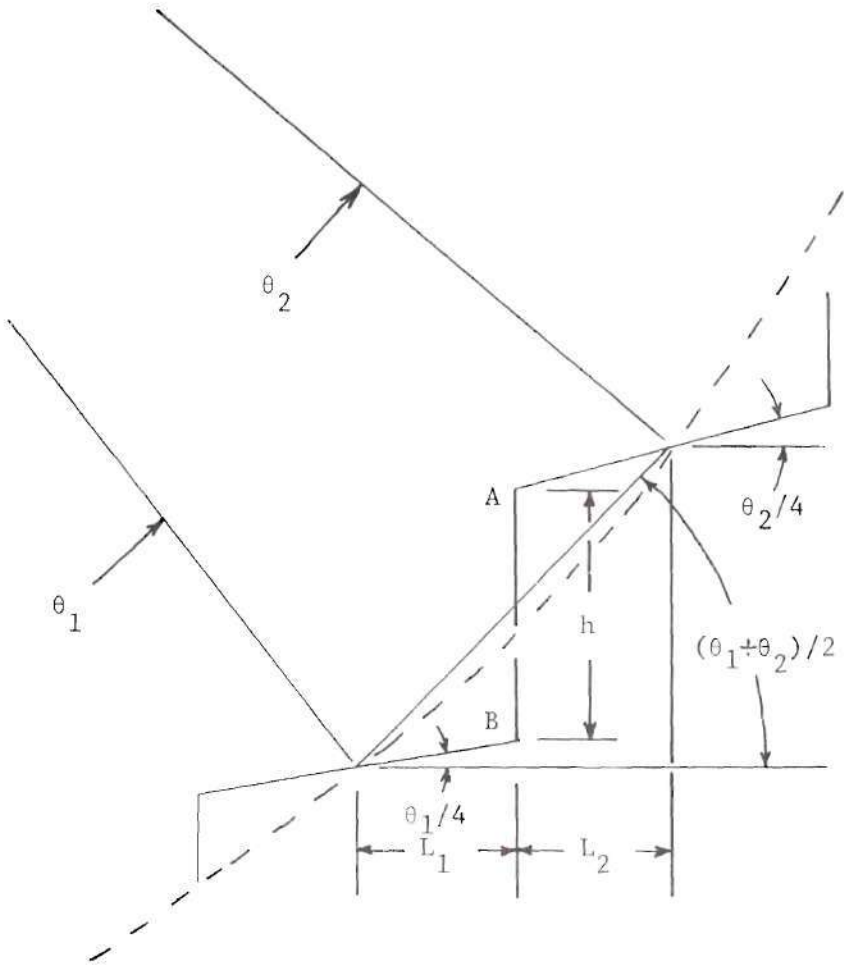

Figure 34. Labeling of Geometry Used in Calculating h Values

The value of direct solar energy incident on the mirror slat was given a normalized value of I. All the mirror slats were given a constant reflectivity value ρ, of 85.1%. This reflectivity was determined experimentally and will be discussed later. The heat flux fall-off curve shown in Figure 30 was used to connect points k, g, and 1, and m, j, and n as shown in Figure 33. Noting that the angle as described in Equation (1) and Figure 25 is $\theta/2$ in Figure 33, the heat flux profile shown in Figure 35 was plotted.

The method described above illustrates the general method applied to all the mirror slats for each given solar angle, ϕ, at which the analysis was carried out. This is a total of 140 construction diagrams similar to Figure 33. Figure 33 illustrates just one slat and edge position. There were, however, a number of different groups of similar slat positions which were treated slightly differently. Any single slat position and solar angle combination could be placed in one type of these groups. These different slat reflection types will now be discussed.

Slat Reflection Types

Figure 33 is an example of two slat reflection types. Generally a given heat flux profile can be considered to have two "end sections" (sections (k1) and (mn) in Figure 35) and a midsection. It is in these "end sections" where the profile starts at a zero value then builds up, following the characteristic fall-off curve shown in Figure 30, to a maximum value of the heat flux. The midsection (section (1m) in Figure 35) consists of an area of constant heat flux which varies in width down to zero. In that case the curve is

essentially bell shaped. Now, the type of slat reflection which occurs at the given mirror slat will determine how and where the "end section" points k, g, l, m, j, and n (Figure 33) will be located on the focal plane. Generally, the slat reflections were broken down into four basic types. In presenting these types only the composite diagrams as shown in Figure 29(d) are illustrated. The notation of light rays (1) and (3) from the edge of the sun's disk and ray (2) from the center of the sun's disk will also be used. Where needed, approximations used in the heat flux construction diagrams will also be shown.

Type I occurs when no vertical edge intersects either the incident or reflected rays (1), (2), and (3). The edges of the mirror slat then become the boundaries where reflection begins and ends. This is shown in Figure 36.

Type II occurs as shown in Figure 37(a) when all or some of the rays (1), (2), and (3) intersect the edge (ps) before being reflected off the slat. The calculations needed to determine where rays (1), (2), and (3) intersect the focal plane as shown in Figure 37(a) were of such length that the approximation shown in Figure 37(b) was deemed necessary. The approximation consists of a type I reflection from point o, where ray (2) intersects the slat as shown in Figure 37(b). Rays (1)* and (3)* are the approximations for rays (1) and (3). The differences between Figure 37(a) and the approximation, which are the two distances B_1 and B_2, are very small due to the fact that angle 2Ω is only 32 minutes and edge (ps) is only a few inches in length.

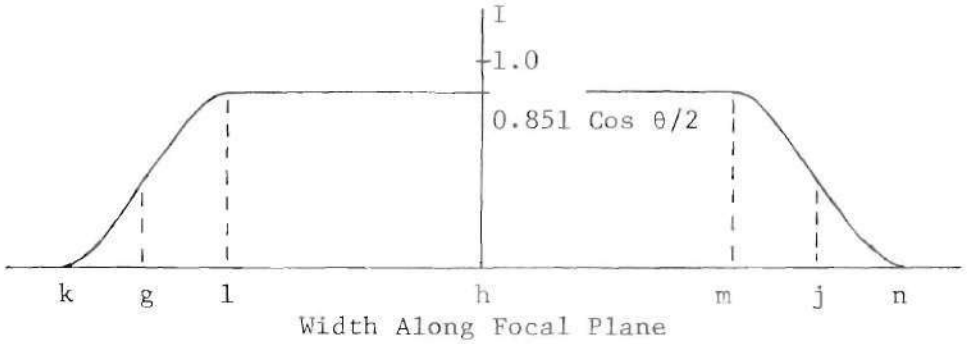

Figure 35. Heat Flux Profile at the Focal Plane from a Single Mirror Slat

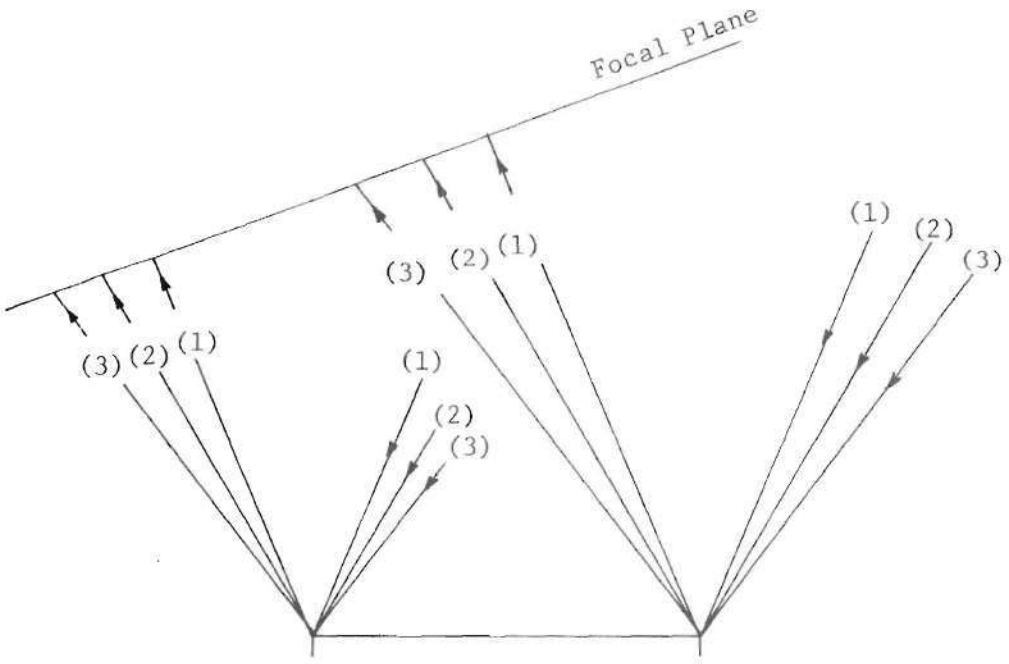

Figure 36. Slat Reflection Type I

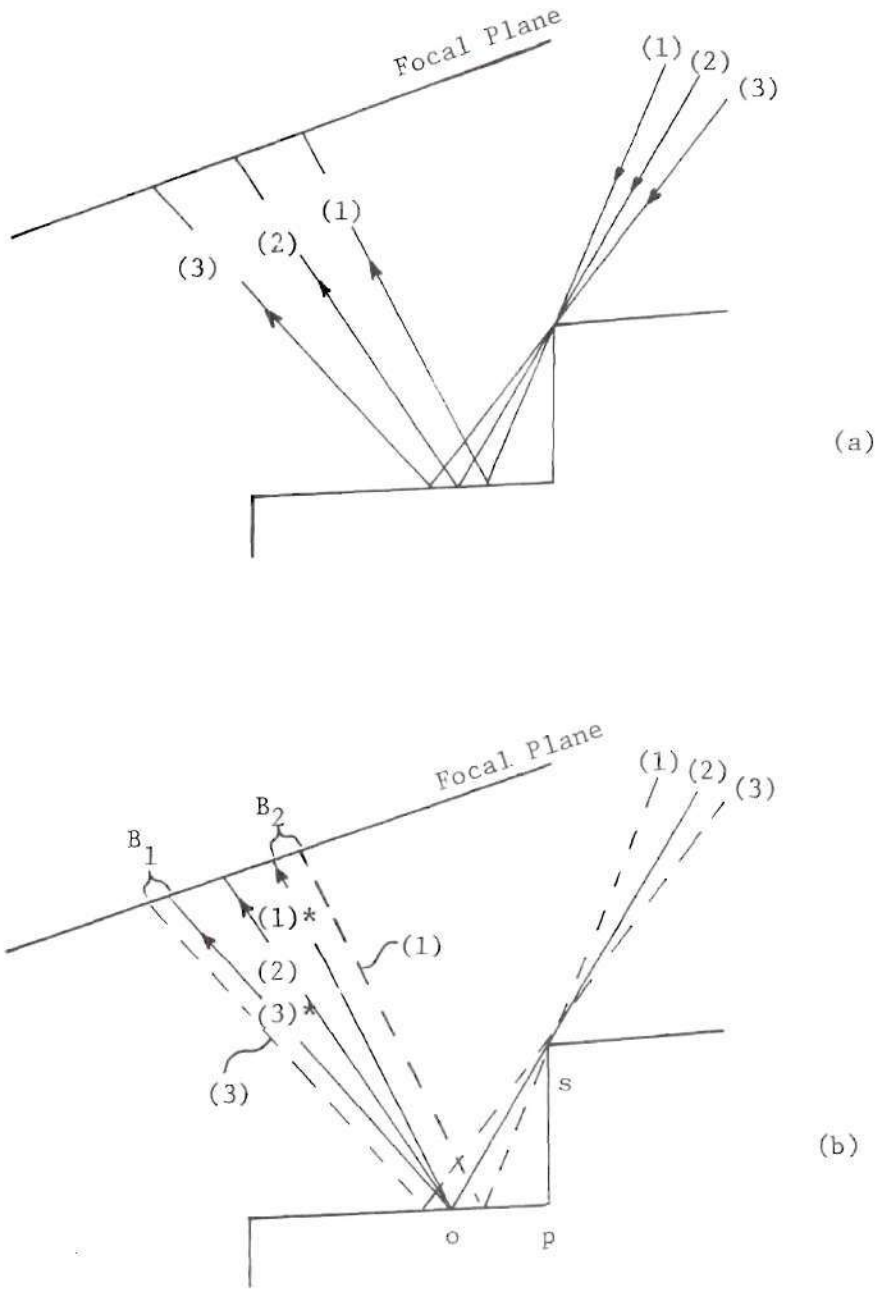

Figure 37. Slat Reflection Type II

A type III reflection occurs when rays (1), (2), and (3), incident on a mirror slat, are reflected off and must pass point s which is the top of edge (ps) in Figure 38. Figure 33 has a type III reflection *off edge* (de). As shown in Figure 38, this reflection can be handled as a type I reflection from point s on edge (ps), along the direction of the reflected ray (2).

A type IV reflection occurs when the solar angle ϕ is small enough that a shadow would extend from the inside edge of one of the edge slats ll_R or ll_L across several adjacent slats. This reflection type is very similar to type II except that point s (as shown in Figure 37) would be located several feet away. In this case, even though angle 2Ω is only 32 minutes, the distances B_1 and B_2 become relatively large and must be accounted for. Figure 39 shows the general situation. The mathematics and trigonometry involved in determining points a, b, and c, while lengthy, are relatively simple and will not be described in detail. Basically, the distances x and y in Figure 39, between the centers of the edge slat and affected slat were first determined in a manner similar to that used to find distance D_{bh} in Figure 32. From this, the point o on the affected slat where ray (2) intersects it, was determined. With this information, points w and z where rays (1) and (3) intersect the affected slat were located. Finally, a construction diagram similar to Figure 33 was used to locate points a, b, and c on the focal plane.

As mentioned above the general heat flux profile has two end sections and a midsection. The end sections are located on the focal plane through the use of the slat reflection types discussed above.

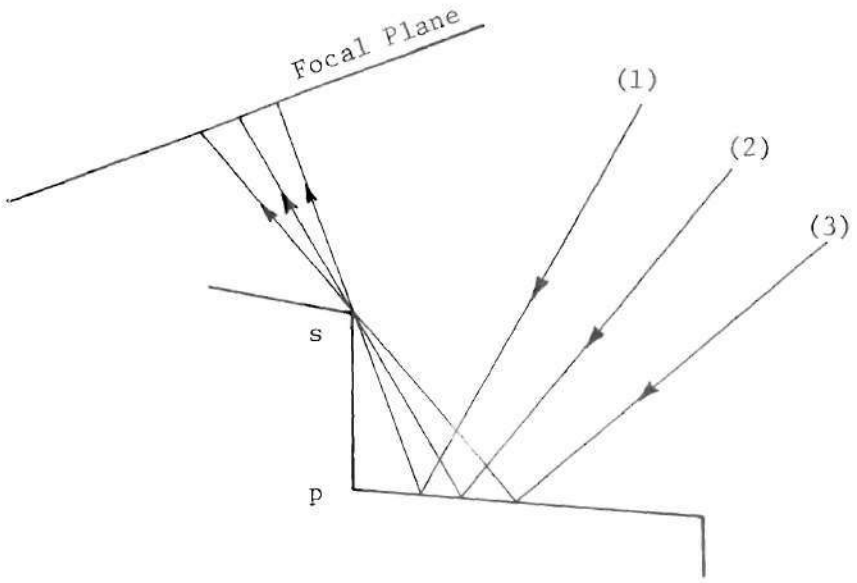

Figure 38. Slat Reflection Type III

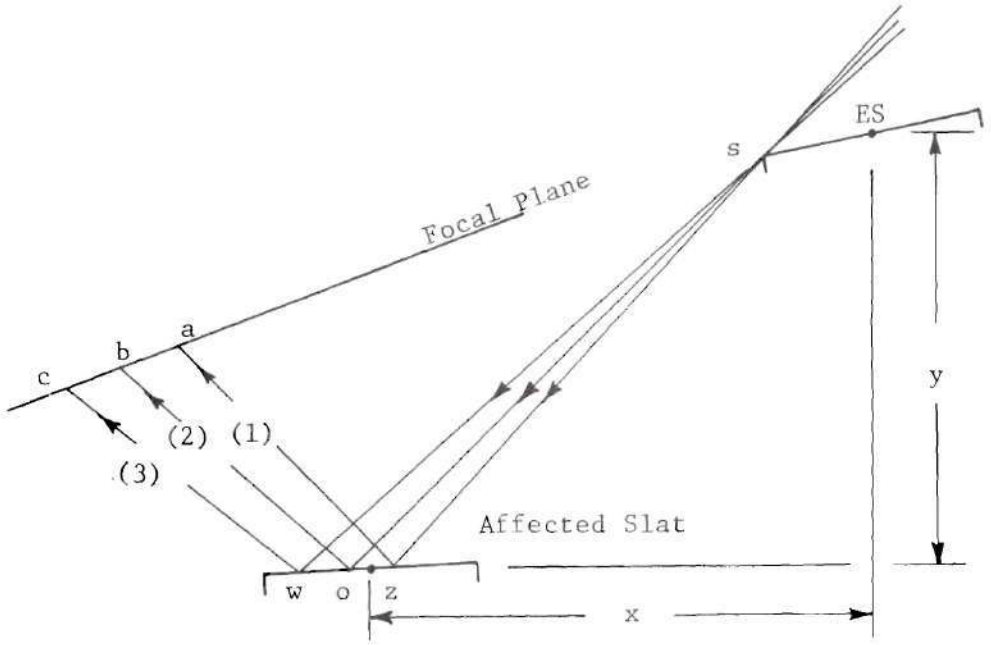

Figure 39. Slat Reflection Type IV

If the situation exists as described in type IV, the end section produced by the type IV reflection may overlap into the other end section on the heat flux profile because it is much larger than normal. This is the situation in which the width of the portion of mirror slat which actually refelcts light is so small that an observer at any point on the focal line never sees the entire solar disk. To plot the heat flux profile in this case, the two fall off curves were plotted in their overlapping state using the information taken from the construction diagram. Then, the overlapping section was marked off in points. At each point the percentage of the solar disk not seen due to each fall-off curve was determined. The total percentage of the solar disk not seen at the particular point was just the sum of the above percentages from each fall off curve. The percentage of the sun's disk seen at the point was then easily obtained. The procedure was repeated for the rest of the points along the overlapping section, thus completing the curve.

Total Heat Flux Profile

For a given solar angle ϕ, the individual heat flux profiles were arrived at, as described previously. With this information, the curves were added to produce the total heat fulx profile at the focal plane. To do this each individual heat flux profile was marked off with "addition" points every tenth of an inch using the center of the focal plane, point h in Figure 35, as a reference point. The points at a given distance from the reference point h, on all the individual slat profiles were then summed up to produce a total point at the same

given distance from the reference point on the total heat flux profile. This was repeated for all the addition points along the width of the focal plane. The resulting set of points was then connected using a French curve to produce the theoretical heat flux profile for the given solar angle ϕ.

Edge Losses

The fixed mirror concentrator's edge loss was defined as the percentage of energy incident on the concentrator which does not reach the focal plane due to self-shadowing. This is light that is not reflected back to the focal plane, but is either incident directly on a vertical edge between two slats or reflected into such a vertical edge.

The first step in these calculations was to determine the total amount of direct solar energy incident on the concentrator. Using a two dimensional analyses, this is given by the following Equation

$$S = W\sin\phi I \tag{3}$$

where S - Total direct solar energy incident on the concentrator

W - Width of concentrator as measured between the outside edges of the edge slats

I - Normalized value of direct solar energy

ϕ - Solar angle

Both reflections and edge losses reduce the amount of direct solar energy which finally reaches the focal plane. The theoretical total heat flux profiles at the focal plane were obtained using a constant

mirror slat reflectivity of ρ = 85.1% and a normalized value for direct solar energy I. The area under such a profile represents the amount of solar energy reaching the focal plane after edge and reflection losses. By dividing the area under the total heat flux profile by the constant reflectivity ρ, the amount of solar energy reaching the focal plane after edge losses only, S_E, was obtained. The percentage of incident solar energy lost due to self shadowing (edge losses) is simply

$$\text{Edge Loss} = \left(\frac{S - S_E}{S}\right) \times 100 \tag{4}$$

These calculations were carried out for the solar angles ϕ, listed in Table 2. Now a correction is applied to the edge losses obtained using Equation (4), at the solar angles of 78 degrees and 90 degrees. At these angles the cross pipe (aluminum pipe which holds the heat collecting tube in the focal plane) casts a shadow on slats $10_L - 11_L$ and $1_R - 2_R$. This shadow, which causes a type IV reflection, was taken into account when determining the individual heat flux profiles at the four slats affected. As a result, the final total heat flux profile at solar angles 78 degrees and 90 degrees contained reflection losses, edge losses, and a shadow loss caused by the cross pipe. To obtain the correct value for S_E in Equation (4) the cross pipe's shadow loss had to be determined.

To do this, the individual heat flux profiles from each of the affected slats were examined. First, the area under the given profile was calculated taking into account the cross pipe's shadow. Next, a new heat flux profile was plotted without the cross pipe's shadow.

The difference in the two areas was the cross pipe's shadow loss affecting that particular mirror slat. These cross pipe shadow losses affecting the two slats at the given solar angle were calculated and then added to the value S_E, to obtain the correct value for the amount of solar energy reaching the focal plane after edge loss only (S_E*). That is

$$S_E^* = S_E + L_{CP} \tag{5}$$

where S_E* = corrected value for energy ariving after edge loss only at ϕ = 78 degrees or 90 degrees

S_E = energy arriving after edge and cross pipe shadow losses

L_{CP} = cross pipe shadow losses.

The new correct value S_E* was then used in Equation (4) to arrive at the percentage edge loss.

Concentration Efficiency

The concentration efficiency is defined as the amount of solar energy arriving at the target area on the focal plane divided by the total amount of solar energy incident on the concentrator, S. As shown in Figure 40, as the target area's width on the focal plane is decreased, the concentration efficiency becomes a function of this width since more and more of the area under the heat flux profile will miss the target area. If the area under the heat flux profile within the target area on the focal plane, S_T, is determined, then the concentration efficiency CE is defined as

$$CE = \frac{S_T}{S} \times 100 \qquad (6)$$

Using Equation (6) and the theoretical heat flux profiles for the solar angles listed in Table 2, the theoretical concentration efficiencies were calculated.

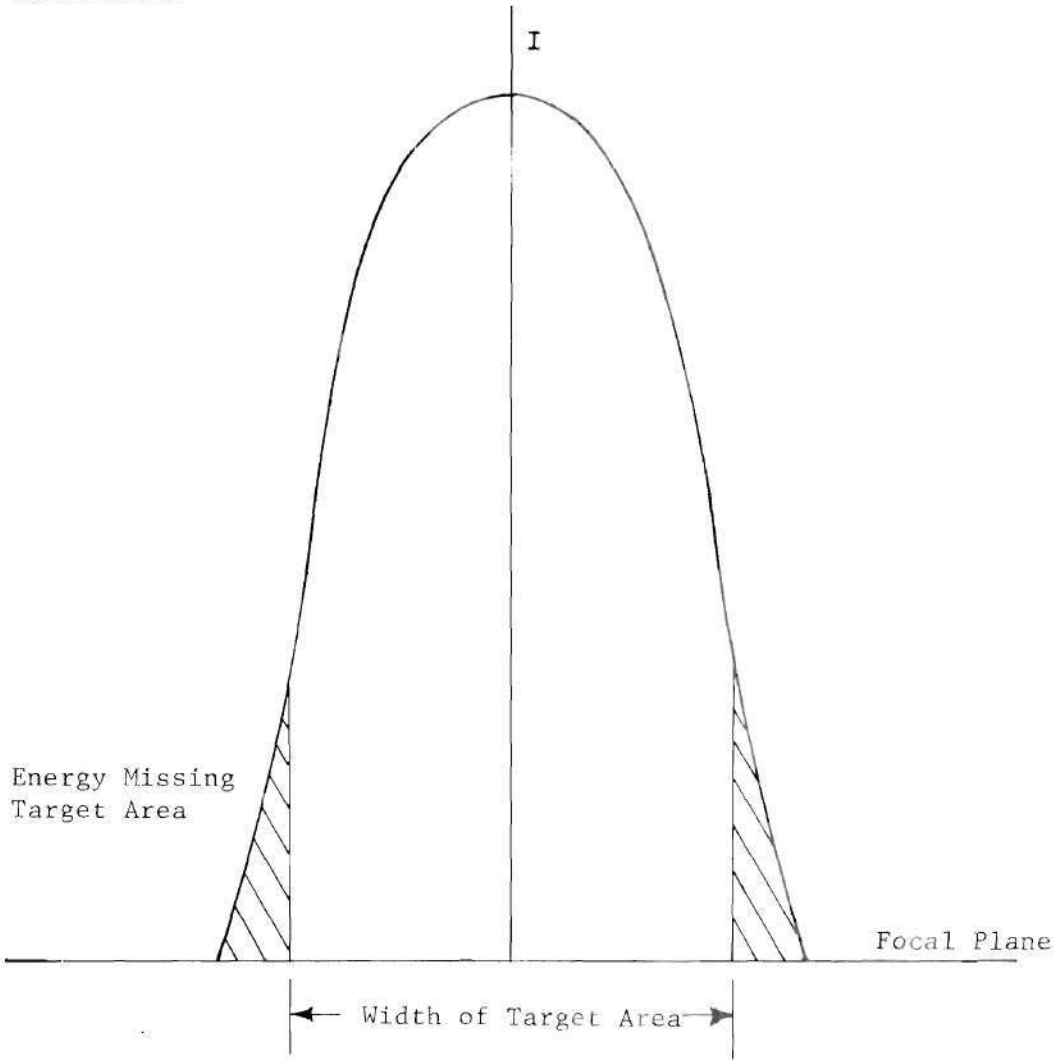

Figure 40. Heat Flux Profile on the Target Area

CHAPTER V

INSTRUMENTATION AND EQUIPMENT

Background

The instrumentation was designed to measure the actual heat flux (in normalized units I) at the focal plane for any solar angle ϕ. To do this, a photomultiplier tube was used as a sensing device to detect thermal radiation at the focal plane. By mounting this tube on a scanning mechanism which moved it across the focal plane, the thermal radiation intensity across the focal plane was recorded. A photomultiplier tube is a device which detects incident radiation over a certain range of wavelengths and linearly amplifies it to a measurable output current. By dividing the output current of the photomultiplier tube when it was used to measure direct solar radiation incident on the concentrator, into the output current produced when the tube measured the radiation intensity across the focal plane of the fixed mirror concentrator, the actual heat flux (in units of direct solar radiation I) at the focal plane was determined. A detailed discussion of this procedure will come later.

Photomultiplier Tube

Thermal radiation, that radiation which produces thermal excitation in matter, is defined by Chapman [18] as radiation with a wavelength between 10^3 and 10^6 Angstroms. This radiation extends from the ultraviolet to the infrared range. Ideally, the photomultiplier

tube chosen for the radiation sensing device should have a spectral range covering the entire range of thermal radiation from the sun. The tube actually chosen, had the widest spectral range of those available for the project. This was an EMI 9558QC, 2 inch diameter, flat faced, end window tube with a 44 mm cathode and 11 venetial blind dynodes having CsSb secondary emitting surfaces. The tube has a fused silica window and a tri-alkali cathode giving it a spectral range of 1,650 to 8,500 Angstroms. This is from the middle of the ultraviolet range to the beginning of the infrared range of radiant energy. Other specifications are listed below.

EMI Type 9558QC Electrical Ratings

Over sensitivity, Rated	200A/lm
MaX	2000 A/lm
Max. anode current (mean)	1 mA
Max. operating temperature	140° F
Transit Time	55 ns
Maximum cathode to anode voltage	2200 V
subject to not exceeding	2200 A/lm

As discussed above, the spectral range of the phototube chosen for this project covers a range of 1,650 to 8,500 Angstroms. By examining a spectral irradiance curve of the solar energy arriving at the surface of the earth, it can be seen that the phototube's broad spectral range covers most of the incident solar energy. Some of the infrared portion of the incident solar energy (that whose wavelength is greater than 8,500 Angstroms) will not be detected by the phototube. This, however, does not present a problem under the assumption of constant mirror slat reflectivity independent of angle of incidence

and wavelength. The phototube under this assumption will measure a constant portion of the total radiation spectrum incident on the tube window whether the tube is measuring the direct radiation incident on the fixed mirror concentrator, or when it is measuring the concentrated radiation at the focal plane. Therefore, the actual heat flux profile can be determined since the constant percentage factor will be eliminated by division.

The phototube is designed to detect extremely low levels of radiation. Therefore to utilize the tube in detecting direct and concentrated solar radiation, it had to be encased in a special housing which is shown in an exploded view in Figure 41. This housing is essentially a light tight case with a pin hole at one end which allows radiation to enter. A series of neutral density filters placed before and after the pin hole further reduced the solar radiation to acceptable levels that can be measured by the phototube. The tube housing was covered in white tape to reflect heat and keep the tube as cool as possible. Aluminum foil was placed on the front of the tube housing facing the focused radiation for the same reason.

One other problem had to be overcome in utilizing the phototube to measure the concentrated radiation at the focal plane. In Figure 24 it can be seen that the radiation striking the focal plane does so over a range of incident angles. When radiation strikes the boundary between two transparent mediums of different indices of refraction, part of the radiation is reflected and part is transmitted through one medium. The amount of the incident radiation transmitted and reflected will be a function of its angle of incidence. Generally, the further

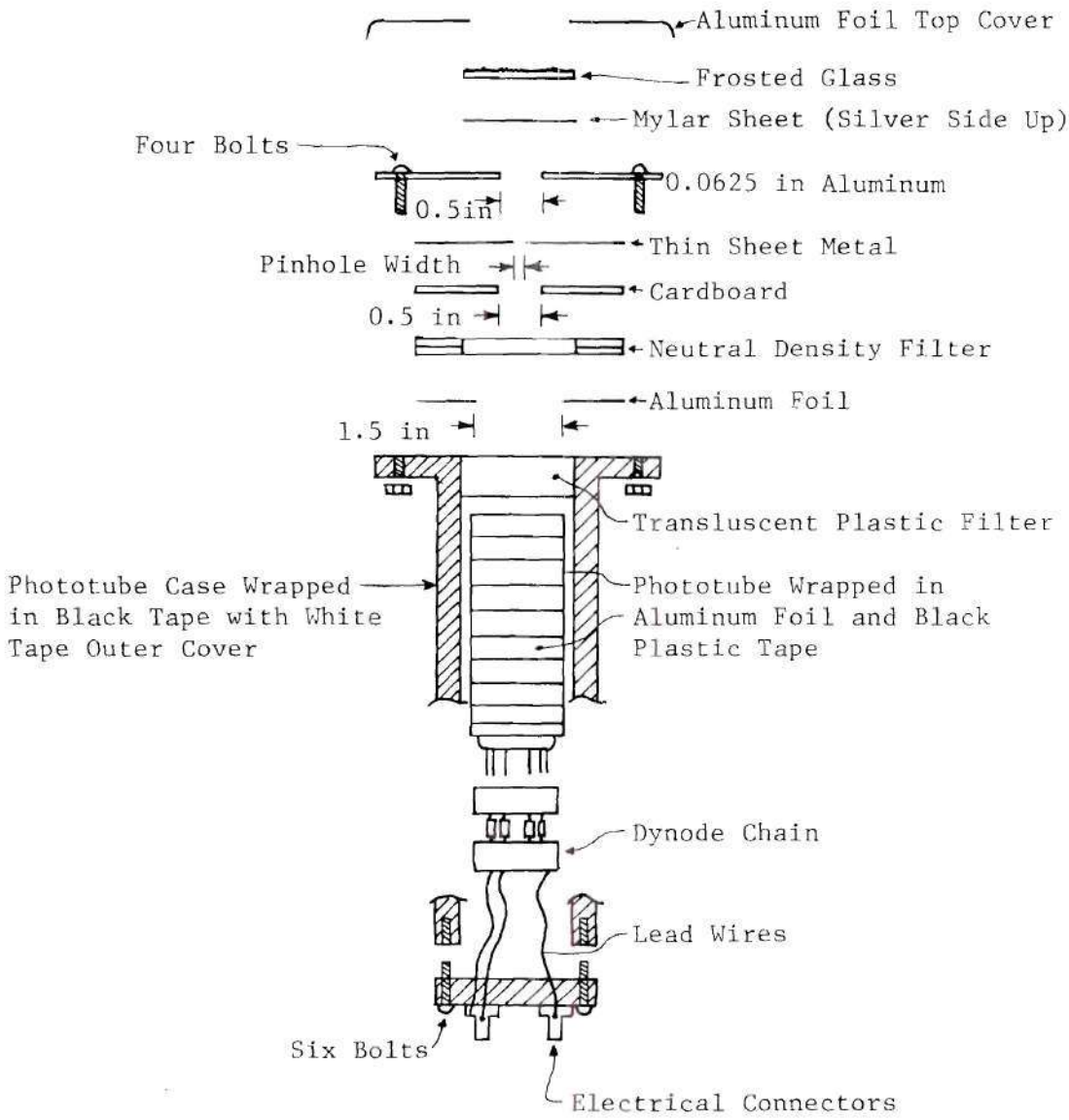

Figure 41. Detail of Photomultiplier Tube

the angle of incidence is from a perpendicular to a given medium, the larger will be the percentage of incident radiation reflected from the medium. Similarly, the less will be the percentage of incident radiation transmitted through the medium. For a phototube placed perpendicular to the focal plane, it can be seen in Figure 24, that a greater percentage of incident radiation reflected from the tangent slat will be transmitted through the tube's filter and be detected, than incident radiation reflected from the edge slats.

The phototube must produce a constant output current for radiation of constant intensity no matter what its angle of incidence. This will allow the phototube to measure a constant percentage of both direct solar radiation which is incident at an angle perpendicular to the phototube's end window (hence little reflection) and the concentrated radiation at the focal plane which will be incident on the end window of the phototube over a range of angles (hence varying reflection under normal conditions). To accomplish this, radiation incident at any angle on the photomultiplier tube, must have an equal change of going through the pinhole and striking the phototube's cathode. The solution to this problem is shown in Figure 42. A frosted piece of glass was laid on top of all the filters and pinhole.

Theoretically, since the frosted upper surface of the glass window should reflect isotropically, it would also transmit isotropically a constant percentage of incident radiation no matter what its angle of incidence on the window. This constant transmitted percentage of radiation would have an equal change of going through the pinhole. This would be true for incident light hitting any single

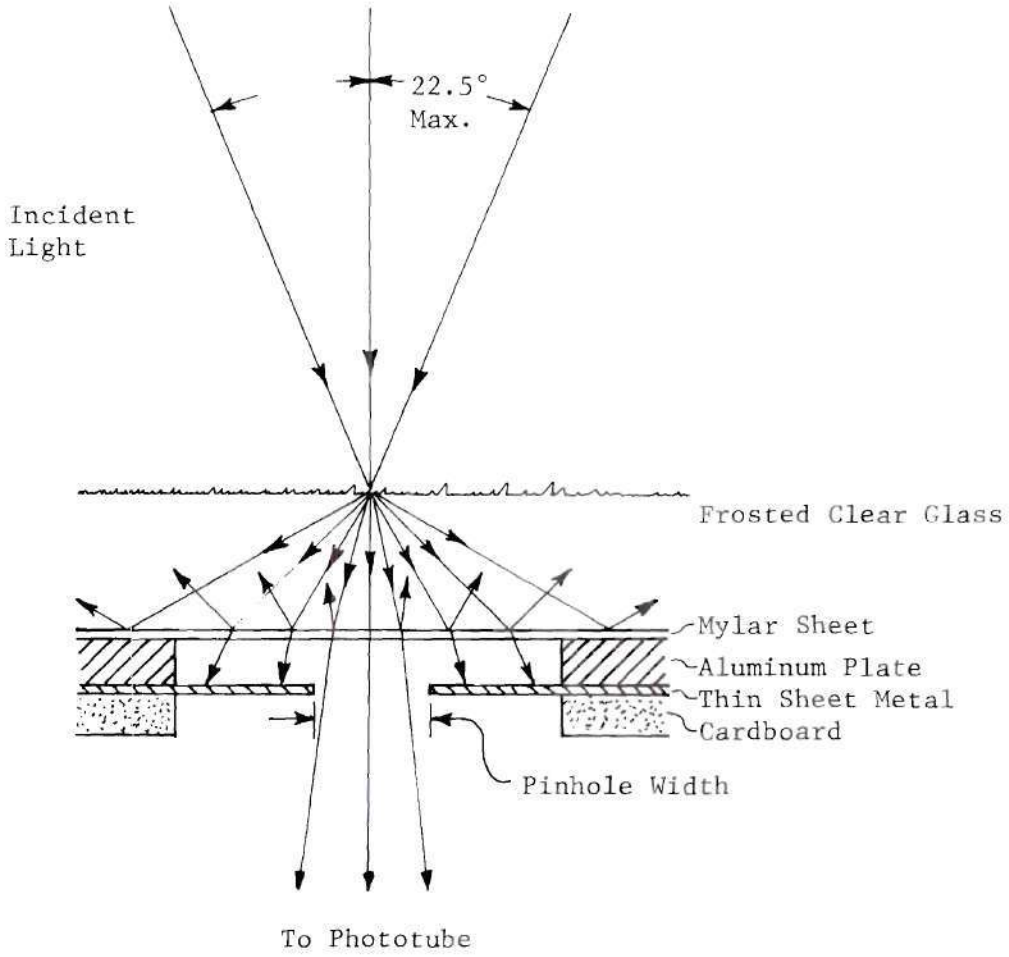

Figure 42. Frosted Glass Front Window

point on the frosted glass with any angle of incidence. As a result the phototube would detect a constant amount of radiation from a ray of light of constant intensity with any angle of incidence. In reality, the actual reflection and transmission should be very close to the theoretical isotropic assumption since the maximum angle of incidence on the phototube for this particular fixed mirror concentrator with θ_{in} = 90 degrees, as measured from the perpendicular, is only 22.5 degrees as shown in Figure 42.

Scanning Mechanism

As mentioned previously, the phototube was mounted on a scanning mechanism which moved the tube across the focal plane to obtain a record of the radiation intensity. This mechanism consisted of a modified optical scanner, a variable speed motor control, and an automatic reversing device.

The optical scanner of unknown brand originally consisted of a heavy multipartitioned aluminum beam on which were mounted an aluminum guideway and D.C. electric motor. The motor was connected to a threaded shaft which ran through a platform that sat in the guideway. When the motor turned the shaft, the platform would move along the guideway. A piece of piano wire with stops clamped on each end was fitted through the platform to detect when the platform reached either end of the guideway. At this point the piano wire was pushed or pulled by the platform, tripping a reverse sensor switch which activated the automatic reverser to reverse the direction of the platform along the guideway. When the platform reached the other end of the guideway, the reversing action was repeated. A variable speed motor control set

the scanning speed at any desired level. This level was held constant for varying loads on the motor by regulating circuitry in the control. The scanning platform could cover a distance of 7.5 inches before reversing. This distance was more than enough to record the width of the focal image at the focal plane.

The optical scanner was modified for this project to meet the special requirements placed on it. The scanner was mounted on the cross pipe and had the capability to be positioned at any point desired along the cross pipe. To decrease the weight of the scanner as much as possible, the heavy aluminum beam was replaced by an aluminum channel of the same type used for the mirror slats. The distance from the motor to the guideway was lengthened with a drive shaft extension to balance the whole mechanism about the cross pipe to which it was mounted. The platform was modified to accept the mounting of the phototube with a screw type adjustable steel band. The whole mechanism was then turned on its side so that the mounted phototube would face the focal plane. A clamping device was then added so that the scanning mechanism could be easily mounted or removed from the cross pipe through the use of four screws. Once mounted, tightening a single set screw would lock the scanning mechanism in any position on the cross pipe. Handles for use in maneuvering the mechanism and a bubble level which could be rotated to any angle were then added as shown in Figures 43 and 44. The bubble level (round object in Figure 43) was used to quickly reposition the mechanism at any desired angle around the cross pipe. This will be described in detail later.

A focusing target was added to determine when the proper solar

angle had been reached. This target seen in Figure 44, consisted of two pieces of aluminum mounted on either side of the path that the front face of the photomultiplier tube housing traveled. These two pieces of aluminum were painted white with three bare aluminum lines two inches apart left in the center. In actual operation the focusing target and front face of the photomultiplier tube housing were positioned exactly in the focal plane. When the proper solar angle for testing was reached, the focused image of the concentrator was centered on the three bare aluminum lines on the white focusing target as seen in Figure 44. In Figure 44 the scanning mechanism was exactly in the midpoint of its scan across the focal plane.

When the electrical connections were made to the phototube and electric motor, the scanning mechanism was ready for operation. Listed below are the specifications for the scanning mechanism motor, motor control and automatic reverser:

Scanning Mechanism Motor

Bodine Electric Company
D.C. Motor Type NSH-12
H.P. 1/50, RPM 1725
Power Input 115 VDC, .36 A
Continuous Duty
Temperature Rise 40° C

Variable Speed Motor Control

Minarik Electric Company
Model SL 14 for Bodine Type NSH-12 motor
Power Input 115 VAC .8 A
Line fuse - 1.5 A
Control Weight - 1.75 lb.
Maximum D.C. Output
Field 115 V - .08 A
Armature 130 V - 0.25 A

Automatic Reverser

Velmex, Inc.
Model 312

Complete Equipment Set-Up

A schematic diagram of the complete equipment set-up is shown in Figure 45. All the instruments took initial power from a standard 110 Volts 60 cycles grounded outlet. The high voltage power supply then fed a high voltage low amp. D.C. current into the phototube. The output current of the phototube which was linearly proportional to the incident radiation was then fed into the ammeter which amplified the signal and fed it into the strip chart recorder. In this way a record of the incident radiation intensity across the focal plane was produced.

As shown in Figure 46, the high voltage power supply (bottom shelf), ammeter and motor speed control (middle shelf), and strip chart recorder (top shelf) were placed on a mobile cart for ease of storage when not in use. Out of sight in Figure 46 is also the automatic reverser. Listed below are the specifications for the recorder, ammeter, and high voltage power supply.

Strip Chart Recorder

Keithley Instruments
Model 370 Recorder
Range 0 - 1.0 mA DC
Power Input 120 VAC
Single Pen
Chart Speeds: .75, 1.5, 3, 6, or 12 in/hr or in/min

Ammeter

Keithley Instruments
Model 414 Micro-Microammeter

Output 0 - 5 mA
Input 0 - 10 mA
Power Input 117 VAC

High Voltage Power Supply

John Fluke Manufacturing Company, Inc.
Model 415-B High Voltage Power Supply
Power Input 115 VAC
Output 0 to 3.1 KV DC

If the phototube in its housing, is pointed directly at the sun and a measurement taken, the measurement will record all the radiation incident on the tube's end window. This incident radiation will consist of both direct and diffuse radiation. A fixed mirror concentrator cannot focus diffuse radiation at the focal plane. In order to determine the actual heat flux profile in units of incident direct solar radiation I, a device was built to measure only the direct solar radiation incident on the concentrator. This device, shown in Figure 47, consisted of a long, slender, hollow tube (1.96 inches inside diameter x 31 inches long) painted flat black inside and out, and mounted on a tripod to facilitate aiming at the sun. By aiming the black tube directly at the sun and placing the phototube at the other end, a measurement of direct solar radiation only was obtained. An observer looking through the black tube can only see the sun's disk and a minute fraction of the sky above. Practically all of the diffuse radiation, which is the radiation reflected and scattered by the atmosphere is not seen by the observer looking through the black tube. Also, diffuse radiation entering the upper end of the tube at an angle other than normal would be reflected and absorbed by the flat black paint along the tube's walls. The end result is that only direct solar radiation is measured through the tube.

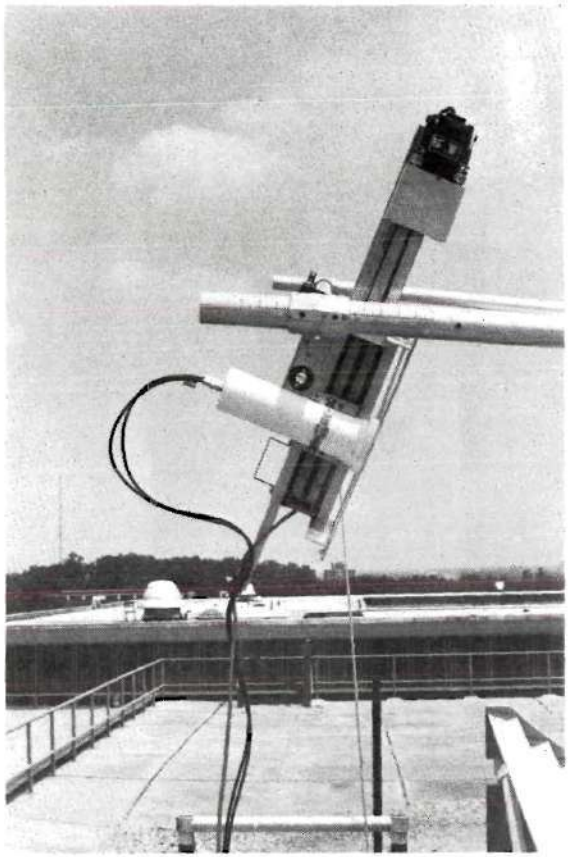

Figure 43. Side View of Scanning Mechanism and Photomultiplier Tube, Mounted on Cross Pipe

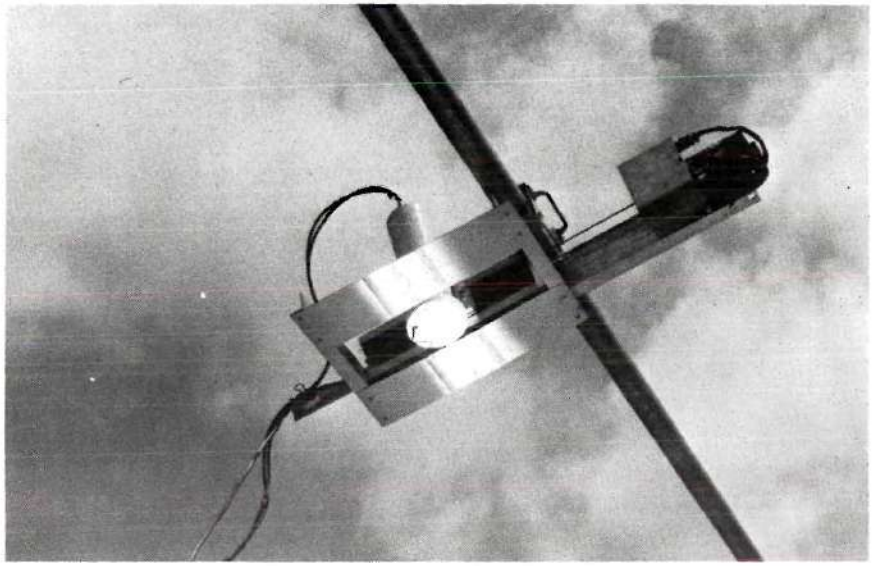

Figure 44. Scanning Mechanism in Operation with Photomultiplier Tube at the Midpoint of its Scan

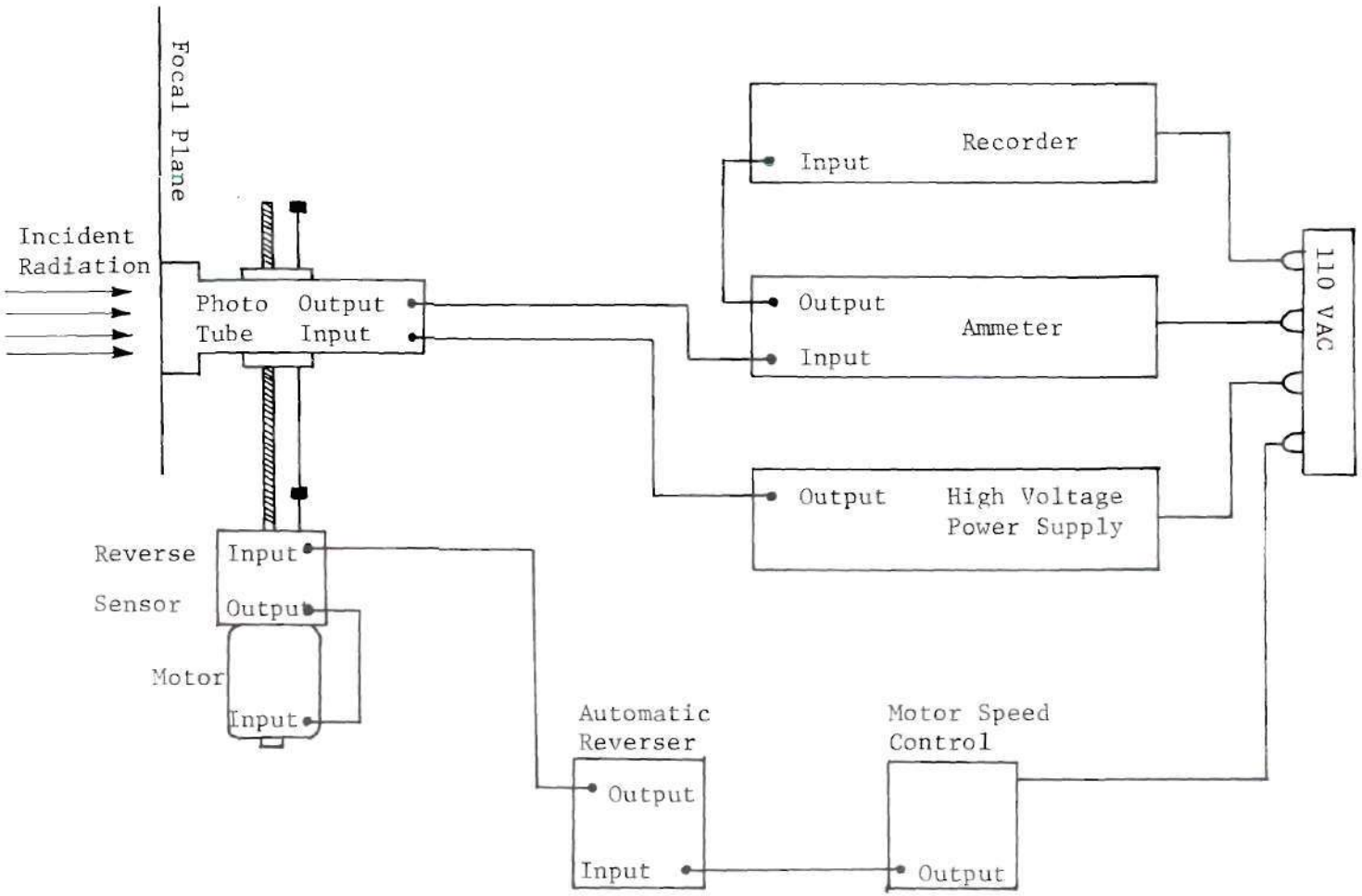

Figure 45. Schematic of Experimental Equipment Set-Up

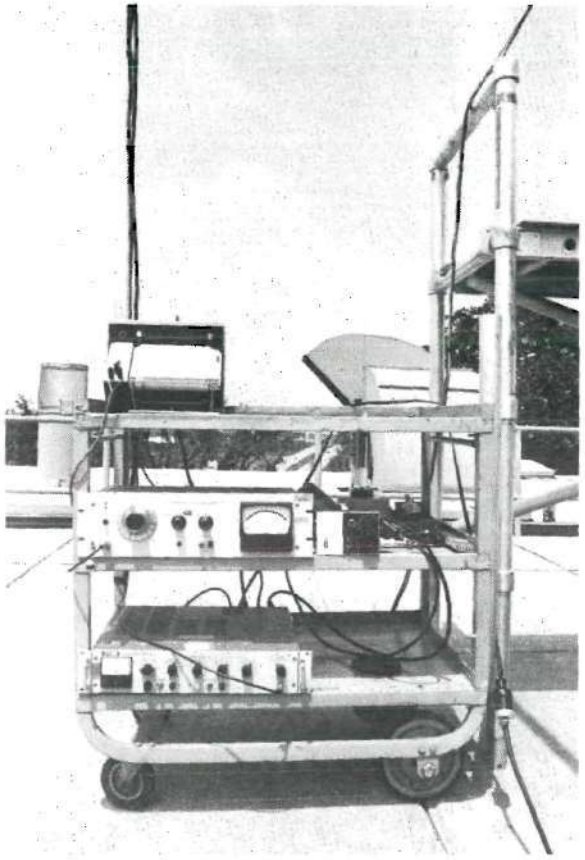

Figure 46. Equipment Cart

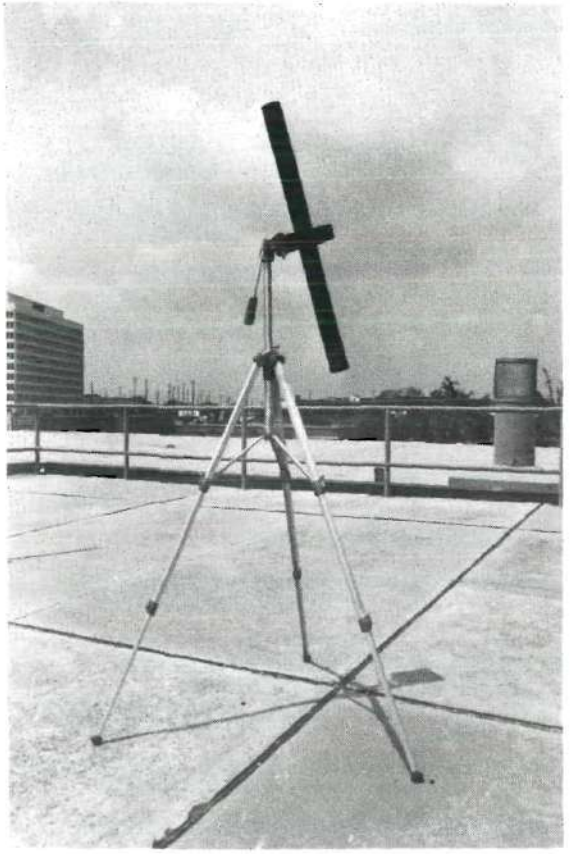

Figure 47. Direct Solar Radiation Measuring Device

The final piece of experimental equipment was a draftsman's adjustment triangle, used to set the correct pivot arm and scanner angles. Figure 48 shows the complete equipment set-up in actual operation. The direct solar radiation measuring device is at the far left. The equipment cart can be seen next to the concentrator and the scanning mechanism can be located in the middle of the cross pipe.

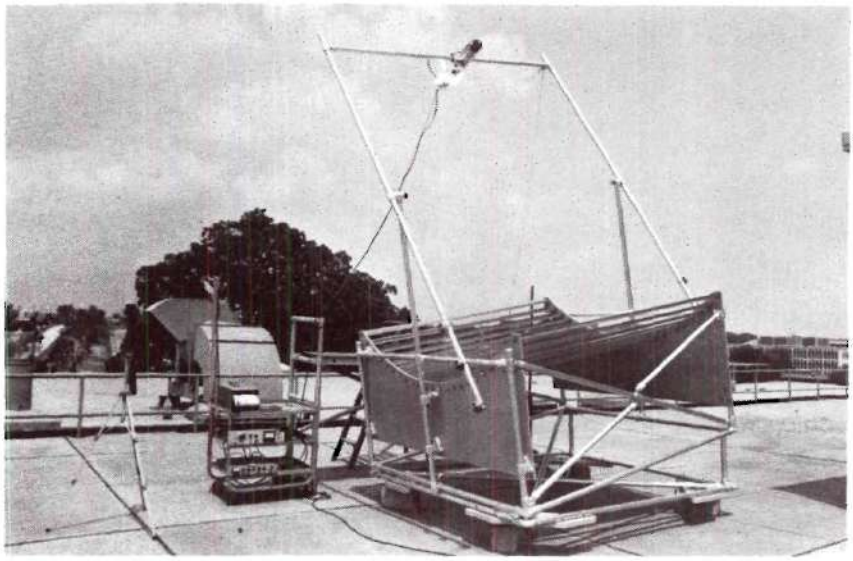

Figure 48. Complete Equipment Set-Up in Operation

CHAPTER VI

EXPERIMENTAL PROCEDURE

Initial Equipment Calibration

As mentioned previously, the phototube used in this project had a voltage and current limitation placed on it for proper operation. The first step in the experimental procedure was to determine the proper input voltage to the phototube at which all the testing would be done. The proper input voltage would insure:

1. The phototube was operating within its designed sensitivity range
2. The output current of the phototube was below 10×10^{-6} A (the maximum level for continuous operation [19])
3. Full use of the complete width of the strip chart recording scale with the ammeter scale placed on a given setting

The scanning mechanism and phototube were placed on the concentrator and intensity readings were taken with the solar angle of $\phi = 90$ degrees (solar noon position). At $\phi = 90$ degrees the edge losses of the fixed mirror concentrator designed for this project are at a minimum [13], and the incident solar radiation is at its most intense level. Therefore, the concentrated radiation as detected at the focal plane by the phototube will also be at its most intense level. By applying varying combinations of phototube input voltages and ammeter scale settings, equipment settings which met the above three limitations were established. An appropriate input voltage for the phototube was

determined to be 850 VDC. The scale factor on the ammeter was determined to be 0 - 10 μA when reading concentrated solar radiation at the focal plane and 0 - 1 μA when reading direct solar radiation or radiation reflected off a single mirror slat. The above equipment settings were utilized throughout the experimental testing.

During the initial calibration it was determined that after the high voltage power supply was warmed up, an additional warm up period of at least 30 seconds was required once the high voltage was switched to the phototube. This allowed the high voltage input to the phototube to stabilize to a constant level. During all tests, time was allowed for this warm up period before any measurements were taken.

Reflectivity Measurements

After a literature search failed to turn up the required information, an attempt was made to determine reflectivity of a mirror slat (made of ordinary rear surfaced window glass mirror section) as a function of angle of incidence of the incoming radiation for use in the theoretical calculations. The arrangement illustrated in Figure 49 was used to measure the reflectivity of a mirror slat for various incident angles of radiation. The mirror slat tested was kept outdoors until an average coating (by visual observation) of dust was deposited on its surface. Using a carpenter's adjustable level, the tube angle and mirror slat angle were set to obtain a given angle of incidence Γ'. The mirror slat was positioned so that radiation from the entire solar disk could be detected by the phototube. This was

done by visually sighting down the tube through a dark sun filter. When the mirror slat was properly positioned along the horizontal axis the reflected image of the complete solar disk could be seen through the tube. If any misalignment was present, then only part of the sun's disk could be seen.

The phototube was held at the end of the properly positioned black tube and a reading was taken of the reflected intensity level I_R. This was done by slowly shifting the phototube at the end of the black tube until a maximum reading on the strip chart recorder was obtained. The strip chart recorder and ammeter were set to zero before any measurements were taken. Next, very quickly, the black tube was aimed at the sun and a measurement was taken and recorded of the direct solar intensity I. (The method used to obtain the direct solar radiation level I, will be discussed in detail.)

The angle of incidence of the incoming radiation was obtained from the known tube angle and mirror slat angle. The mirror slat reflectivity is given by the following formula.

$$\rho = \frac{I_R}{I} \tag{1}$$

For the solar angles ϕ at which the concentrator was tested, the incoming radiation will hit any given mirror slat with an angle of incidence in the range of 20 degrees to 90 degrees inclusive. The above reflectivity test was carried out 18 times at incident angles in the above range. The data showed that the reflectivity ρ, of a mirror slat with an average coating of dust was approximately

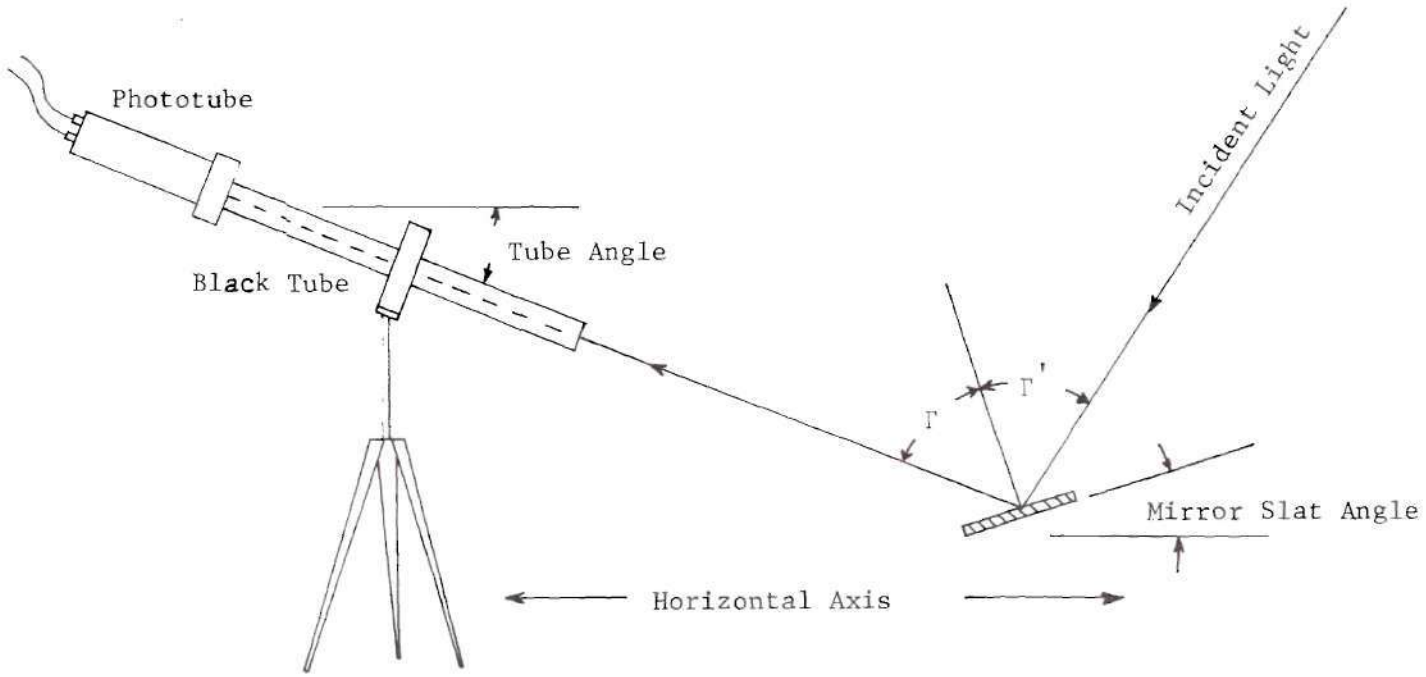

Figure 49. Mirror Slat Reflection Measurement Equipment Set-Up

constant at ρ = 85.1%.

Effect of Dust on Mirror Reflectivity

A test was run to determine the effect a coating of dust has on reducing the reflectivity of a mirror slat. The apparatus used is shown in Figure 50. A section of mirror of the type used on the concentrator was laid on the tangent slat of the concentrator and left to weather for several days. When visual observation of this mirror section determined that it had an unusually heavy coating of dust, it was removed and tested as follows.

A piece of white tape was placed across the four inch width of the mirror section near the center of its length dividing it into two halves. One half was carefully wiped with glass cleaner until it was completely free of dust. The other half was left dirty. A direct solar energy measurement was taken using the black tube. The phototube was then replaced on the scanning mechanism. The mirror section was placed in a horizontal position as shown in Figure 50 so that it reflected incident light to the center of the focusing target from its clean half only. A scan of this reflected image was made and recorded. The mirror section was then quickly moved a few inches so that the incident light was reflected to the center of the focusing target off its dust covered half. A second scan of the image arriving at the focusing target of the scanning mechanism was made and recorded. The procedure was then repeated several times by first reflecting an image off the clean half of the mirror section and then off of the dusty half of the mirror section. Finally, the phototube was removed from the

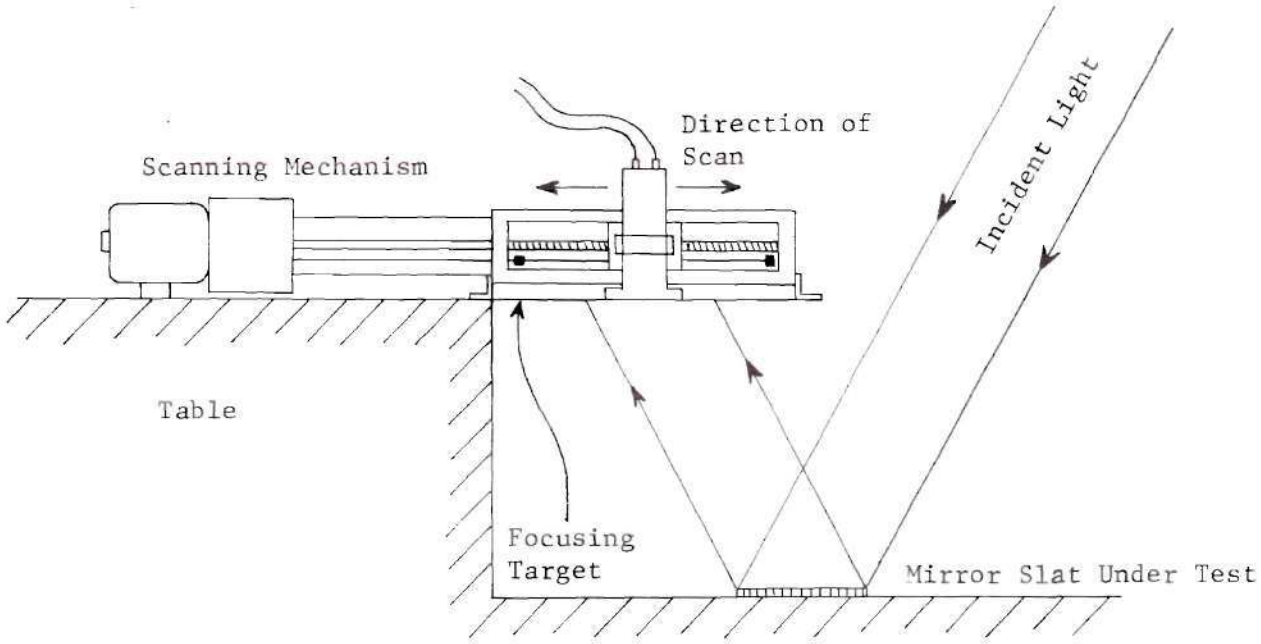

Figure 50. Dust Reflection Equipment Set-Up

scanning mechanism and a second direct solar energy measurement was taken and recorded. With the above data, a general range of the reflectivity value ρ, of a mirror slat with varying degrees of dust on it was determined.

In all of the experimental testing, two direct solar energy readings, one before and one after the test, were taken and recorded. If it was determined that there was a difference in the two intensity levels, then the data acquired during that test was discarded. This would mean that the direct radiation level had varied during the test, automatically eliminating the test's validity. This happened approximately 40% of the time.

Heat Flux Profile at the Focal Plane

Positioning of the Scanning Mechanism

The general method used to measure the heat flux profile at the focal plane is now described. In order that the focusing target of the scanning mechanism be correctly positioned exactly at the focal plane perpendicular to a line from the tangent slat, the scanning mechanism had to be positioned with a certain pivot arm distance D_p, scanner angle η, and pivot arm angle θ_p, as shown in Figure 51 for each different solar angle ϕ. This was made necessary by the design of the scanning mechanism. When it was mounted on the cross pipe, the perpendicular distance from the center of the cross pipe to the focusing target (and focal plane) was 6.05 inches. The distance from center of the cross pipe along a line parallel to the focal plane, to the center of the focusing target was 6.72 inches as shown in Figure 51.

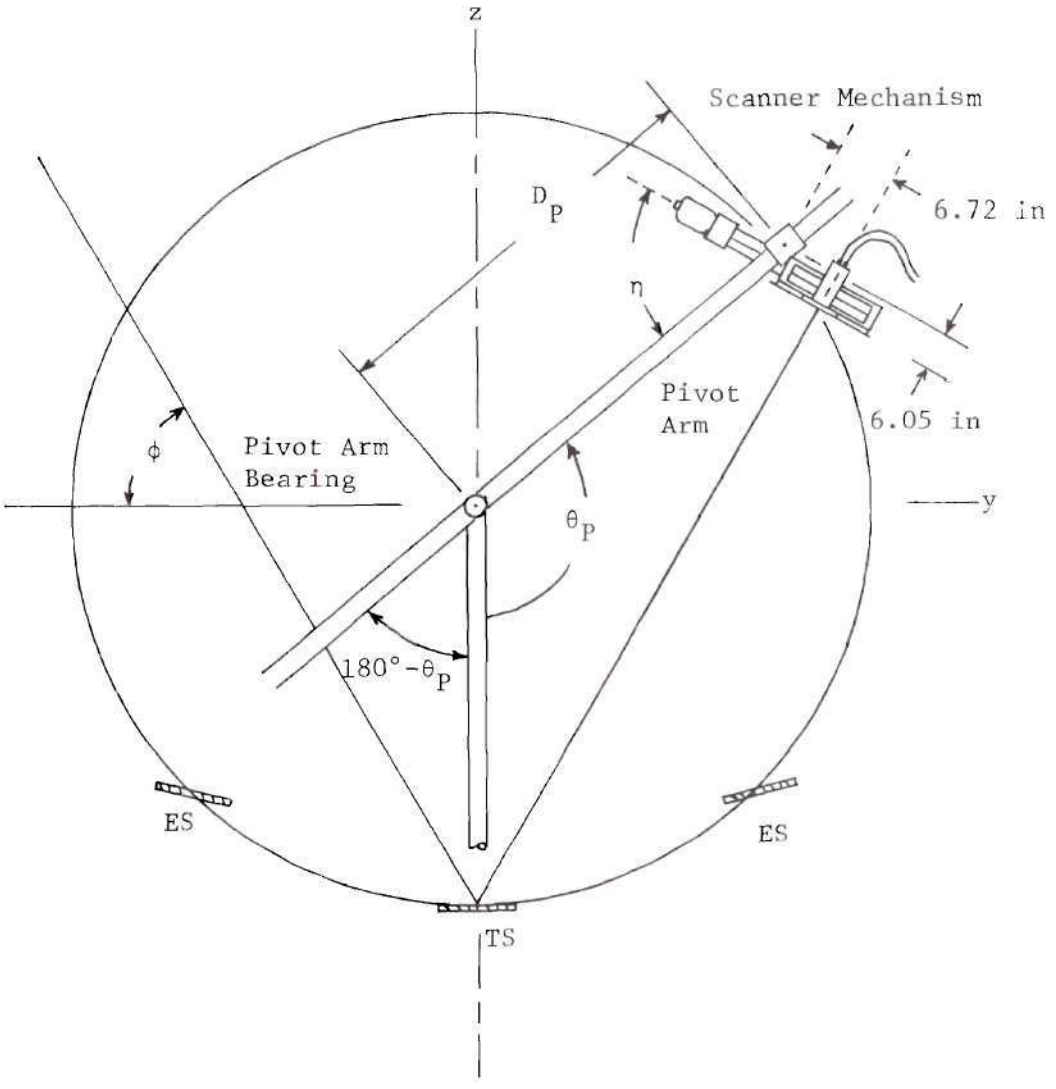

Figure 51. Positioning of Scanner Mechanism

Table 3 shows the various D_P, η, and θ_p values needed at each solar angle θ.

Table 3. Scanning Mechanism Position Settings

ϕ degrees	θ_P degrees	D_P inches	η degrees
27.5	63	61.32	35
33.75	75.5	62.34	41.5
45	98	64.08	53
56.25	120.4	65.79	64
67.5	142.25	67.37	74
78.75	164	68.98	85
90	185.4	70.32	96

Note, as seen in Figure 51, the solar angles ϕ in Table 3 only represent incident radiation falling on the concentrator with an angle of incidence to one side of the center line C_L. For radiation incident from the other side of the center line, the mirror images of the above scanning mechanism position settings were used.

The fixed mirror concentrator designed for this project was relatively short (8 feet). Because of this, it was oriented with its longitudinal (x) axis in the north-south direction. By tilting the concentrator about its y axis as shown in Figure 48, the focused image could be centered between the two pivot arms, minimizing the end effects described in Chapter II. However, since the sun follows a circular arc in the sky which in general does not stay in the yz plane of the concentrator, the focused image is not always perfectly centered between the two pivot arms for any given concentrator tilt. In general,

the image would be off center at sun rise, gradually become centered as the sun reached solar noon, (ϕ = 90 degrees) and finally move off center as the sun sets again. These end effects gave rise to the problem of how to specify the position along the x axis of where the scan should take place.

In comparing the theoretical heat flux profile with the experimental profile for any solar angle ϕ, an average experimental profile was needed. To arrive at this for any given solar angle ϕ several profiles were measured at varying positions along the x axis of the focal plane (axis parallel to cross pipe) and then averaged. Theoretically, these profiles should be exactly the same, however this was checked experimentally for this concentrator. This process took several weeks during which time the concentrator was tilted at various angles to keep the focused image centered between the pivot arms. During the duration of these tests the focused image shifted up and down the length of the cross pipe many times.

To be perfectly correct, in order to exactly duplicate a particular scan at a given solar angle ϕ (measured in the yz plane) and a given position along the cross pipe, the solar angle ϕ_x as measured in the xz plane would also have to be duplicated (Figure 9). If this were easily done then by simply specifying ϕ, ϕ_x, and the position along the cross pipe as measured from some references point on it, a test at any given scan position could be repeated. Also, scans could be taken at planned positions along the x axis of the focal plane which would effectively cover the focal plane for use in determining an average heat flux profile at the given solar angle ϕ.

The solar angle ϕ_x not only changes hourly, but also seasonly as well at different rates. Add to this the fact that clear weather conditions cannot be depended on for any given day of experimental testing in Atlanta, it can be seen that a given ϕ-ϕ_x combinations would be very difficult to duplicate without being able to rotate the concentrator about its z axis (as originally planned, but made impossible by uneven, rough ground conditions). Therefore, a new reference system was arrived at to locate the scanning positions along the x axis of focal plane of the concentrator.

The reference point used was the midpoint of the focused image at the focal plane. From the discussion above it can be seen that this reference point would shift along the x axis of the focal plane depending on the angle ϕ_x. To locate this reference system, the cross pipe was marked (in inches) starting at its center and extending both directions. The northern half of the cross pipe was defined as the top portion, the southern half as the bottom portion, In this way any location on the cross pipe could be specified as T21 or B16 etc.

The length of the concentrator is approximately eight feet. For light incident with a value of ϕ_x close to 90 degrees, (the situation where the concentrator is properly tilted as in Figure 48) the focused image on the focal plane will also be approximately eight feet long. If the focused image is off center, one of its ends will extend past an end of the cross pipe, and the other end will be located on the other half of the cross pipe at a specific numbered location. Knowing this location, one is able to determine how far up or down on the cross pipe the focused image has shifted. With this information, the location of

a particular scanning position along the x axis of the focal plane can be specified with respect to the center of the focused image by utilizing the numbers on the cross pipe.

It should be pointed out that the reference system is not exactly correct. That is, reflected light from a certain point on each mirror slat will determine the center of the focused image on the focal plane at a given values of ϕ and ϕ_x. The center of a focused image at the focal plane will be determined by reflected light from different points (from those above) on each mirror slat if the light is incident at the same value of ϕ, but a different value of ϕ_x. This reference system is, however, only used to mark locations along the x axis of the focal plane that essentially cover the various combinations of reflections from the concentrator for use in finding the average heat flux profile for a given solar angle ϕ. Since the value for ϕ_x will be relatively close to 90 degrees during all of the experimental tests, the difference mentioned at the start of this paragraph will be small enough so that the defined reference system will serve its intended purpose.

Direct Solar Energy Measurement

The method used to measure the direct solar intensity level I is now discussed. After completing a scan at the focal plane, the high voltage power supply to the phototube was cut off and the electrical connections at the phototube disconnected. The phototube was then quickly removed from the scanning mechanism by loosening the adjustable band holding it, and the electrical connections re-connected. The high voltage power supply to the phototube was then turned back on and given the 30 second warm up to stabilize. The

ammeter at this time was also changed from 0 - 10 μA to 0 - 1 μA scale factor. During this 30 second time period the direct solar radiation measuring device was aimed directly at the sun. When this was accomplished no shadow caused by the top of the black tube could be seen on the square block connecting the tube to the tripod (Figure 47).

Next, the ammeter and strip chart recorder were checked for a zero reading. The phototube was then picked up by hand and held approximately 1/8 inch from the end of the black tube as shown in Figure 52. When the black tube was aimed directly at the sun (thus receiving all of the direct and essentially no diffuse solar energy) the sunlight falling on the front face of the phototube housing through the black tube formed a clear, sharp circle. If the black tube was not aimed directly at the sun, then this image would have some or all of its circular edge appear blurred. By watching this image on the front face of the phototube housing, the black tube was kept pointed directly at the sun. Finally, the strip chart recorder was turned on and the phototube shifted slightly until a maximum reading was obtained and recorded. After this, the power supply to the phototube and the strip chart recorder were switched off. The entire process described above, from the time the high voltage power supply to the phototube was first turned off, until the measurement was completed, took about 1.5 minutes.

It should be pointed out that in shifting the phototube at the end of the black tube, very little change in intensity was recorded on the strip chart recorder.

Figure 52. Measuring Direct Solar Intensity Level

Experimental Average Heat Flux Profile

The first step in obtaining an experimental heat flux profile was to position and level the concentrator. This was done by setting the concentrator in a north-south direction on top of concrete blocks. A carpenter's level was used to insure that the y axis of the concentrator was horizontal. Next, the scanning mechanism was mounted on the cross pipe and the six counter balance weights were adjusted on the two pivot arms. The concentrator was then tilted to the proper angle to center the focused image at noon between the two pivot arms. This was done by fitting the proper length tilt pipes as shown in Figure 15 in the fittings on the back of the aluminum frame.

The aluminum scaffold and upright metal pipe were positioned as shown in Figure 53. When the cross pipe and pivot arms were rotated down as far as they would go, the tip of one pivot arm fit into the top end of one upright pipe in the scaffold, and the tip of the other pivot arm fit into the top end of the upright metal pipe. (Seen as a slender black pipe directly under the tip of the far pivot arm in Figure 53) When the cross pipe was held down and the two pivot arm tips touched their respective uprights, this was defined as the locking position. The height of the upright metal pipe was adjustable. It was properly adjusted so that the two pivot arms and cross pipe were all in the same plane when placed in the locking position. The concentrator was now ready for testing.

The pivot arm distance was set for the given solar angle to be tested as shown in Figure 43. The cross pipe was mounted on the two pivot arms by two simple set-screw fittings which could slip up and

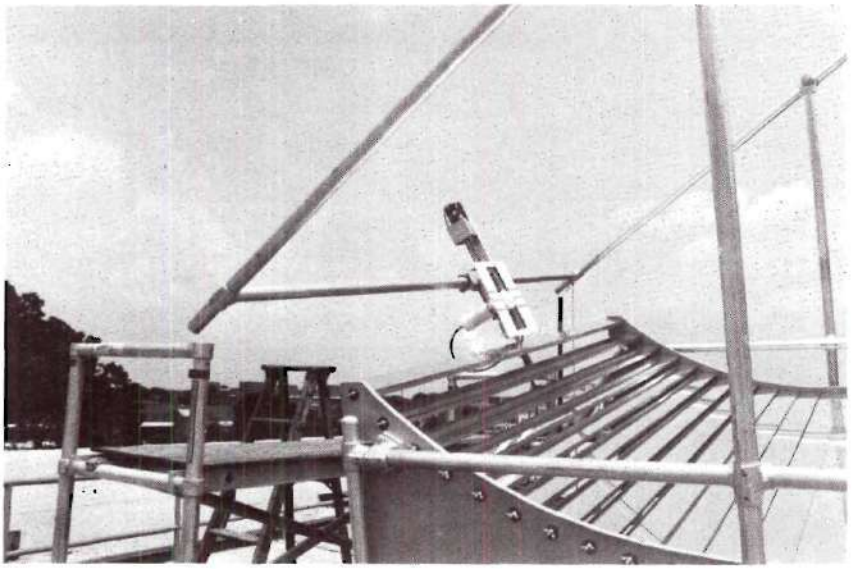

Figure 53. Concentrator Locking Position

down on the pivot arms. The proper pivot arm distances as measured, from the center of the reference circle to the edge of the slip fitting, were marked on the pivot arms (Figure 43). By loosening the two slip fitting set screws, the cross pipe could be moved up or down on the two pivot arms and then locked at the correct pivot arm distance D_P. This was done in the locked position to insure that the cross pipe and pivot arms would remain in the same plane.

Next, with the pivot arms still in the locked position the scanning mechanism was set at its proper scanner angle η, and first test position along the cross pipe (which would later be translated to the position relative to the center of the focused image on the focal plane). The scanner angle was set by visually sighting down the plane of the two pivot arms with an adjustable triangle set to the proper angle. With the setscrew on the scanning mechanism slightly loosened, the mechanism was tilted about the cross pipe until the proper angle was reached. The setscrew was then retightened. The bubble level (round object in Figure 43) on the scanning mechanism was then rotated until the leveling bubble was centered in its glass vial. Using the bubble level, the scanning mechanism could be quickly moved and reset at another position along the cross pipe. This was done by placing the pivot arms in the locked position and then moving the scanning mechanism along the cross pipe to the new position. By rotating the mechanism about the cross pipe at the new position until the leveling bubble was centered, the proper scanner angle η, could be duplicated.

Next, the proper pivot arm angle θ_p was set by rotating the pivot arms while visually sighting down an adjustable triangle set at the junction of the pivot arm and upright support. When the pivot arm angle became greater than 90 degrees, the angle between the upright support and the other end of the pivot arm ($180 - \theta_p$) was used as shown in Figure 51. With the proper pivot arm angle set, a set screw in the pivot arm bearing was turned, locking the cross pipe at the proper position. At this time there was a pause until the sun moved into the proper solar angle ϕ. This would be the position when the sun's focused image was centered on the scanning mechanism's target. During this time the equipment was turned on and checked out.

It should be mentioned that before the tests were made the scanning speed of the scanning mechanism and the paper speed of the strip chart recorder were synchromized. This was done, using a stop watch, by adjusting the scanning speed with the variable speed motor control until it matched a convenient scale on the strip chart recorder. The speed finally arrived at was one inch of paper travel to four inches of scan with the paper speed set at 12 in/min.

By observing the focusing target on the scanning mechanism, the focused image could be seen slowly moving into the three centering lines signifying that the sun had reached the proper solar angle ϕ (Figure 44). When one edge of the focused image first touched an outside line on the focusing target the pivot arm bearing set screw was loosened and the pivot arms rotated down to the locking position. The phototube was removed from the scanning mechanism and a direct solar intensity reading taken as described previously. The phototube

was then replaced and the pivot arms returned to the appropriate pivot arm angle using the adjustable triangle. After the equipment was zeroed for the second time, there was approximately another minute wait until the focused image reached the centered position on the focusing target (as seen in Figure 44). At this time the first heat flux profile scan was taken.

To accomplish this, the paper feed of the strip chart recorder was turned on, and then the motor control was switched from brake to forward. The scanning mechanism moved the phototube across the focal plane and then reversed its direction returning the phototube back across the focal plane to its original position. In this way two heat flux profiles, mirror images of each other, were recorded. Upon later examination, if these two mirror image profiles were not exactly alike the data was discarded. This was a check to see if atmospheric conditions were changing at the time the particular scan was taken. Care was taken to be sure that the initial scan across the focal plane was in the same direction as the paper feed on the recorder, so that the experimental data was examined correctly in the yz plane and not reversed.

When the phototube was returned to its initial position at one end of the scanning mechanism, the motor control was quickly returned to the brake position, (note the motor had separate brake-forward and speed adjustment controls). This completed the heat flux profile scan. The pivot arms were then rotated back down to the locked position and the scanning mechanism moved to another location on the cross pipe. By centering the leveling bubble, the correct scanner angle was

repositioned. The pivot arms were then moved back up until the focusing target of the scanning mechanism had the focused image centered on it. At this time another pair of mirror image scans were taken as described previously. The scanning mechanism was then repositioned along the cross pipe and a third pair of mirror image scans recorded.

At the end of the last scan, the pivot arms were rotated until the focused image fell along the cross pipe. At this time the location of the focused image's center position on the scale on the cross pipe was recorded. Finally, the pivot arms were again rotated to the locked position and a second direct solar intensity level was recorded. This completed the measurements at the solar angle ϕ.

A maximum of three positions along the cross pipe were scanned during a single test at any given solar angle ϕ. Examining only one position at a time might have been better since obviously, the solar angle did change for the three positions tested. However, through practicing the test procedure in taking early data that was not used, the time to complete the three scans was kept below two minutes. During this time, the solar angle ϕ would change less than one degree, so this change could be neglected. Also, because the weather would not cooperate, it was soon determined that taking data at only one position along the cross pipe for each solar angle ϕ during a given day, would considerably increase the time needed to take enough data.

In repositioning the pivot arms during scans at a given solar angle, special spring loaded friction pads at each pivot arm bearing applied enough force to hold the scanning mechanism at any position desired. At the same time these pads allowed the pivot arms to be

rotated at will. This was accomplished by adjusting the spring tension in the pads and pivot arm counter balance weights.

In testing the concentrator at various solar angles care was taken to be sure that the scanning mechanism and its trailing electrical connections did not cause shadows to fall on the concentrator which would be detected by the phototube. At solar angles of 78.75 degrees and 90 degrees particular care was taken to adjust the tilt of the concentrator so that the light reflected to the phototube did not reflect from an area of the concentrator's surface close to the scanning mechanism's shadow.

Raw Data Preparation

After the appropriate heat flux profile scans were taken, the raw data was transformed into an average heat flux profile for the given solar angle in the following manner. First, the two direct solar intensity measurements, one before and one after the series of heat flux profile scans, were examined. If the two levels differed by any appreciable amount, the data was discarded. This showed that the direct solar energy level changed during the series of scans, thus making them invalid. Next for a usable set of data, each pair of mirror image scans was examined to see if they were exactly alike. If they were not, then that pair of scans (taken at one cross pipe position) was eliminated. This problem was usually due to a gust of wind moving the scanning mechanism during a scan. This would obviously invalidate a particular scan since the scanning rate would be affected by the scanning mechanism's movement.

A set of scans at a given solar angle and at different positions

along the focused image which passed the above checks was then taken and transferred to a common reference system. This involved taking each profile whose vertical scale was in units of phototube output current, and dividing it by its measured direct solar intensity level I, also in units of phototube output current. The result was a heat flux profile in units of direct solar energy I, for the given solar angle ϕ and position along the focused image.

The above set of heat flux profiles at different positions along the focused image and at the same solar angle were then superimposed on one another in the following manner to obtain an average heat flux profile. Each profile was transferred to a clear plastic sheet. A plastic sheet with one profile on it was laid on a piece of glass with a strong light behind it. Another profile on a sheet of paper was laid on top of the plastic sheet so that both profiles could be seen on the paper because of the strong light behind the glass. Keeping both horizontal axes lined up the two profiles were adjusted until they lined up as closely as possible. The bottom profile was then plotted on the sheet of paper with the other profile already on it. This procedure was repeated until the one sheet of paper had all the heat flux profiles scanned at a given solar angle ϕ, plotted together. A single profile, following the average of all the above profiles plotted together was then drawn. This was the average heat flux profile for the given solar angle ϕ.

It should be mentioned that the above method of obtaining the average heat flux profile assumed that the concentrator alignment was such that all the profiles at different positions on the x axis

would be similar for the same solar angle. Theoretically, they would be exactly alike in every detail, all beginning and all ending at the same point on the horizontal axis. In reality, the curves were slightly different. Since there was no single reference point to locate the exact point where each profile began on the common horizontal axis, (width of focal plane) the above method of fitting the curves one on top of another was utilized to arrive at an average heat flux profile.

Longitudinal Scan

The average heat flux profile was arrived at using experimental tests which covered a period of several weeks. During this time, the solar intensity level, atmospheric conditions, and dust coating on the mirrors all varied with each particular day of testing. As a result, while the above data is satisfactory for determining average heat flux profiles at each solar angle ϕ, it can not be used to examine how the heat flux profile varies longitudinally along the x axis of the focal plane, for any single solar angle ϕ. To do this, a new quick scan technique was developed.

The technique involved utilizing two people to operate the equipment. One person operated the scanning motor control and strip chart recorder while the other person repositioned the scanning mechanism on the cross pipe and then moved the mechanism so that it was centered in the focal plane for the next scan. A special arm was attached to the end of the cross pipe to shorten the time needed for centering the scanning mechanism at the focal plane. In this way 12 scans at 10 different positions along the focused image were carried out for a single solar angle ϕ, in approximately four minutes.

The direct solar intensity level was checked before and after the heat flux scans were taken. From this it was determined that the direct solar intensity level had not varied during the duration of the test. The dust coating on the mirrors and the general atmospheric conditions had obviously not varied during the test either, so it can be said that the results of this test do indicate how the heat flux varies longitudinally along the focal plane.

CHAPTER VII

RESULTS

Concentration Efficiency

The concentration efficiency, as determined theoretically and measured experimentally, is shown in Figure 54. The method used to determine the theoretical concentration efficiency was discussed in Chapter IV. To determine the experimental concentration efficiency the same method was used utilizing the experimentally determined heat flux profiles.

The solar angle ϕ as used in Figure 54 was measured from the eastern horizon for the north-south oriented fixed mirror concentrator. Essentially the sun would rise at 0 degrees and set at 180 degrees. The theoretical heat flux profiles were only calculated for solar angles from 27.5 degrees to 90 degrees. Since the fixed mirror concentrator designed for this project was symmetrical about its center line, the theoretical heat flux profiles and concentration efficiencies for solar angles between 90 degrees and 152.5 degrees were simply mirror images of those between 27.5 degrees and 90 degrees.

Edge Losses

The theoretical edge losses for solar angles ϕ from 27.5 degrees to 90 degrees are shown in Figure 55. As discussed previously, the theoretical edge losses for solar angles from 90 degrees to 152.5 degrees are simply mirror images of the edge losses between 27.5 degrees and

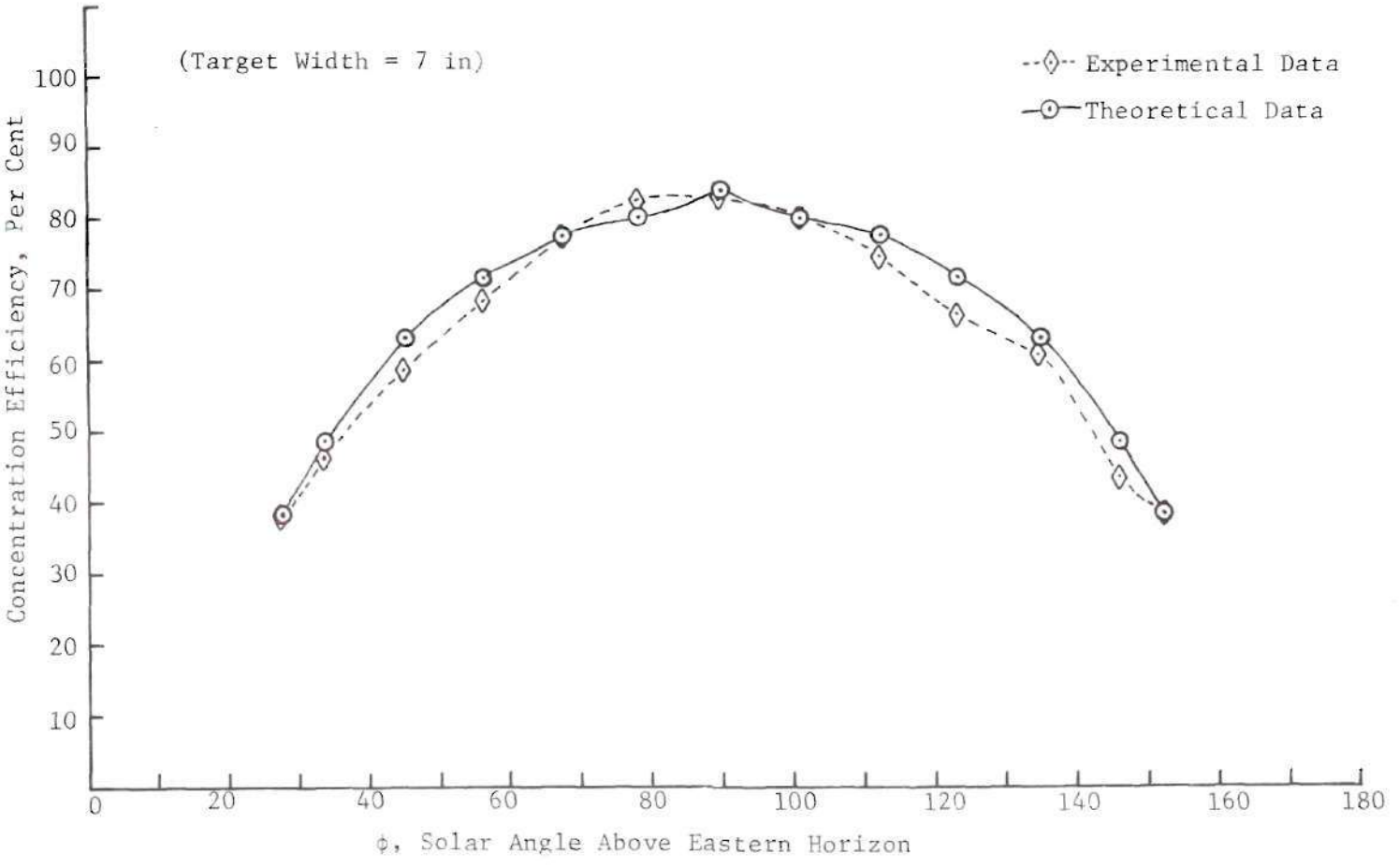

Figure 54. Concentration Efficiency

90 degrees. The method used to calculate these edge losses is discussed in Chapter IV.

For a comparison Russell's [13] calculations of the edge losses for a similar fixed mirror concentrator (symmetrical, θ_{in} = 90 degrees) are also shown in Figure 55. It should be pointed out that Russell defines the aperture angle θ_{in} as that angle extending from the center of one edge slat to the center of the opposite edge slat. Russell's calculations also assume very thin mirror slats. The aperture angle as defined in this report extends from the outside edge of one edge slat to the outside edge of the opposite edge slat. For a fixed mirror concentrator with wide mirror slats, defining the aperture angle from center to center of the edge slats would in effect, not include a significant percentage of the concentrator's surface. For a concentrator with very thin mirror slats the difference in using either definition is negligible.

Theoretical Heat Flux Profiles

The theoretical heat flux profiles for solar angles of 27.5 degrees to 90 degrees as calculated for the fixed mirror concentrator designed in this project are shown in Figure 56. The method used in calculating these profiles was discussed in Chapter IV. As mentioned previously, since the concentrator is symmetrical, the theoretical heat flux profiles, for solar angles of 90 degrees to 152.5 degrees are simply mirror images of those shown in Figure 56. The vertical scale in Figure 56 is in units of heat flux where direct solar flux incident on the concentrator has a value of one. The area under such a curve has units of flux inches.

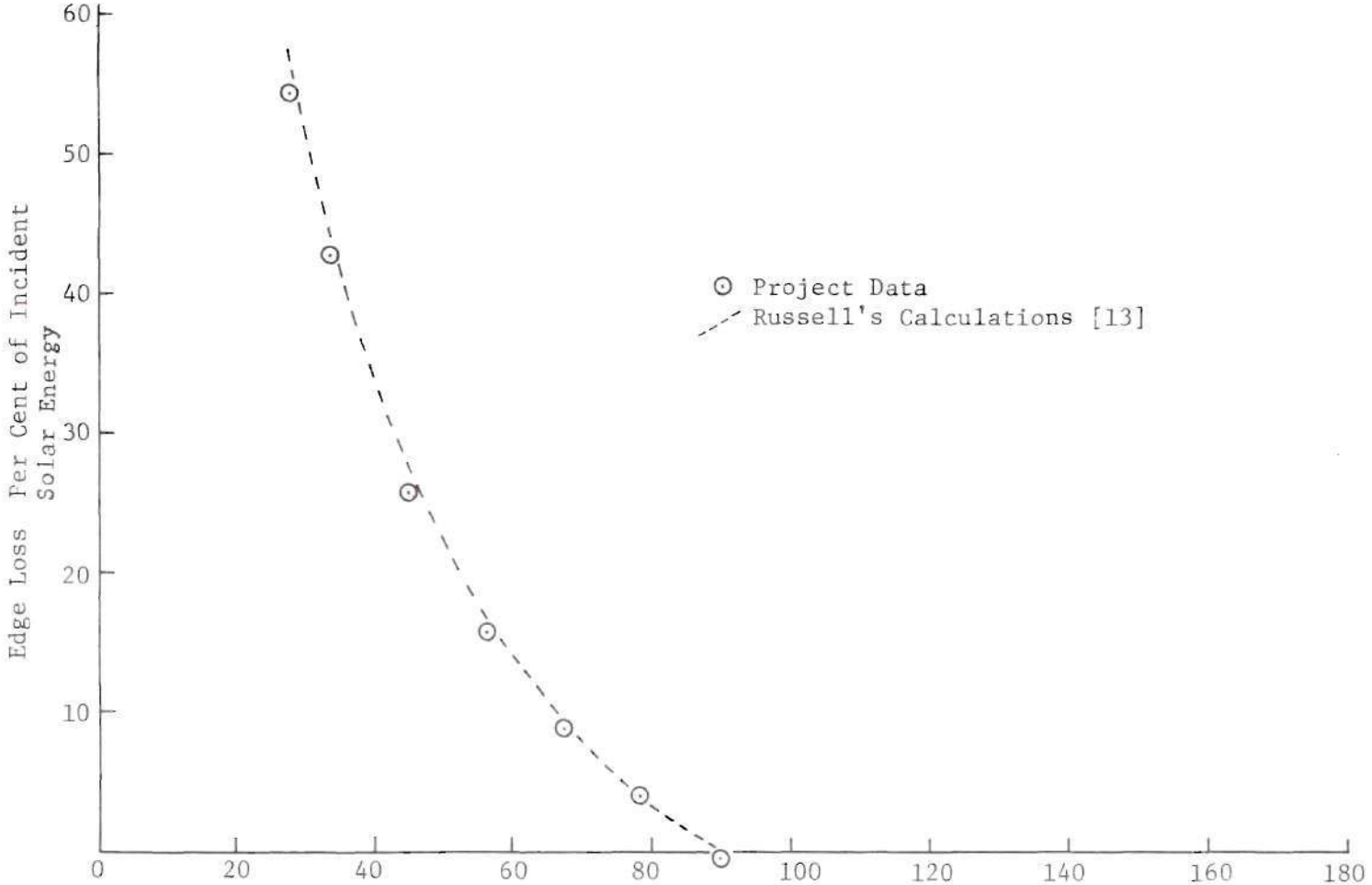

Figure 55. Theoretical Edge Losses (θ_{in}=90° TS=0°)

As discussed in Chapter IV the general shape of the heat flux profile is determined by mirror slat reflectivity and edge losses associated with a particular solar angle ϕ. For solar angles of 78.75 degrees and 90 degrees there is the additional shadow of the cross pipe which falls on particular mirror slats. The theoretical profiles were calculated assuming that the cross pipe was positioned above the concentrator as it actually was during the experimental tests. The theoretical profiles then took into account the shadow of the cross pipe which fell across the concentrator. As discussed previously in Chapter VI, in order to correctly position the scanning mechanism at the focal plane, the pivot arm was placed at the proper pivot arm angle. This determined the position of the cross pipe.

It can be seen in Figure 51, to measure the heat flux profile at ϕ = 90 degrees, there are two sets of scanning mechanism position settings mentioned in Table 3. The cross pipe can be located on either side of the center line of the concentrator as long as the focusing target of the scanning mechanism is positioned horizontally, directly over the tangent slat. In other words, in the yz plane of Figure 51, no matter how the pivot arms are rotated, the end of the scanning mechanism with the motor, will always face toward the sky, except at ϕ = 90 degrees. In this position, the scanning mechanism will be horizontal with its motor and the cross pipe on the left or right side of the center line.

Thus, the theoretical heat flux profile must be calculated based on whether the assumed cross pipe position was on the right or left side of the center line. This is because the two profiles would be

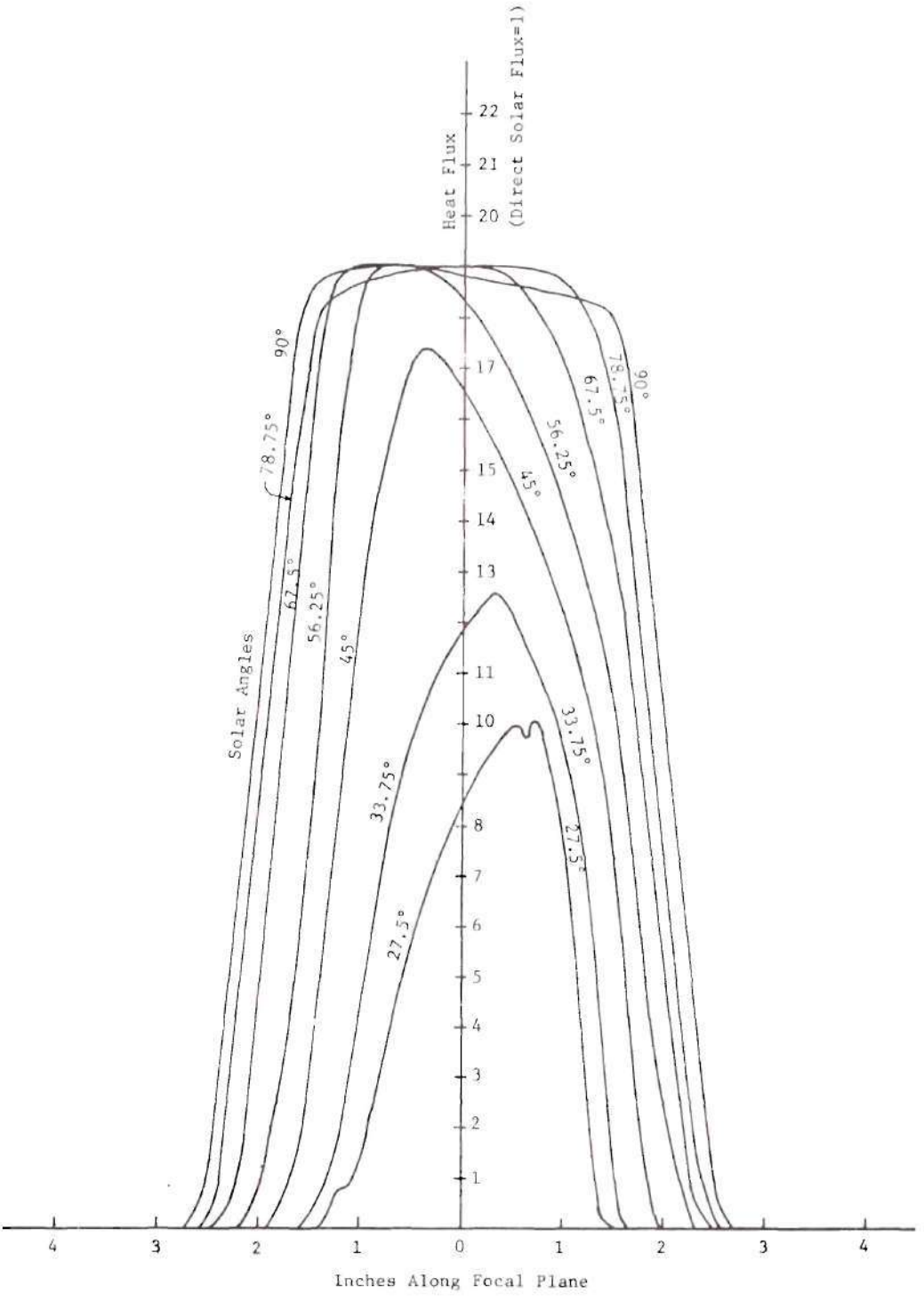

Figure 56. Theoretical Heat Flux Profiles

mirror images of each other, caused by the shadow of the cross pipe. For the purposes of uniformity all theoretical and experimental heat flux profiles for ϕ = 90 degrees were calculated and measured with the cross pipe on the eastern side of the concentrator. (This is the right side in Figure 51.)

It can be seen in Figure 56 that the shadow of the cross pipe located on the eastern side of the center line caused the theoretical heat flux profile at ϕ = 90 degrees to dip slightly on its top right side.

Average Experimental Heat Flux Profiles

The average experimental heat flux profiles are shown in Figure 57 and Figure 58. The method used to measure these profiles was discussed in Chapter VI. The vertical scale in all the profiles is in units of heat flux where direct solar flux incident on the concentrator has a value of one. The area under such a curve has units of flux inches.

Appendix A contains the experimental heat flux profiles used to determine the average profile at each solar angle ϕ.

If the average direct solar radiation falling on the concentrator is assumed to be 260 Btu/hr - ft^2 for solar angles from ϕ = 27.5 degrees to 152.5 degrees, the following estimate of the power output of the concentrator can be made. The heat collecting tube is assumed to consist of a metal cylinder with an appropriate selective coating surrounded by an evacuated glass cylinder. The metal cylinder is seven inches in diameter and eight feet long. The focused image remains

centered on the heat collecting tube. The heat collecting tube has an effective total emissivity of 0.10 and a surface temperature of 500°F. In addition, 10% of the focused radiation is assumed reflected off of the glass envelope and 5% is lost due to convection and conduction.

The average area under all of the average experimental heat flux profiles from ϕ = 27.5 degrees to ϕ = 152.5 degrees was found to be 46.92 flux-inches. This gives an average of 8133 Btu/hr focused to the eight foot heat collecting tube. When the radiation, reflectivity and convection losses are accounted for a heat collection efficiency of 59% can be calculated.

In the hypothesized system air would be the working fluid supplying heat to a steam generator. The air would receive 59% of the energy incident on the heat collecting tube or 4787 Btu/hr. If 10% is lost due to piping losses and heat transfer to the environment in the steam generator, then the working fluid of the power plant would receive 4308 Btu/hr. Assuming a Rankine cycle efficiency of 33%, then the average power output of the concentrator would be 1421.64 Btu/hr or 23 Btu/hr - ft^2 of concentrator.

Longitudinal Scan of Heat Flux Profiles

The results of the single longitudinal scan taken at ϕ = 67.5 degrees are shown in Figure 59 and Figure 60. The position along the focal plane in both figures is given in inches top (T) or bottom (B) with respect to the center of the focused image as discussed in Chapter VI. The vertical scale in Figure 59 represents the area under the heat flux profile taken at the given positions. This area is

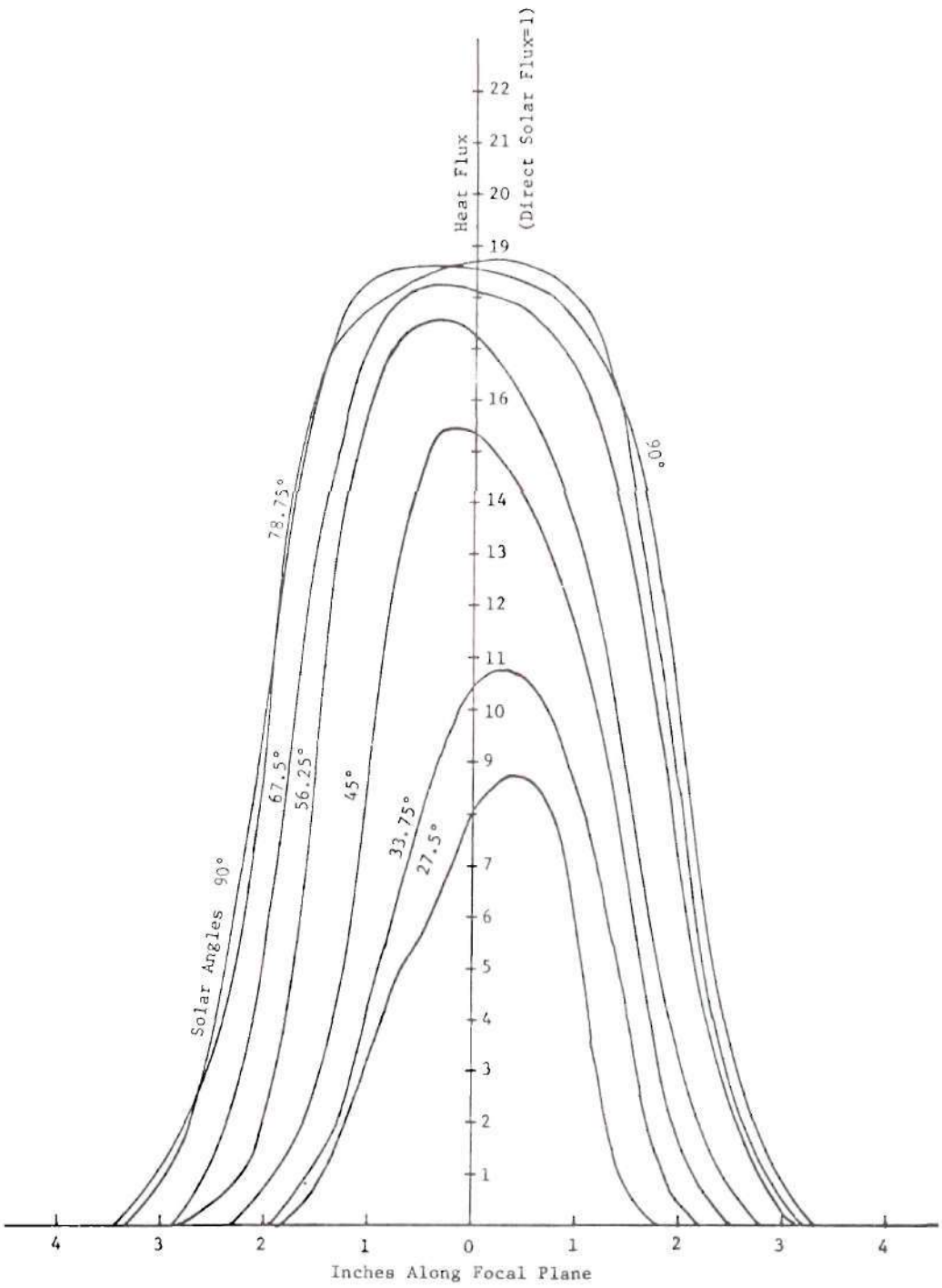

Figure 57. Average Experimental Heat Flux Profiles
ϕ = 27.5° to 90°

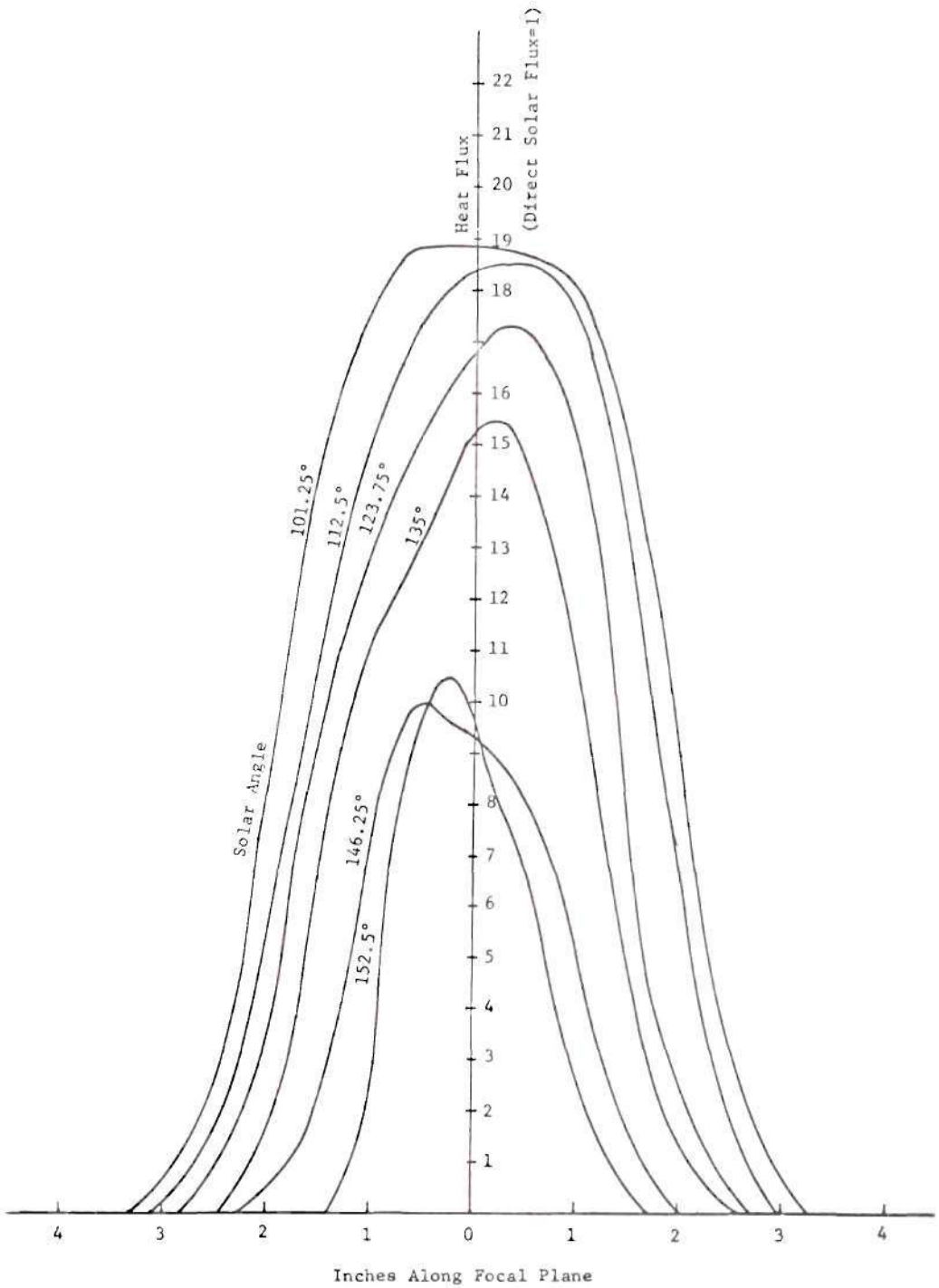

Figure 58. Average Experimental Heat Flux Profiles
ϕ = 101.25° to 152.5°

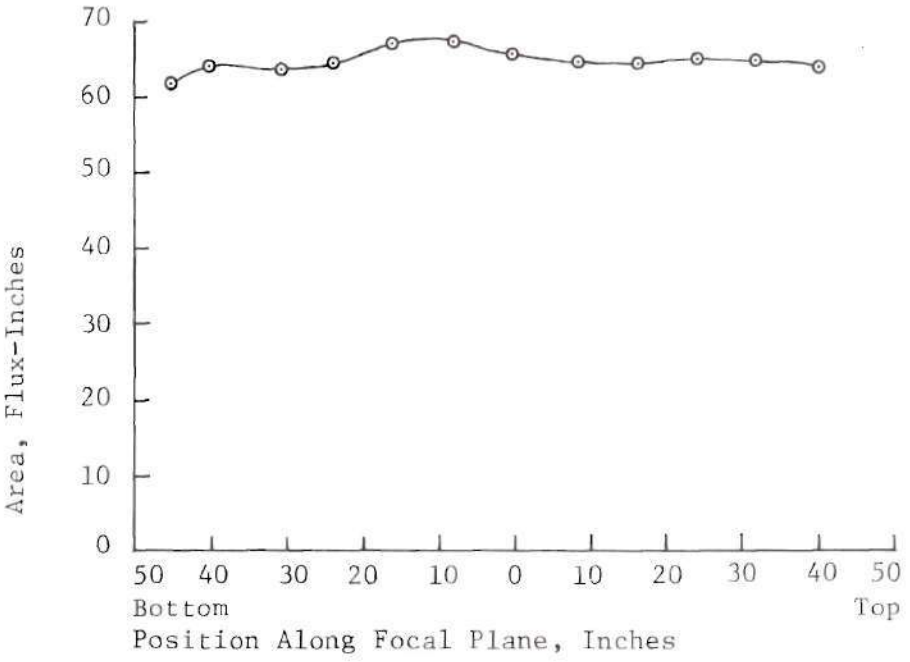

Figure 59. Area Under Heat Flux Profiles Along Focal Plane at $\phi = 67.5°$

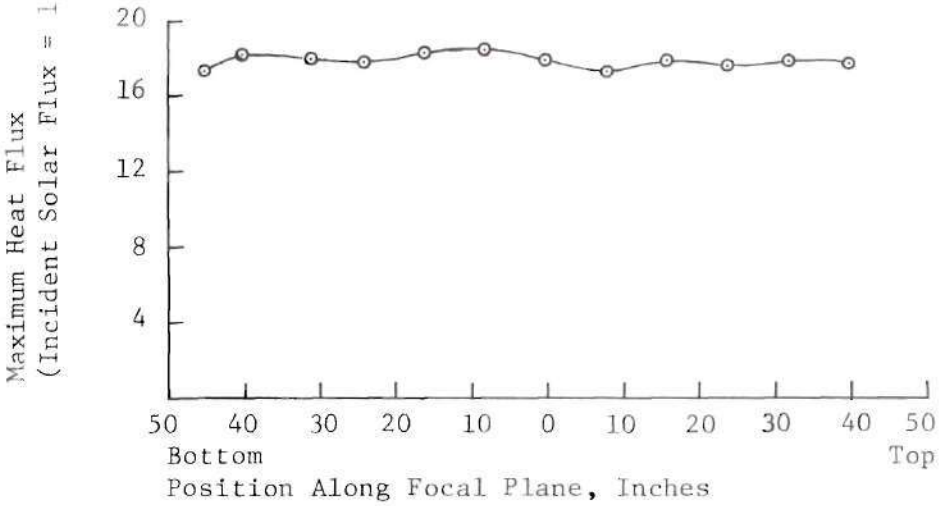

Figure 60. Maximum Heat Flux Along Focal Plane at $\phi = 67.5°$

given in units of flux-inches where the direct solar flux has a value of one. The vertical scale in Figure 60 has units of heat flux where direct solar flux has a value of one. The general shape of the profiles used to calculate and plot Figure 59 and Figure 60 is shown in Figure 57.

Reflectivity Measurements

Measurements were made to determine the relationship between the angle of incidence of incoming radiation and reflectivity of a rear surfaced mirror slat with an "average" coating of dust. The data showed no definite relationship other than a constant reflectivity value of ρ = 85.1% with a standard deviation of 2%.

Figure 61 shows the results of the measurements used to determine the effect dust has on mirror slat reflectivity. The curve on the left (clean surface) was plotted by superimposing three heat flux profiles reflected from a clean section of a four inch wide window glass mirror and measured as shown in Figure 50. The three profiles were measured by reflecting sunlight off positions on the mirror section within two inches of each other.

The curve on the right in Figure 61 was plotted by superimposing three heat flux profiles reflected and measured from a dusty, six inch long section of mirror. The layer of dust on the mirror section was determined by visual observation before the test to be unusually heavy. Because of this, the reflectivity measured from this dusty mirror section should be considered a minimum value for the rear surfaced window glass mirror slats used on the concentrator.

It should be noted that the reflectivity from a clean mirror slat as shown in Figure 61 differs very little, if any, from that determined to be the average reflectivity (for angles of incidence of 20 degrees to 90 degrees) of a mirror slat with an "average" coating of dust. The "average" coating of dust (determined by visual observation) was very little when compared to the heavy coating used in the dust reflectivity test. The difference between a clean mirror slat and one with an average coating of dust could only be visually detected from a distance of less than six feet. A heavy dust coating was very noticeable at a much greater distance.

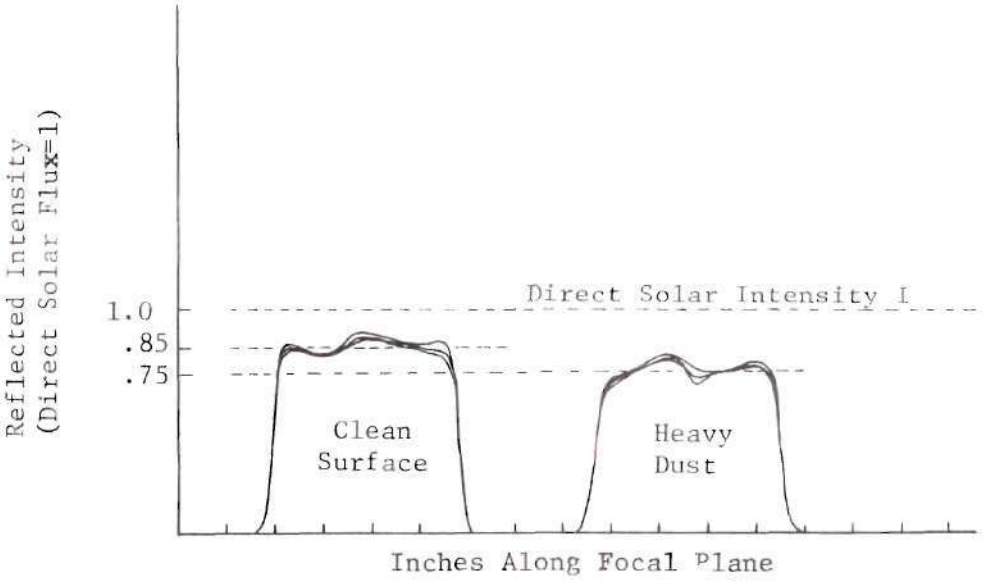

Figure 61. Reflectivity of Rear Surfaced Window Glass Mirror Sections as a Function of Surface Dust Coating, as Shown by Their Heat Flux Profiles

CHAPTER VIII

CONCLUSIONS AND RECOMMENDATIONS

Conclusions

The method used to design and build the fixed mirror concentrator out of aluminum pipe, aluminum channels, plywood and rear surfaced window glass mirror sections was successful. This method produced a working concentrator using low cost, readily available materials requiring no unusual construction techniques.

The second method of mirror alignment as described in Chapter III was successful in that theoretical and experimental concentration efficiencies at solar angles from 27.5 degrees to 152.5 degrees did not differ greatly as shown in Figure 54. This is also supported by the fact that the theoretical and average experimental heat flux profiles for the above solar angles did not differ significantly either, as shown in Chapter VII.

The experimental performance of the concentrator compared very well with the predicted theoretical performance. This is supported by the fact that the experimental concentration efficiencies for the solar angles tested did not differ a great deal from the predicted theoretical concentration efficiencies. Also as previously mentioned, the experimental heat flux profiles were very similar to the predicted theoretical profiles for the solar angles tested as shown in Chapter VII.

The longitudinal scan supported the theoretical assumption that

for any solar angle ϕ, the heat flux profile along the x axis of the focal plane should be constant. Figures 59 and 60 show that the maximum heat flux and area under the heat flux profile vary only slightly along the axis of the focal plane for a solar angle of ϕ = 67.5 degrees. The slight rise in the center of the curves in Figures 59 and 60 is probably due to the small midspan deflection in each mirror slat described in Chapter III.

From Figure 61 it can be seen that the reflectivity of the rear surfaced window glass mirror section lies somewhere in the range of 70% to 85% depending on the front surface dust coating. As mentioned in *Chapter III*, "average" dust coatings have negligible effect on reflectivity. The reflectivity value of 70% for a heavy dust coating should be noted as a special case. The conditions which brought about the unusually heavy dust coating on the reflecting surface of the concentrator were only observed one day out of the three and one half months that the concentrator was under test. These conditions were a short heavy rain followed by a dusty wind which deposited large amounts of dust on the wet surface of the concentrator. In the opinion of the author, 95% of time during which the concentrator was under test the surface dust coating was of an average level.

The dust coating on the surface of the concentrator was a function of the atmospheric conditions surrounding the concentrator. The general weather conditions contributing to an "average" coating of dust were as follows [20]. In Atlanta, Georgia, the average temperature (over a 24 hour period) for the three month testing period from April to July was 73^{o}F. During the same period the average rainfall was approximately

four inches per month. The average particulate concentration [21] was 140 mg/m^3.

Recommendations

In designing and constructing the concentrator the only major problem encountered was with the wing nut end bolt assembly used to lock the individual mirror slat into position while still permitting slat rotation about its x axis during concentrator alignment. As discussed in Chapter III, movement of the concentrator caused the mirror slats to move out of alignment because the wing nut end bolts failed to hold the mirror slats in position. It is obvious that future designers of fixed mirror concentrators should pay particular attention to the method used to position and hold the individual mirror slats so that the above problem does not occur. While future commercial fixed mirror concentrators might not suffer vibrations caused by frequent movement from one location to the other, over a period of years wind and rain might have some effect on the alignment of a large stationary concentrator. In addition, thermal cycling effects on the mirror slats might cause loss of alignment.

In the experimental tests on the concentrator only one major problem was encountered. Forty per cent of the time the results of tests had to be discarded because the direct solar intensity level changed during the test. This was probably due in part to the fact that the length of time between direct solar energy measurements was as long as two minutes. This problem could have been eliminated by utilizing experimental equipment which had the capability of taking a heat flux profile scan while simultaneously taking a direct solar energy measurement.

This would mean that the direct solar energy would be required to remain constant only for a few seconds rather than minutes for the test to be valid. Such equipment should be developed for future study of fixed mirror concentrators utilizing the experimental techniques in this report.

It would be very valuable if further work were done on the average reflectivity versus angle of incidence of incoming radiation on various low cost reflecting surfaces which must be used in an economical solar concentrator. A thorough literature study revealed very little in this area. Such economical reflecting surfaces, while being very satisfactory in overall performance, do have numerous surface imperfections which make the prediction of their average reflectivity at various incident angles very difficult. It can be seen in Figure 61 how the heat flux profile varies considerably over the width of the rear surfaced window glass section tested. Such information on the reflectivity of various economical reflecting surfaces would be very useful in accurately predicting the performance of low cost solar concentrators.

Also, the reflectivity of these economical reflecting surfaces as a function of surface dust coatings would be extremely useful. A method of quantatively describing the surface dust coating on different reflecting surfaces should be determined. Research should then be done to determine exactly how surface dust coatings affect reflectivity for various economical reflecting surfaces.

Finally, it should be pointed out that only the fixed mirror concentrating surface was examined in this report. Before a final decision on the feasibility of the fixed mirror concentrator for

particular situations is made, an entire system consisting of the fixed mirror concentrator, heat exchanging tube and heat storage system should be designed, built, and thoroughly tested. This would provide information on what the complete system was capable of and what it would cost.

In testing the complete fixed mirror concentrating system a commercial pyroheliometer should be set up near the system to obtain data on incident solar flux which could be related back to the output of the system. This information which is not generally available, along with a record of the atmospheric conditions during the experimental testing would prove very useful in the design of an efficient heat collecting tube.

The problems associated with wind should also be examined during these experimental tests. The convective losses associated with particular heat collecting tube designs for winds of various speeds and directions should be examined. The loss of collection efficiency from vibration of the pivot arms due to high wind loadings might also be examined.

APPENDIX

APPENDIX

EXPERIMENTAL HEAT FLUX PROFILES

This appendix contains the experimental heat flux profiles measured at various positions along the focal plane and at solar angles 27.5 degrees to 152.5 degrees as measured from the eastern horizon. The vertical scale is in units of heat flux where the direct solar flux incident on the concentrator has a value of one. The position along the focal plane where each profile was measured is given with respect to the center of the focused image. This position is given in inches, in either the top (T) or bottom (B) direction from the center of the focused image as discussed in Chapter VI.

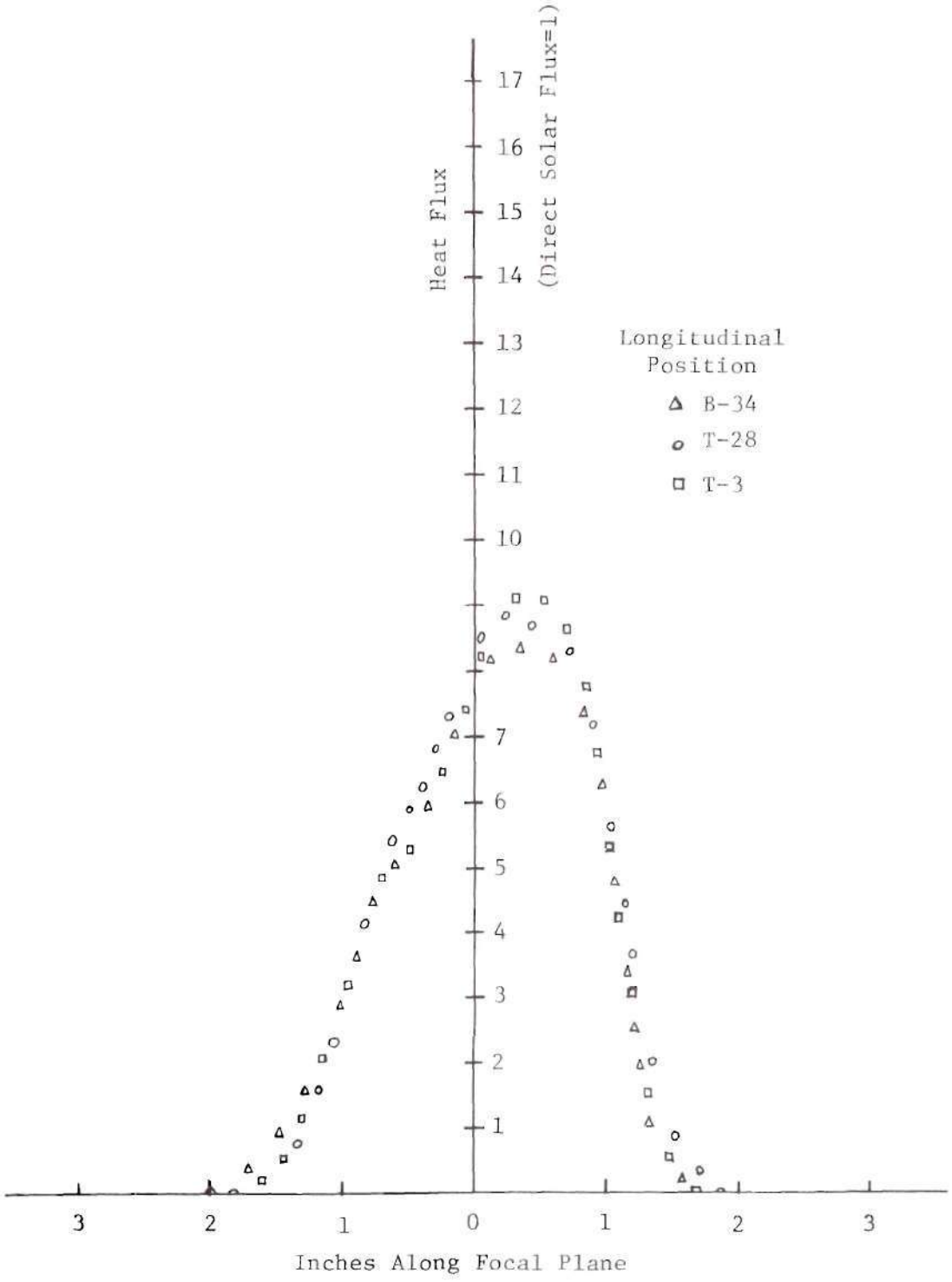

Figure A-1. Experimental Heat Flux Profiles, ϕ = 27.5°

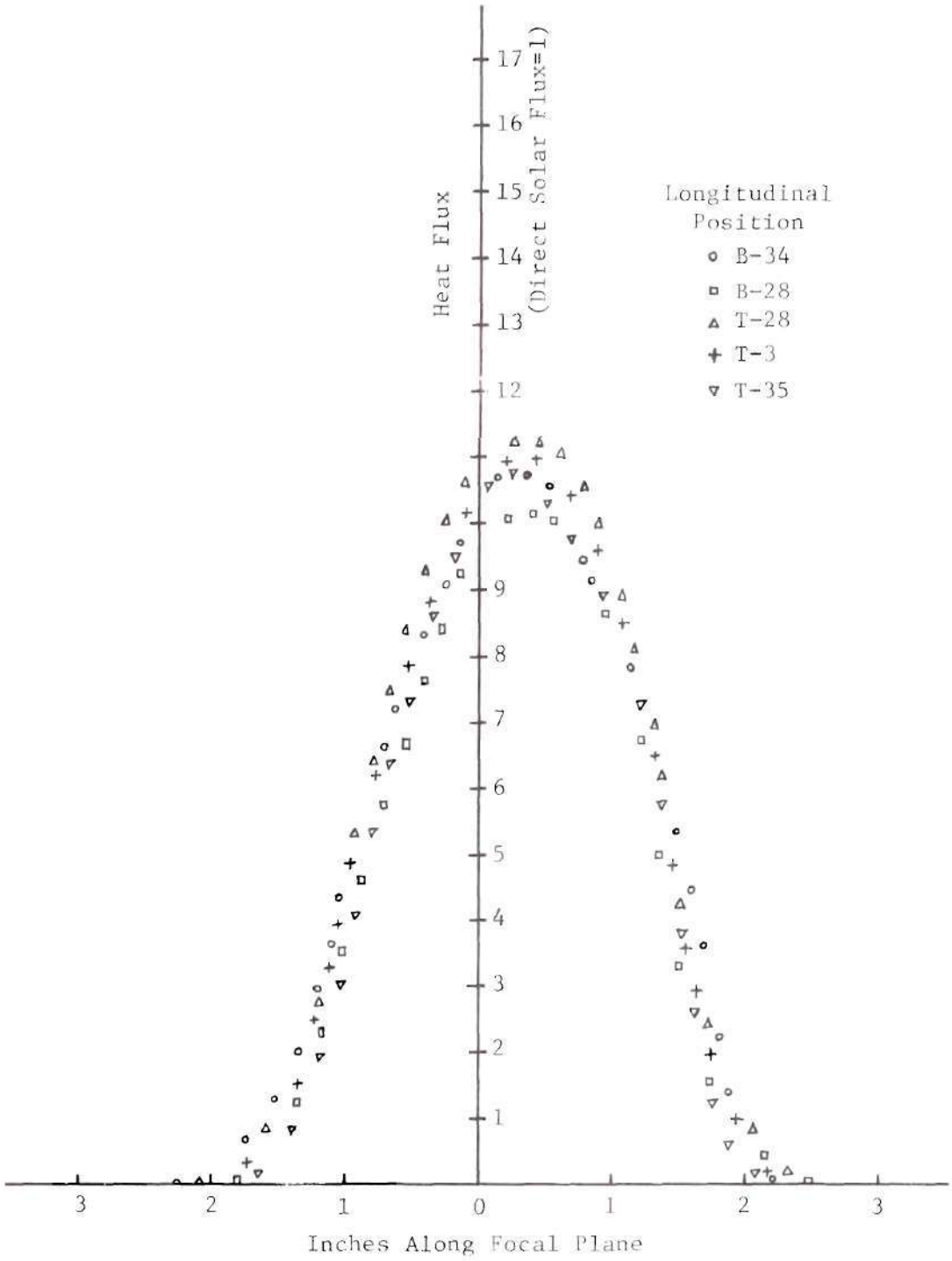

Figure A-2. Experimental Heat Flux Profiles, ϕ = 33.75°

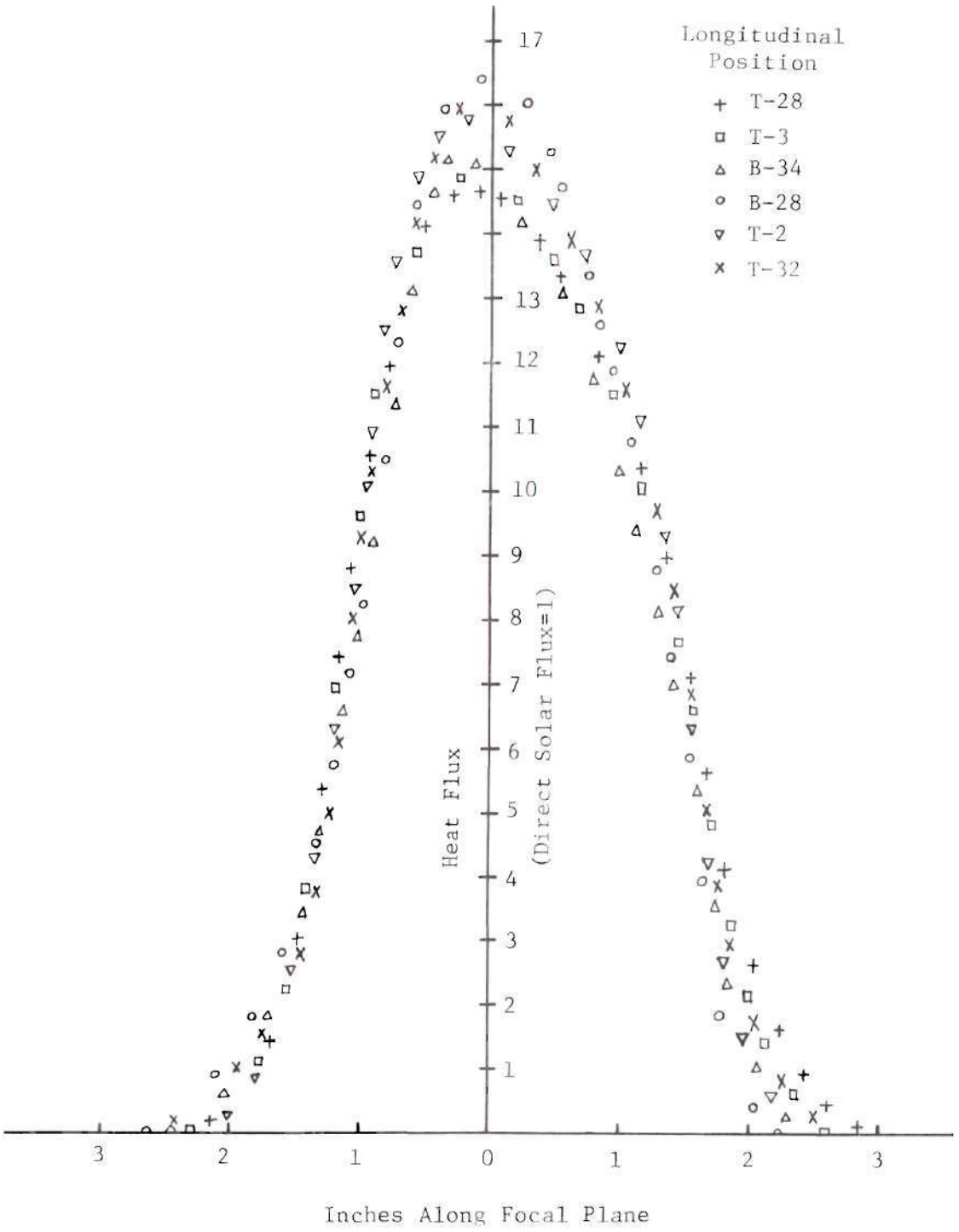

Figure A-3. Experimental Heat Flux Profiles, $\phi = 45°$

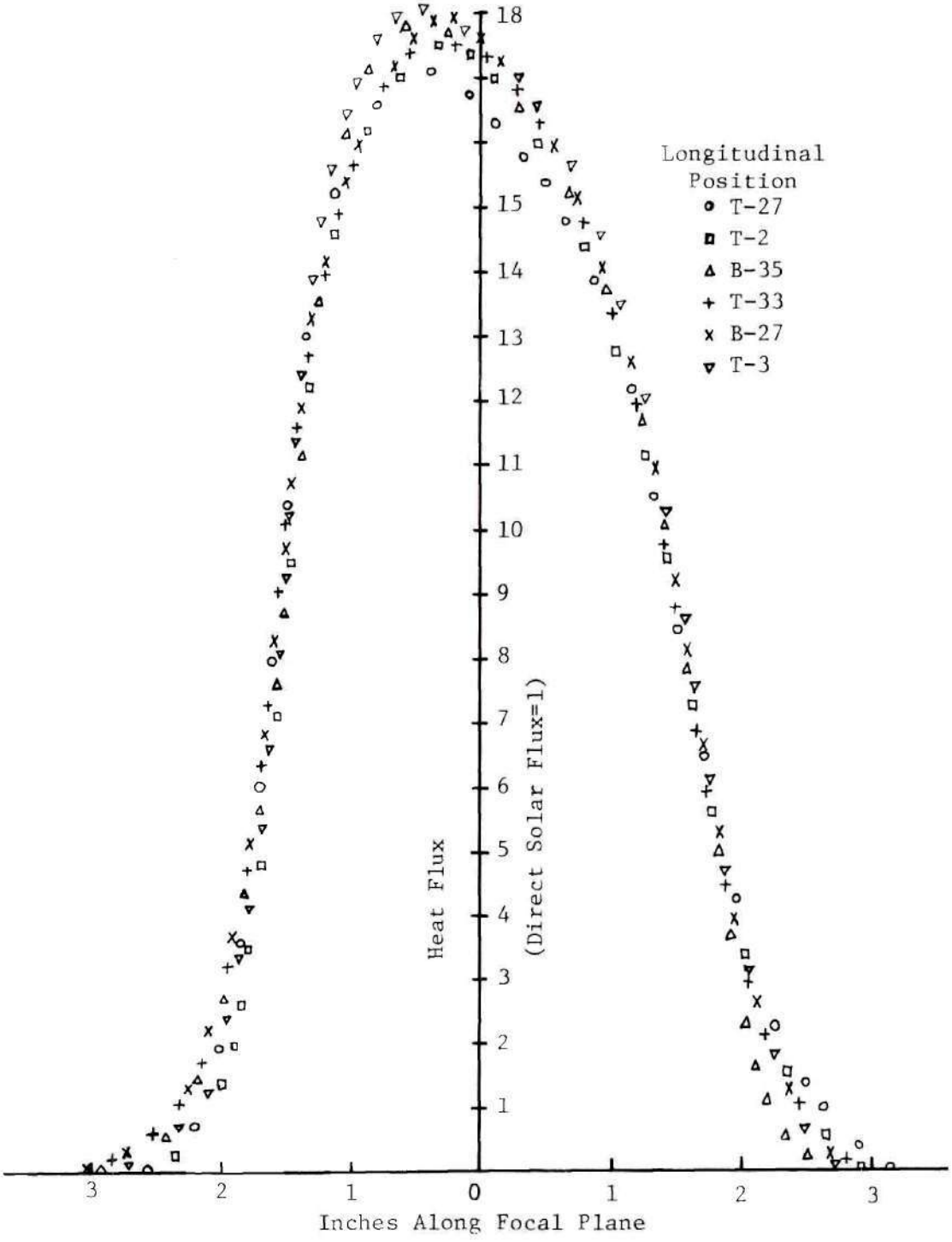

Figure A-4. Experimental Heat Flux Profiles, $\phi = 56.25°$

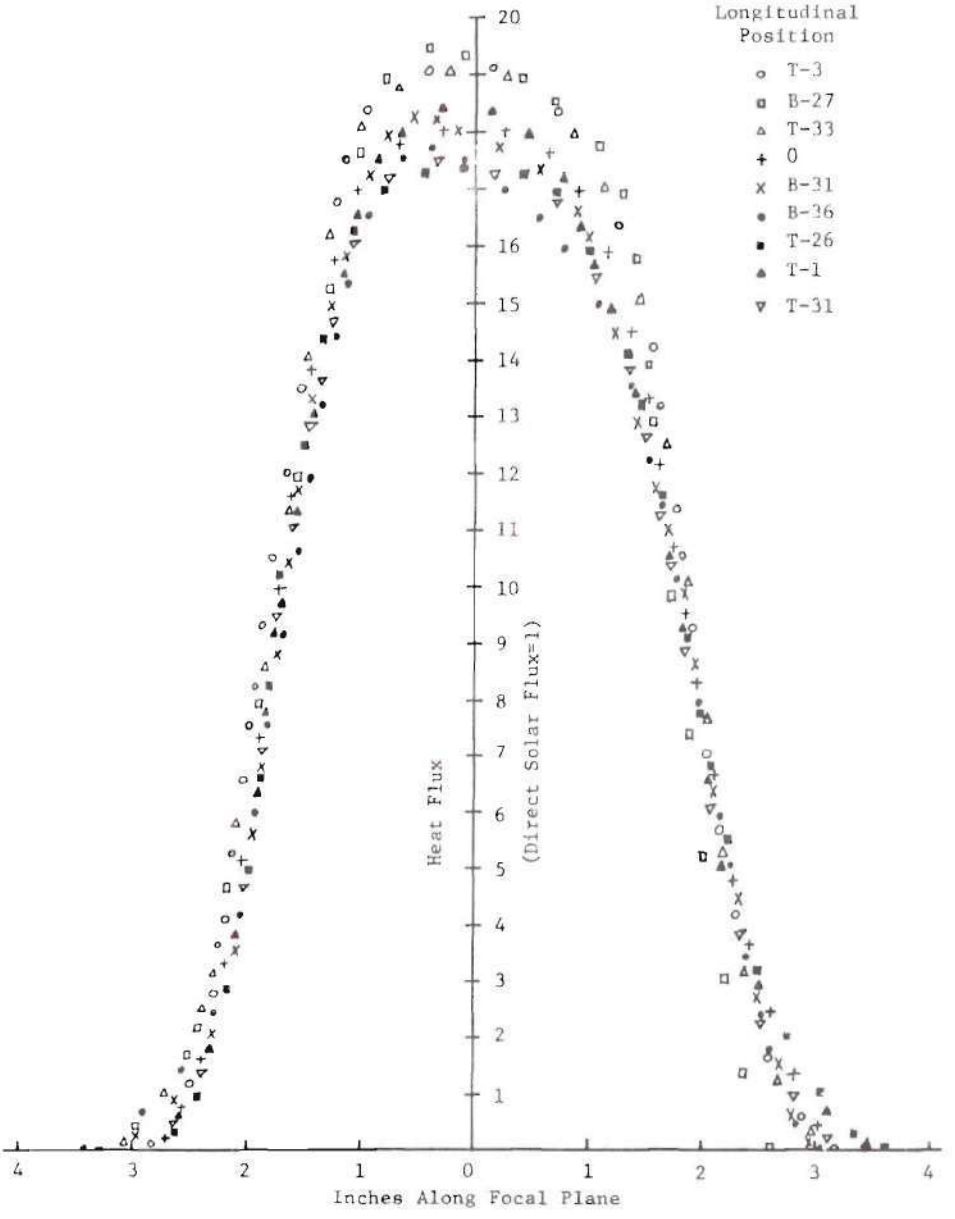

Figure A-5. Experimental Heat Flux Profiles, $\phi = 67.5°$

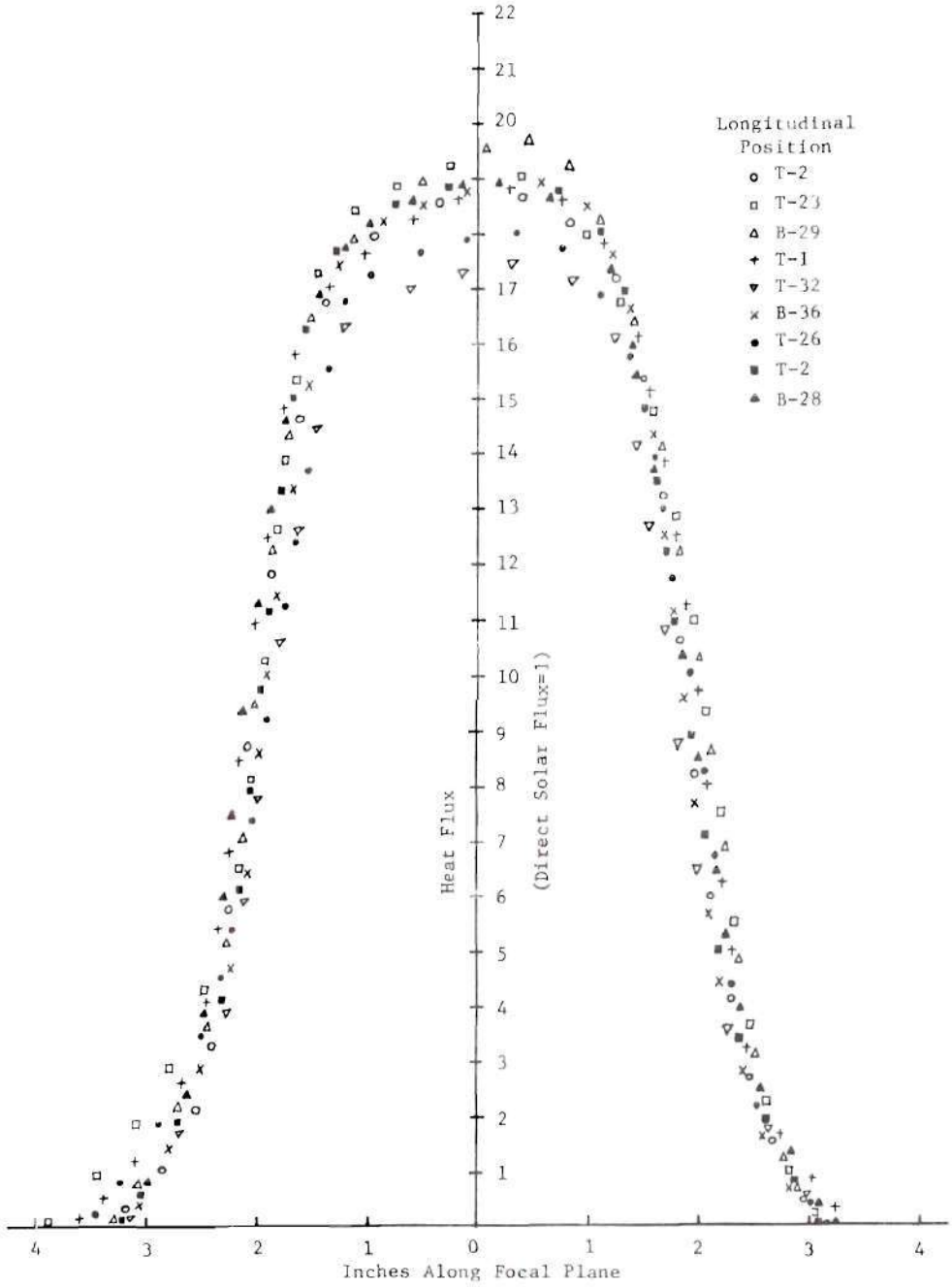

Figure A-6. Experimental Heat Flux Profiles, ϕ = 78.75°

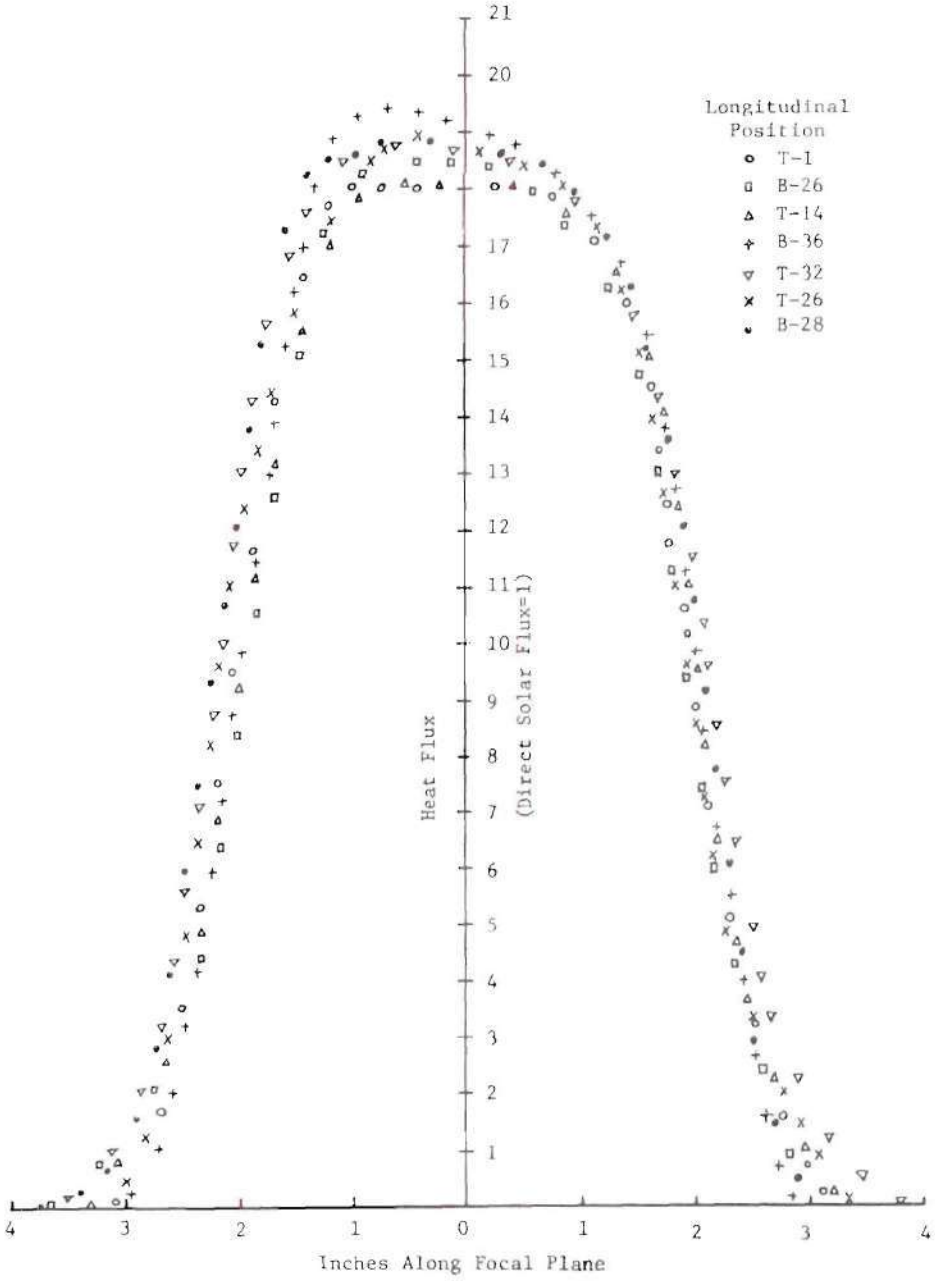

Figure A-7. Experimental Heat Flux Profiles, $\phi = 90°$

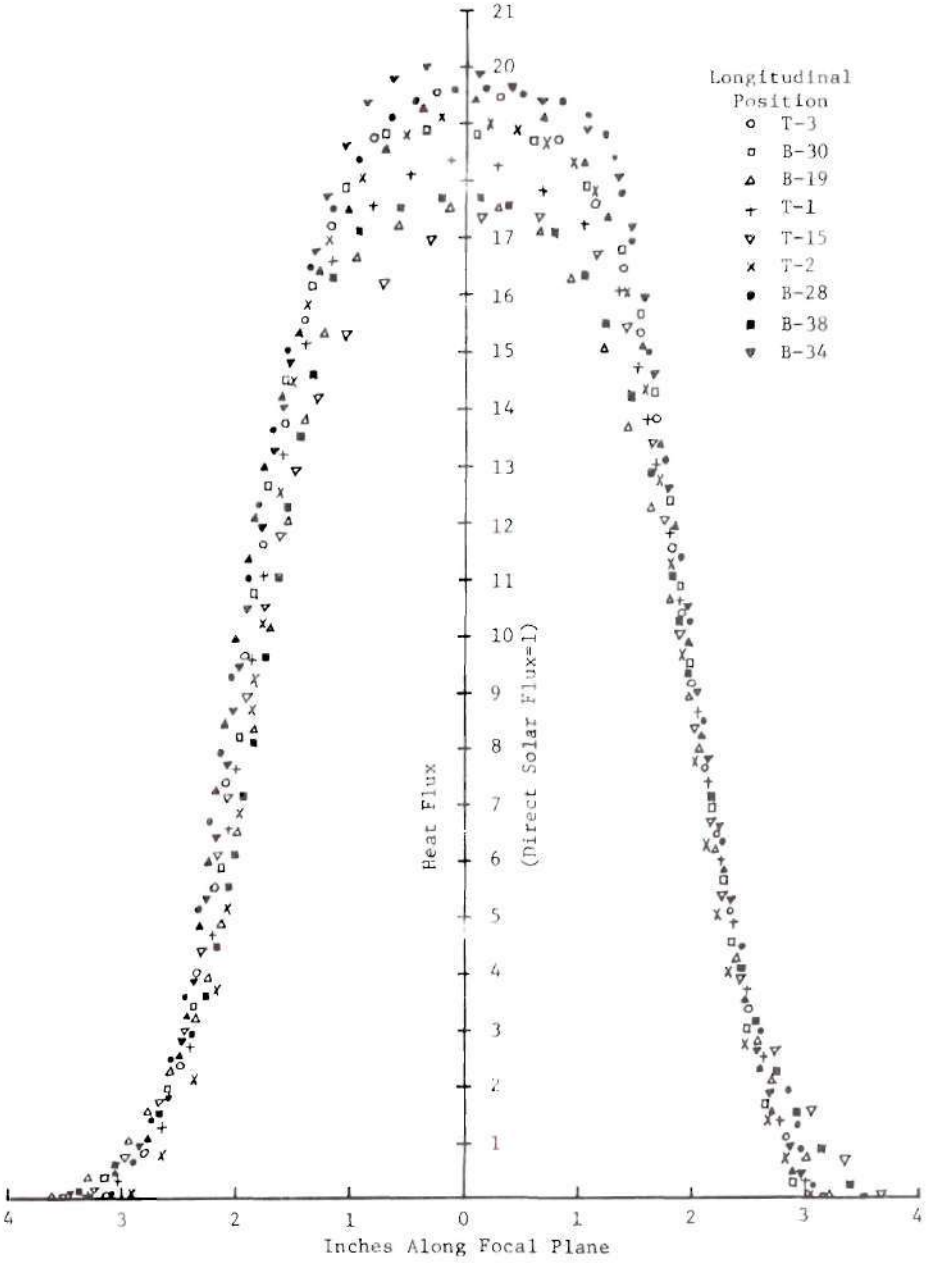

Figure A-8. Experimental Heat Flux Profiles, ϕ = 101.25°

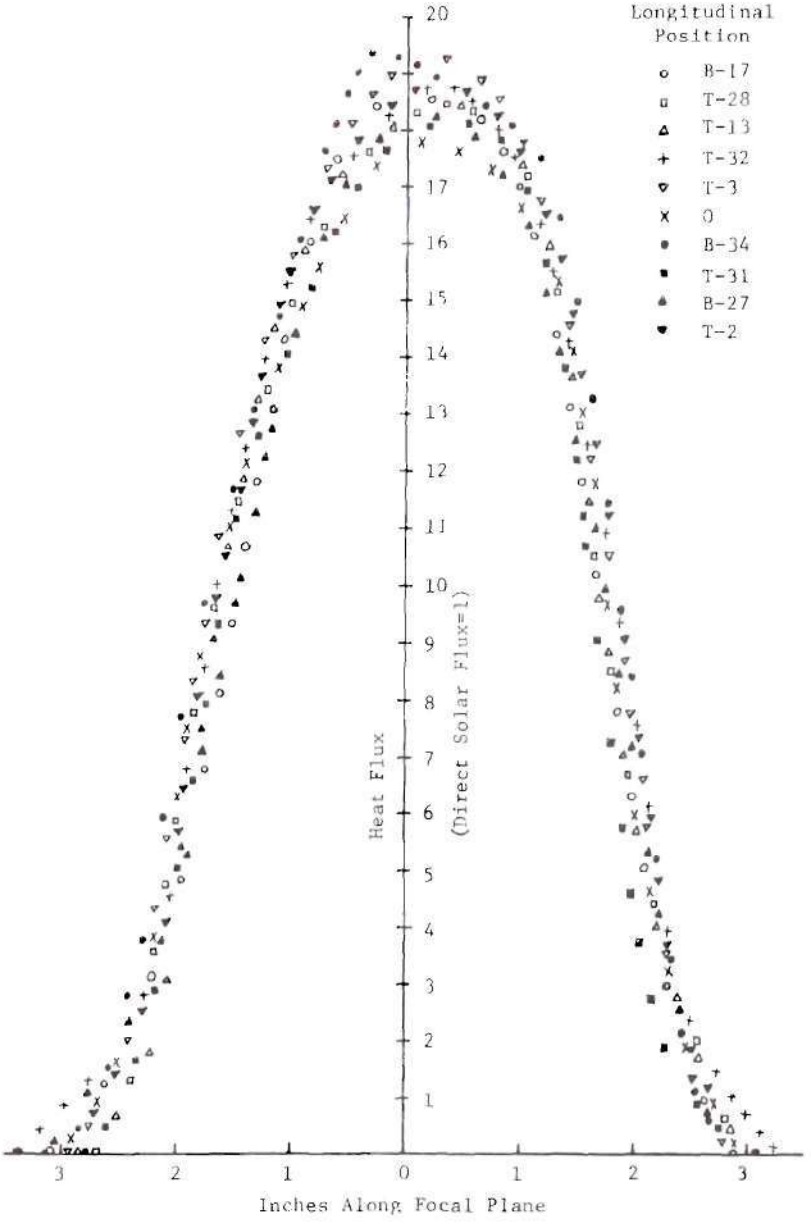

Figure A-9. Experimental Heat Flux Profiles, ϕ = 112.5°

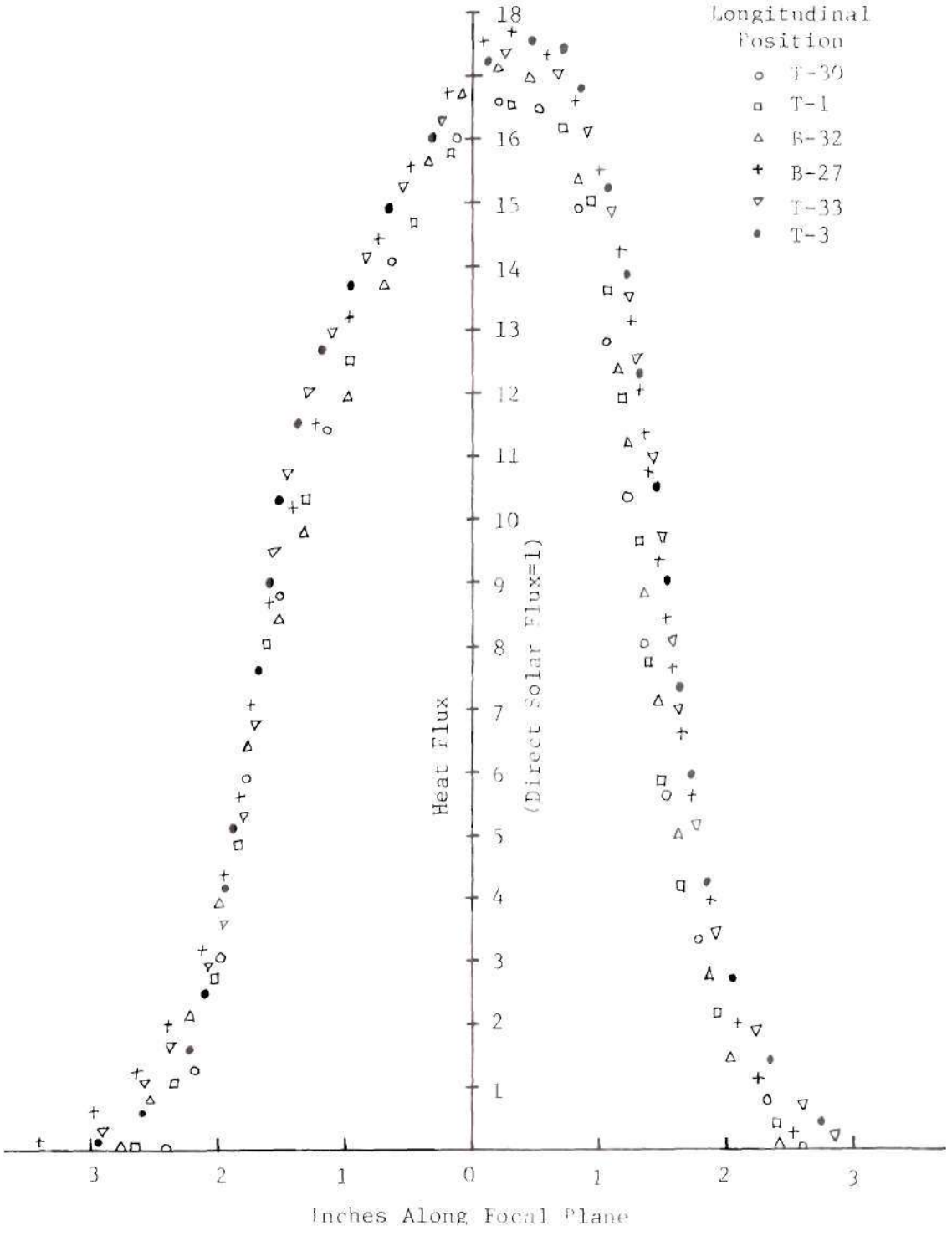

Figure A-10. Experimental Heat Flux Profiles, ϕ = 123.75°

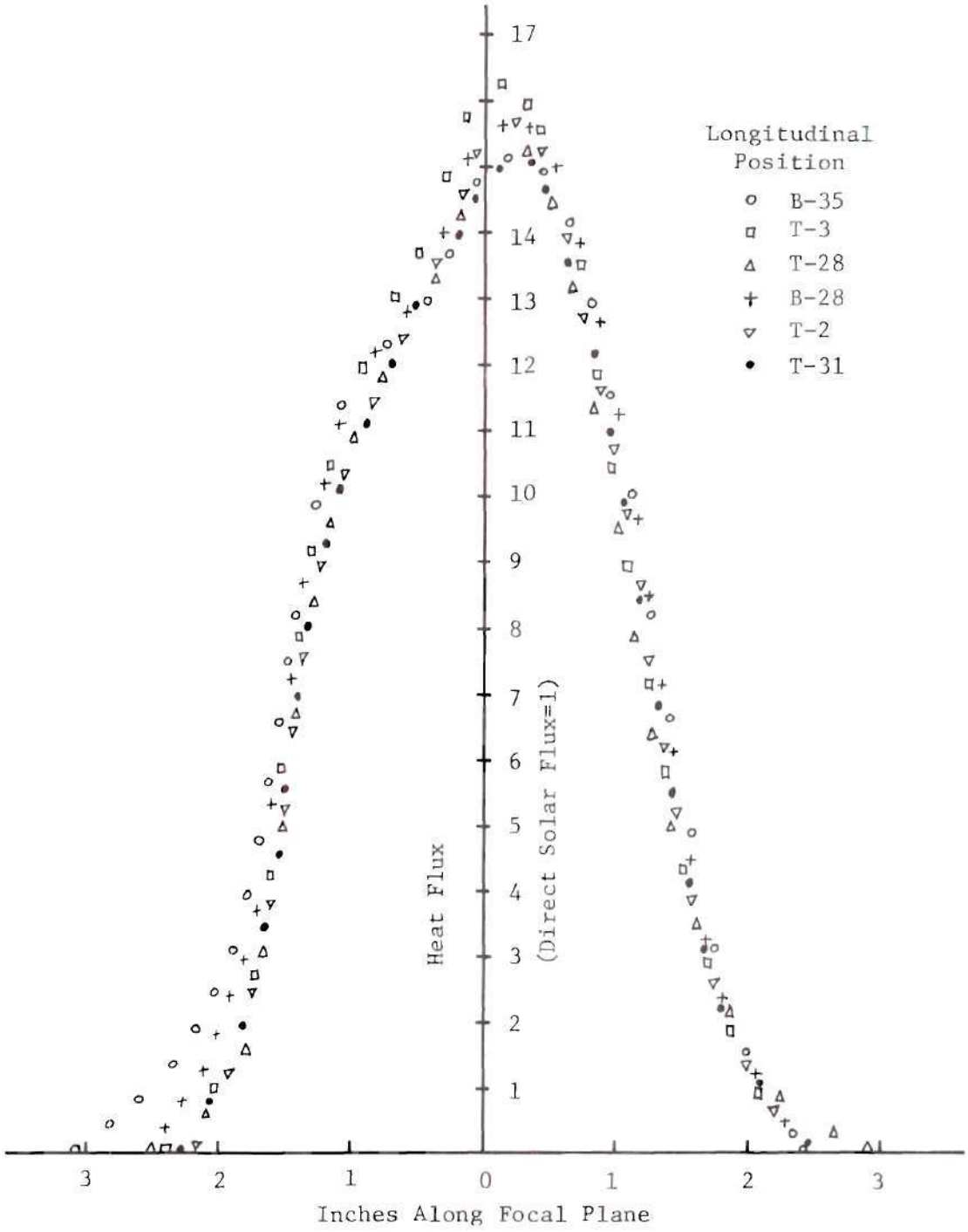

Figure A-11. Experimental Heat Flux Profiles, ϕ = 135°

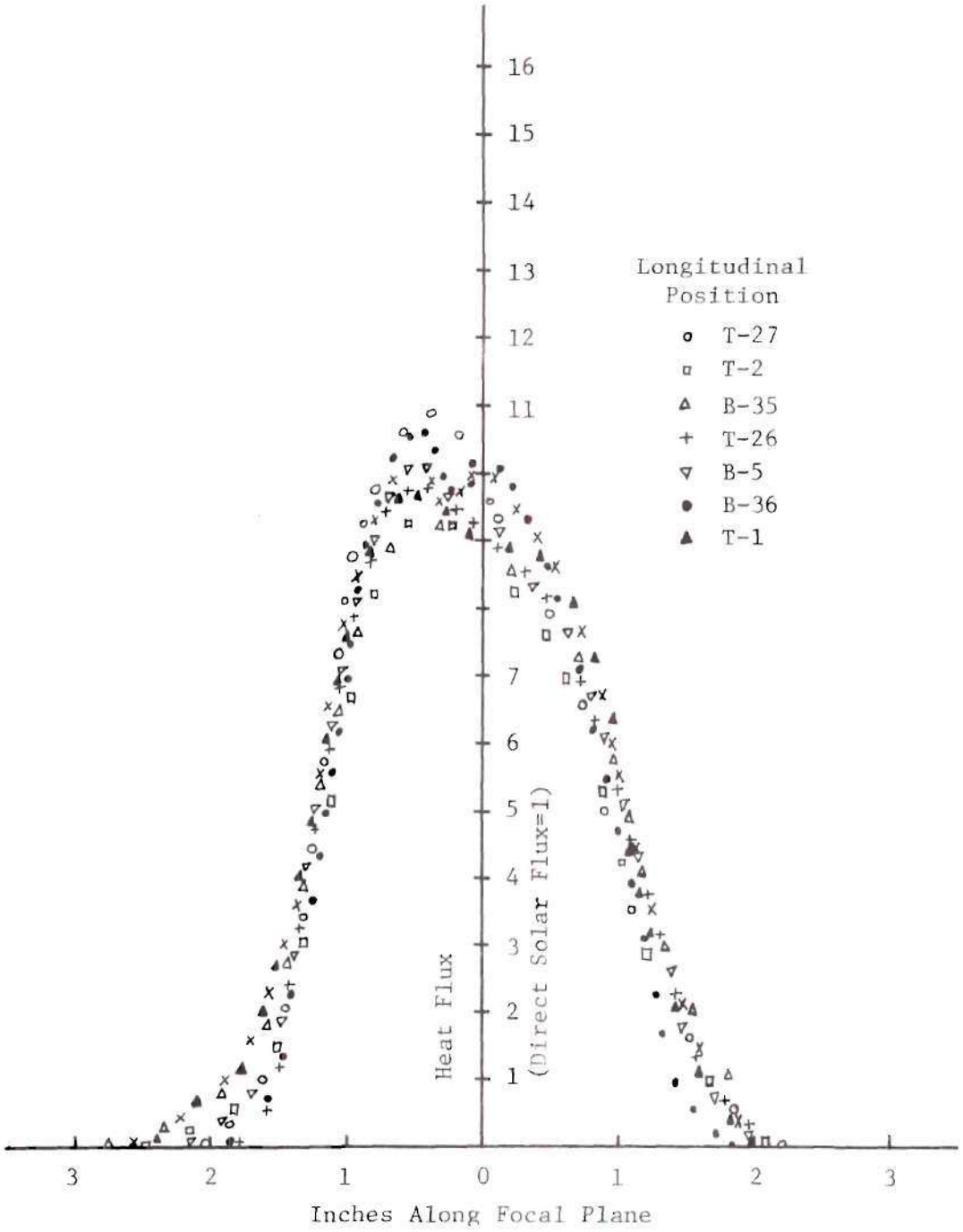

Figure A-12. Experimental Heat Flux Profiles, ϕ = 146.25°

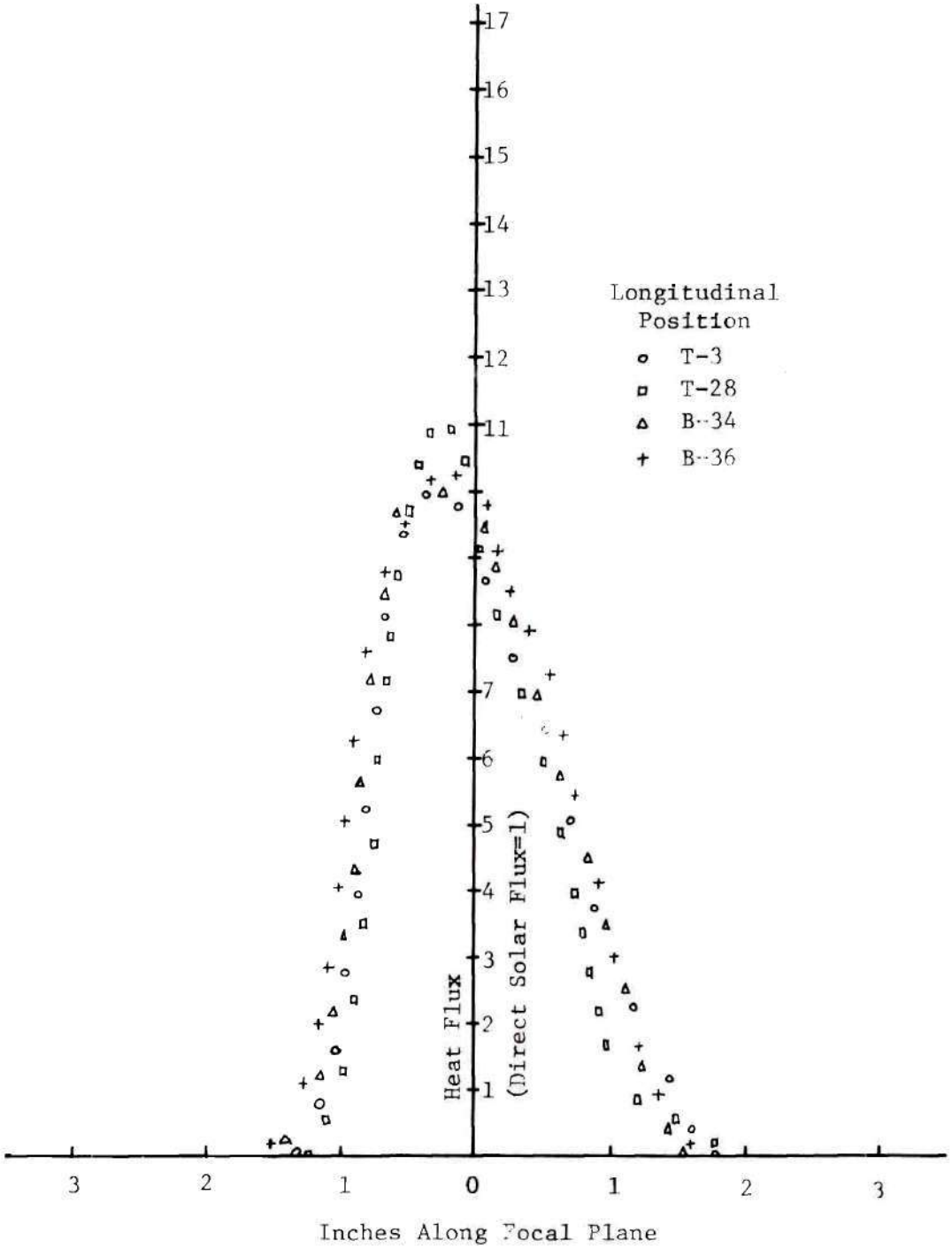

Figure A-13. Experimental Heat Flux Profiles, ϕ = 152.5°

BIBLIOGRAPHY

BIBLIOGRAPHY

1. Williams, J. R., Solar Energy Technology and Applications, Ann Arbor Science Publishers Inc., Ann Arbor, Michigan, 1974.

2. Eibling, J. A., "A Survey of Solar Collectors", Proceedings of the NSF/RANN Solar Heating and Cooling for Buildings Workshop, Washington, D. C., pp. 47, March 21-23, 1973.

3. Daniels, F., Direct Use of the Sun's Energy, Yale University Press, New Haven, 1964.

4. Guntner, C., "The Utilization of Solar Heat for Industrial Purposes by Means of a New Plane Mirror Reflector", Scientific American, May 26, 1906.

5. Lindsey, A. M., "Investigation of a Segmented Plane Solar Energy Concentrator", Thesis, Georgia Institute of Technology, August, 1974.

6. Fairbanks, J. W. and Morse, F. H., "Passive Solar Array Orientation Devices for Terrestrial Application", Solar Energy, Vol. 14, pp. 67-79, 1972.

7. Baum, V. A., Aparase, A. R. and Garf, B. A., "High-Power Solar Installation", Solar Energy, Vol. 1, No. 2, pp. 6-13, 1957.

8. Francia, G., "Pilot Plants of Solar Steam Generating Stations", Solar Energy, Vol. 12, pp. 51-64, 1968.

9. Walton, J. D. and Blake, F. A., Update on the "Solar Power System and Component Research" Program, International Solar Energy Society U. S. Section Annual Meeting, Fort Collins, Colorado, August 21-23, 1974.

10. Tabor, H., "Stationary Mirror Systems for Solar Collectors", Solar Energy, Vol. 2, pp. 27-33, July-October, 1958.

11. Steward, W. G., "A Concentrating Solar Energy System Employing a Stationary Spherical Mirror and Movable Collector", Proceedings of the NSF/RANN Solar Heating and Cooling for Buildings Workshop, Washington, D. C., pp. 24-25, March 2.-23, 1973.

12. Winston, R., "Solar Concentrators of a Novel Design", Report from Enrico Fermi Institute and Department of Physics, University of Chicago.

13. Russell, J. L., DePlomb, E. P. and Ravinder, R. K., "Principles of the Fixed Mirror Solar Concentrator", Solar Energy, Submitted for publication.

14. Russell, J. L., "Investigation of a Central Station Solar Power Plant", Proceedings of the Solar Thermal Conversion Workshop, Washington, D. C., January, 1973: [also published as Gulf General Atomic Report No. Gulf-FA-A12759, August 31, 1973].

15. Handbook of Tables for Applied Engineering Science, 2nd Ed., Chemical Rubber Company Press, Cleveland, 1973, p. 217.

16. Popov, E. P., Introduction to Mechanics of Solids, Prentice-Hall, Inc., Englewood Cliffs, N. J., 1968.

17. Bansal, Ravinder K., "Theoretical Analysis of a Fixed Mirror Solar Concentrator", Thesis, Arizona State University, May, 1974.

18. Chapman, A. J., Heat Transfer, 2nd Ed., The Macmillan Company/ Collier-Macmillan Limited, London, 1967.

19. Lion, K. S., Instrumentation in Scientific Research, McGraw Hill Book Company, Inc., New York, 1959.

20. U. S. Department of Commerce, Climatological Data, Georgia, Annual Summary 1973, Vol. 77, No. 13.

21. Williams, J. R. and Justus, C. G., "The Georgia Air Quality Implementation Plan", No. 72-94, Presented at 64th Annual Meeting of APCA, Miami Beach, Florida, June, 1972.